UNIVERSITY OF CALIFORNIA

Los Angeles

Manifesting Hidden Structure in Scattering Amplitudes

A dissertation submitted in partial satisfaction

of the requirements for the degree

Doctor of Philosophy in Physics

by

Michael Enciso

2019

ABSTRACT OF THE DISSERTATION

Manifesting Hidden Structure in Scattering Amplitudes

by

Michael Enciso

Doctor of Philosophy in Physics

University of California, Los Angeles, 2019

Professor Zvi Bern, Chair

This dissertation explores hidden structure within scattering amplitudes in quantum field theory, both at tree-level and at loop-level, and introduces some novel methods for making this hidden structure manifest. In Chapter 1 we give a brief introduction to the field of scattering amplitudes. In Chapter 2, we examine two-loop amplitudes in half-maximal supergravity (SUGRA) and discuss different ways of manifesting the underlying and surprising UV-finiteness. In particular, we apply state of the art techniques for performing integration by parts (IBP) reduction on families of multiloop integrals and introduce a new way of exposing UV-cancellations by performing IBP reduction directly on vacuum diagrams in a way that does not mix up UV and IR divergences. In Chapter 3 we continue to explore IBP reduction, now from a different perspective. Here we focus on planar Feynman diagrams and use the properties of dual conformal transformations to identify a family of IBP vectors that do not double propagators, and are therefore compatible with the highly successful unitarity method of computing loop amplitudes. A natural extension of these ideas is to try to apply similar methods to nonplanar diagrams, and doing so leads to some very preliminary steps towards uncovering a nonplanar analog of dual conformal symmetry, which is believed to exist from other considerations. Initial steps along this direction are discussed at the end of this chapter. In Chapter 4 we continue on from Chapter 3 in uncovering a nonplanar analog

of dual conformal symmetry. Here we show that through three loops in $\mathcal{N} = 4$ super-Yang–Mills (sYM) theory at four points and through two loops at five points, a representation of the amplitudes exist such that every relevant nonplanar diagram enjoys this hidden nonplanar symmetry. In Chapter 5 we leave the world of loop amplitudes and consider one of the simplest classes of scattering amplitudes—tree amplitudes in planar $\mathcal{N} = 4$ sYM. A novel geometric perspective on this class of amplitudes is afforded by the amplituhedron picture. We introduce a new formalism for computing these amplitudes in the NMHV helicity sector, and a new and purely combinatorial description of the underlying polytopes. Our formalism makes the equivalence of different triangulations of the underlying space manifest by introducing a new set of objects that can be used to express the amplitude uniquely. In Chapter 6 we discuss ongoing work. In the first section, we discuss some progress that has been made in extending the formalism introduced in Chapter 5 to different MHV sectors. This would provide new insight on the geometric underpinning of these amplitudes, which is currently not understood. Finally, in the last section of this chapter we describe an algorithm for finding complete sets of numerical solutions to the scattering equations, and doing so faster than other implementations currently available.

The dissertation of Michael Enciso is approved.

Eric D'Hoker

Michael Gutperle

Per J. Kraus

Zvi Bern, Committee Chair

University of California, Los Angeles

2019

To everyone who has helped me.

Contents

List of Figures

Acknowledgements

I would like to thank Zvi Bern for his mentorship, for encouraging me to explore my own ideas, and for keeping those ideas on the right track. I would also like to thank the Bhaumik Institute for its support. I would like to thank Julio Parra-Martinez for many fruitful discussions and for always pointing me in the direction of good papers. I also thank Mao Zeng for helping me get up to speed with things, and Chia-Hsien Shen for always answering my questions.

To Chrysostomos Marasinou and Justin Kaidi, thank you for putting up with my office antics and for being open minded about the mini basketball hoop. To the two aforementioned, as well as Julio, Alex Edison, Andrea Trivella, Fenner Harper, and Allic Sivaramakrishnan for their lunch company over the years and for indulging me in my incessant talk about the NBA.

Finally I need to thank the non-physicists in my life. To Luke, Billy, Evan, Eric, Martin, and Fenner (the latter two of which are, incidentally, physicists), thanks for keeping me sane. I hope my wife, Finja, has even half an understanding of how grateful I am for her support. I thank my mom, my dad, and my bonus mom for all they have done, of which they are very aware. I also thank my sister Jen and brother-in-law Skii for providing me with two awesome nephews that constantly remind me of what it's all about.

Contribution of authors

Chapter 2 is based on Ref. [1] with Zvi Bern, Julio Parra-Martinez, and Mao Zeng, Chapter 3 is based on Ref. [2] with Zvi Bern, Harald Ita, and Mao Zeng, Chapter 4 is based on Ref. [3] with Zvi Bern, Chia-Hsien Shen, and Mao Zeng, and Chapter 5 is based on Ref. [4], which itself is a follow up to Ref. [5]. The work in Chapter 6 on numerical solutions to scattering equations was done in collaboration with Joseph Farrow.

Vita

2008 – 2012	B.A. (Physics and Mathematics), Columbia University
2012 – 2014	M. Sc. in Mathematics, Oxford University
2014 – 2018	Teaching Assistant, Department of Physics and Astronomy, UCLA
2018 – 2019	Dissertation Year Fellowship, UCLA

Publications

"Manifesting enhanced cancellations in supergravity: integrands versus integrals,"
Bern, Z., Enciso, M., Parra-Martinez, J., Zeng, M., JHEP 1705 (2017) 137
DOI: 10.1007/JHEP05(2017)137 arXiv:1703.08927 [hep-th]

"Dual Conformal Symmetry, Integration-by-Parts Reduction, Differential Equations and the Nonplanar Sector,"
Bern, Z., Enciso, M., Ita, H., Zeng, M., Phys.Rev. D96 (2017) no.9, 096017
DOI: 10.1103/PhysRevD.96.096017 arXiv:1709.06055 [hep-th]

"Dual Conformal Structure Beyond the Planar Limit,"
Bern, Z., Enciso, M., Chia-Hsien, S., Zeng, M., Phys.Rev.Lett. 121 (2018) no.12, 121603
DOI: 10.1103/PhysRevLett.121.121603 arxiv:1806.06509 [hep-th]

"Logarithms and Volumes of Polytopes"
Enciso, M., JHEP 1804 (2018) 016, DOI: 10.1007/JHEP04(2018)016
arXiv:1612.07370 [hep-th]

"Volumes of Polytopes Without Triangulations"
Enciso, M., JHEP 1710 (2017) 071, DOI: 10.1007/JHEP10(2017)071
arXiv:1408.0932 [hep-th]

Chapter 1

Introduction

In elementary particle physics, one of the most fundamental observables is the scattering cross section, either in its full form (σ) or its differential form ($\frac{d\sigma}{d\Omega}$). The reason for this is simple: elementary particles are difficult, and sometimes even impossible, to obtain and manipulate on their own. Therefore, the best recourse that physicists have available to them is to collide beams of particles together many times and study the statistical properties of the resulting events. In slightly more detail, we take two beams of (possibly identical) particles, collide them at various energy scales, and study the counts, lifetimes, charges, masses, and other properties of the particles that come out of this process. The theoretical description of these processes is contained in the scattering amplitude $\mathcal{A}$ for the relevant particles in the relevant theory. The scattering amplitude is directly related to the measured (differential) scattering cross-section via a theory-independent phase space integral. Schematically,

$$\frac{d\sigma}{d\Omega} = \int_{\mathcal{P}} |\mathcal{A}|^2 d\mu, \tag{1.0.1}$$

where the amplitude $\mathcal{A}$ is stripped of its momentum-conserving delta function[1] and the integral is performed over the kinematically allowed portion of phase space, which accounts

[1]There must still be one overall momentum-conserving delta function, and we implicitly include this is in the phase-space measure.

for overall momentum conservation as well as the on-shell and positive-energy conditions of the external particles.

With scattering amplitudes carrying all of the theory-dependent information for one of the most fundamental observables in elementary particle physics, it is imperative that the underlying theoretical framework is amenable to their computation. This underlying framework is quantum field theory, and the method for using this framework to compute scattering amplitudes has been worked out in great detail decades ago. Most notably, it was Richard Feynman who clarified many of the computational methods for computing these observables order-by-order in perturbation theory, using diagrams that have now been named after him.

In short, one picks a quantum field theory in which to compute a scattering amplitude and a particular order (of a suitable parameter g) in perturbation theory on which to focus. The latter corresponds to tree-level, one-loop, two-loop, and n-loop (at order g^n, roughly speaking) amplitudes. These names come from the topology of the relevant diagrams that one must draw, which in turn come from the order n expansion of the path integral

$$\mathcal{A} \overset{f.t.}{\sim} \int \mathcal{D}\phi I(\phi) e^{i\int d^D x \mathcal{L}(\phi,\partial\phi)}. \tag{1.0.2}$$

In this schematic expression, the quantum fields are generically denoted by ϕ, $I(\phi)$ is a monomial in the fields encoding the interaction that is being considered, and $\mathcal{L}$ is the Lagrangian defining the quantum field theory[2]. We have also used $f.t.$ to denote the fact that we fourier transform the fields so that the amplitudes are functions on momentum space.

For a given theory and at a given order, Feynman's calculus tells us how to compute any scattering amplitude we wish to obtain. When computing at orders that involve loops, one often encounters ultraviolet (UV) and/or infrared (IR) divergences. The latter are well-understood and do not affect the finiteness of any observable quantities. UV divergences

[2]This formula does not address many subtleties, such as Wick rotation, the presence of gauge redundancy in the path integral, how spinor fields are dealt with, and so on. For the sake of the current discussion, however, we will not need to address these issues.

pose a more troubling problem, but even these can be regulated and either reabsorbed in the couplings and masses of the theory (in the case of a renormalizable theory) or absorbed by the coefficients of higher-order operators in an effective field theory. It therefore would appear that, after many decades of work, the problem of computing scattering amplitudes is solved and one simply needs to sit down and patiently perform whatever computation the experimentalists might desire.

Philosophically, this is indeed the case, but in practice things are not quite as simple. In particular, even some of the simplest processes in phenomenologically relevant theories, at orders of perturbation theory that experimentalists can resolve, would require amounts of computation that are entirely intractable even with modern supercomputers. For example, when two gluons scatter into eight gluons—a reasonably frequent process, given the nonlinear self-couplings of gluons—one would need to compute over ten million Feynman diagrams in order to obtain the scattering amplitude, and this would only provide the lowest-order (tree-level) contribution. Therefore, while a mathematician might consider the issue of computing scattering amplitudes in perturbation theory a solved problem, a physicist does not have this luxury, since these quantities must also be computed with reasonable efficiency in order to keep up with experiment.

Indeed, the experimental need for these gluon-to-gluon scattering amplitudes motivated Stephen Parke and Tomasz Taylor to perform some of these calculations, for reasonably high numbers of gluons. In particular, they chose a particular helicity configuration—the maximally helicity-violating (MHV) configuration in which all but two gluons share the same helicity—and performed these heroic computations. What they found, however, not only provided necessary theoretical predictions, but also spearheaded a new industry. In particular, they found that the (color-ordered) amplitude for $2 \to n-2$ gluon scattering, with gluons i and j having opposite helicities from the others, can be written simply as

$$\mathcal{A}_{\text{Parke-Taylor}} = i(-g)^{n-2} \frac{\langle ij \rangle^4}{\langle 12 \rangle \langle 23 \rangle ... \langle (n-1)n \rangle \langle n1 \rangle} \tag{1.0.3}$$

when expressed in terms of spinor-helicity variables[3]. Recalling that for $n = 10$ this is the result of summing over ten million Feynman diagrams, we see that this result is simply astounding.

In fact, this result teaches us (at least) three important lessons. First and foremost, it shows us that scattering amplitudes can be simpler than one could have ever reasonably hoped for. Second, it shows us that sometimes one needs to use non-standard variables (in this case, spinor-helicity variables as opposed to the usual 4-momentum variables) in order to expose this simplicity. Third, and perhaps most importantly, it shows us that there is a **structure** hiding inside scattering amplitudes that is completely obscured by the standard (i.e., Feynman diagramatic) way of computing these objects. To appreciate this, we must note that while the standard approach asks us to increase the number of Feynman diagrams in this calculation with a faster-than-factorial growth as n increases, the above Parke-Taylor formula asks us to include one more term in the denominator. This not only exemplifies the simplicity of any given amplitude but also shows that there is a hidden structure within this class of amplitudes as a whole that the usual field-theoretic approach is blind to.

This, in turn, begs a few questions. How can this simplicity be explained, understood, and exploited? How special is this simplicity to gluon amplitudes and when, more generally, can we expect to find these surprises? Once we know that there is hidden structure and/or simplicity to be found, how can we make it manifest?

Throughout the last couple decades the community has seen tremendous progress in answering these questions and finding hidden structure and simplicity in large classes of theories and in wide ranges of orders in perturbation theory. This was perhaps most strikingly observed when Witten showed in 2004 [7] that the Parke-Taylor amplitudes can be understood as an instanton expansion of a string theory with supertwistor space as its target space. This result opened the floodgates for the study of scattering amplitudes as a theoretical endeavor in its own right, setting an example for the types of connections across seemingly disparate

[3]For a review on spinor-helicity variables, see e.g. Ref. [6].

arenas of particle physics that one might hope to uncover.

Indeed, simplicity is not the only surprising characteristic that can be found in scattering aplitudes. As is well known [8–10], there are amplitudes in various supergravity theories that are UV-finite despite the lack of any well-established symmetry argument, and in Chapter 2 we explore various ways of making this finiteness manifest. The study of amplitudes has also helped to uncover hidden symmetries of theories, since amplitudes can reflect a symmetry even if that symmetry cannot be easily seen at the level of the Lagrangian. In Chapters 3 and 4, we show how dual conformal symmetry—a hidden symmetry in planar $\mathcal{N} = 4$ super-Yang–Mills (sYM)—can not only be used to simplify the computation of higher-loop amplitudes, but also be extended in certain cases to the nonplanar sector of the theory. In these chapters we therefore see some of the surprises that one can find in an amplitude—simplicity, finiteness, and hidden symmetry—as well as different ways of exploiting these surprises for computational efficiency.

Understanding where these surprises come from, however, presents a new (though related) challenge, and progress in this direction has also been immense in the last two decades. One such example is the discovery of the amplituhedron [11], which gives a unified geometric understanding of the tree-level amplitudes and loop-level integrands of planar $\mathcal{N} = 4$ sYM, making no explicit reference to many of the usual field-theoretic paradigms such as locality and unitarity. While this geometric picture is elegant and surprising, it is often obscured in any explicit representation of the amplitudes. In Chapter 5, we present a new formalism for computing the simplest class of these amplitudes—the tree-level NMHV amplitudes—in such a way that makes manifest the underlying geometric picture. Finally, in Chapter 6, we discuss some progress that has been made in extending this picture to other, more complicated tree-level amplitudes in this (admittedly very special) theory, as well as some other ongoing work.

Chapter 2

Manifesting enhanced cancellations in supergravity: integrands versus integrals

Examples of 'enhanced ultraviolet cancellations' with no known standard-symmetry explanation have been found in a variety of supergravity theories. By examining one- and two-loop examples in four- and five-dimensional half-maximal supergravity, we argue that enhanced cancellations in general cannot be exhibited prior to integration. In light of this, we explore reorganizations of integrands into parts that are manifestly finite and parts that have poor power counting but integrate to zero due to integral identities. At two loops we find that in the large loop-momentum limit the required integral identities follow from Lorentz and SL(2) relabeling symmetry. We carry out a nontrivial check at four loops showing that the identities generated in this way are a complete set. We propose that at L loops the combination of Lorentz and SL(L) symmetry is sufficient for displaying enhanced cancellations when they happen, whenever the theory is known to be ultraviolet finite up to $(L-1)$ loops.

2.1 Introduction

The study of ultraviolet properties of four-dimensional gravity theories has a long history, starting from the seminal work of 't Hooft and Veltman [12]. Despite this we do not know the answer to the basic question of at which loop order various gravity theories actually diverge. In addition, when divergences occur in graviton amplitudes we now know that they have unusual properties, including dependence on evanescent effects [13] and suspected links to anomalies [14,15]. Even more interesting are indications in certain supergravity theories that the loop order where the first divergence occurs is higher than previous expectations [8–10]. This renews the possibility that certain theories, such as $\mathcal{N} = 8$ supergravity, are ultraviolet finite at any order in perturbation theory. No known symmetry is powerful enough to render a four-dimensional quantum gravity theory ultraviolet finite, so if this were true it would be extraordinary.

Certain cancellations in gravity theories are different from those in supersymmetric gauge theories in that they cannot be made manifest for ordinary local representations. When such cancellations happen they are dubbed 'enhanced cancellations' [9]. In simple cases, these enhanced cancellations can be understood through conventional means by constraining the set of available counterterms from symmetry considerations. For example, at one loop, a well-known counterterm argument [12] explains that the n graviton amplitudes are finite even though the diagrams scale poorly in the ultraviolet. On the other hand, recent examples of enhanced cancellations have as yet no standard symmetry explanation, despite attempts [17–19] and insight from string theory [20]. These examples include $\mathcal{N} = 5$ supergravity at four loops in $D = 4$ [9], $\mathcal{N} = 4$ supergravity at three loops in $D = 4$ [8], and half-maximal supergravity at two loops in $D = 5$ [10]. In the relatively simple case of half-maximal supergravity at two loops the cancellations have been understood using the double-copy structure that allows the amplitudes to be built from gauge-theory ones [10]. Unfortunately, it is not clear how to generalize this understanding to higher loops.

In light of the difficulties in trying to develop a comprehensive explanation for enhanced cancellations, we should consider alternative approaches. For instance one could try to mimic diagram-based proofs of finiteness that were successfully carried out for $\mathcal{N} = 4$ super-Yang–Mills theory (see for example Refs. [21, 22]). These were achieved by finding representations of the integrand where every term is ultraviolet finite by power counting. However, enhanced cancellations are different: By definition they cannot be made manifest diagram by diagram at the integrand level, using only standard Feynman propagators. But one can still wonder if some kind of integrand-level reorganization could be found that makes large loop-momentum cancellations manifest or at least clarifies how the cancellations occur.

An obstruction to pursuing these ideas is that we lack a good definition of global variables for all diagrams of a multiloop amplitude including nonplanar diagrams. One way to approach this difficulty is to use unitarity cuts. At one loop, a systematic program was successfully followed for all one-loop (super)gravity amplitudes in Ref. [23] using a formalism [65] based on generalized unitarity [24]. This was used to demonstrate the existence of nontrivial cancellations between diagrams as the number of external legs increases. However, a general extension of the one-loop analysis to higher loops remains a challenge.

In this chapter instead of attempting a general argument we turn to specific examples in half-maximal supergravity, which we study in some detail. We construct the examples using the Bern–Carrasco–Johansson (BCJ) double-copy construction of gravity loop integrands in terms of gauge-theory ones [25, 26]. These examples are based on the one- and two-loop $\mathcal{N} = 4$ supergravity amplitudes previously obtained in Refs. [27–29].

We first show that at one loop it is not possible to construct integrands where cancellations are manifest in general dimensions. In particular, we identify cancellations in $D = 4$ that require integration identities. At two loops we use unitarity cuts to argue that cancellations cannot be made manifest at the integrand level. To further investigate this case, we use integration-by-parts (IBP) technology [30–34, 73, 98] to reorganize the integrand into pieces that are finite by power counting and pieces that are divergent by power counting,

yet integrate to zero. Although this re-arrangement of the complete integrand is successful, it requires detailed knowledge of the specific integrals and their relations, making it difficult to generalize to higher loops.

To deal with this, we then turn to a simpler approach by giving up on trying to make the full integrand display enhanced ultraviolet cancellations. Instead we series expand in large loop momenta in order to focus on the ultraviolet behavior. We show that at least in the two loop examples we study the integral identities necessary for exposing the enhanced cancellations follow from only Lorentz and SL(2) relabeling invariance. These ideas continue to higher loops, and as a nontrivial confirmation we found that these principles generate all required integral identities for exposing the ultraviolet behavior of maximal supergravity at four loops in the critical dimension where the divergences first occur [35]. Based on these results, we conjecture that at L loops the IBP identities generated by Lorentz and SL(L) relabeling symmetry are sufficient for revealing the enhanced cancellations, when they exist. The principles are generic and present in all amplitudes in the large loop-momentum limit.

This chapter is organized as follows. In Section 2.2, we present one- and two-loop examples showing the lack of integrand-level cancellations. In Section 2.3 we outline how one can arrange complete integrands so that they are manifestly finite by power counting up to terms that integrate to zero. In Section 2.4 we then analyze the large loop-momentum limit, bringing us to a conjecture on symmetries of the integrals responsible for making enhanced cancellations visible. We give our conclusions in Section 2.5. We also include an appendix on subtleties regarding boundary terms in integration-by-parts identities.

2.2 Absence of enhanced cancellations in the integrand

Enhanced cancellations are a recently identified type of ultraviolet cancellation that can occur in gravity theories [8–10]. These cancellations are defined as follows: Start with an amplitude organized in terms of diagrams whose denominators are only the usual Feynman propagators $i/(p^2 + i\epsilon)$. Suppose this amplitude is ultraviolet finite, yet there are terms

that are divergent by power counting and cannot be re-assigned to other diagrams without introducing additional spurious denominators in other diagrams. This implies nontrivial cancellations that cannot be manifest in the integrand of each diagram. We would then say there is an enhanced cancellation.

This notion is distinct from the question of whether it is possible to exhibit the cancellations at the integrand level; one might imagine that with careful choices of loop variables in each diagram, one might be able to align the loop momenta in just the right way so that poor behavior cancels algebraically between diagrams prior to integration. Here we show that this does not happen.

We present examples of enhanced cancellations to illustrate that it is only after integration that divergences cancel. We focus on the relatively simple cases of 16-supercharge half-maximal supergravity at one and two loops in $D = 4$ and $D = 5$. In $D = 4$ this theory is just $\mathcal{N} = 4$ supergravity [36]. Even though the one-loop $D = 4$ cancellation is a well-known consequence of supersymmetry [37], it provides a relatively simple concrete example of cancellations that do not arise at the integrand level, but can be exposed using Lorentz invariance. We then turn to the more interesting case of two-loop half-maximal supergravity in $D = 5$. In this case no known standard-symmetry argument invalidates [17–19, 38] the potential R^4 divergence. However, both field theory [10] and string theory [16] calculations show that there are no R^4 terms in the effective action.

In order to construct the integrands we use the BCJ double-copy construction [25, 26], which we review briefly. The double-copy construction is useful because it directly gives us gravity loop integrands from corresponding gauge-theory ones. In this construction, one of the two gauge-theory amplitudes is first reorganized into diagrams with only cubic vertices,

$$\mathcal{A}_m^{L\text{-loop}} = i^L g^{m-2+2L} \sum_{\mathcal{S}_m} \sum_j \int \prod_{l=1}^{L} \frac{d^D p_l}{(2\pi)^D} \frac{1}{S_j} \frac{c_j n_j}{\prod_{\alpha_j} D_{\alpha_j}}\,, \tag{2.2.1}$$

where the D_{α_j} are the propagators of the j^{th} diagram, L is the number of loops, m is

the number of external legs and g is the gauge coupling. The first sum runs over the $m!$ permutations of external legs, denoted by $\mathcal{S}_m$, while the second sum over j runs over the distinct cubic graphs. The product in the denominator runs over all Feynman propagators. The symmetry factor S_n accounts for any overcounts and internal automorphisms. The c_j are the color factors associated with the diagrams and the n_j are kinematic numerators.

The double-copy construction relies on BCJ duality [25, 26] where triplets of diagram numerators satisfy equations in one-to-one correspondence with the Jacobi identities of the color factors of each diagram,

$$c_i + c_j + c_k = 0 \;\Rightarrow\; n_i + n_j + n_k = 0\,. \tag{2.2.2}$$

The indices i, j, k label the diagram to which the color factors and numerators belong. If the diagram numerators satisfy the same algebraic properties as the color factors, we can obtain corresponding gravity amplitudes simply replacing the color factors of a second gauge theory with numerator factors where the duality holds:

$$c_i \to n_i\,. \tag{2.2.3}$$

The gauge-theory coupling constant is also replaced by the gravitational one: $g \to (\kappa/2)$. In this construction the duality (2.2.2) needs to be manifest in only one of the two gauge theories [26, 39]. This construction also extends to cases where the gauge theory includes fundamental-representation matter particles [40].

2.2.1 One-loop example

We start with the one-loop amplitude of pure half-maximal $\mathcal{N} = 4$ supergravity in four dimensions [36]. This amplitude is well studied and has been computed in Refs. [27, 28]. The double-copy construction of this amplitude is particularly simple. We start from the corresponding $\mathcal{N} = 4$ super-Yang–Mills and pure Yang–Mills amplitudes.

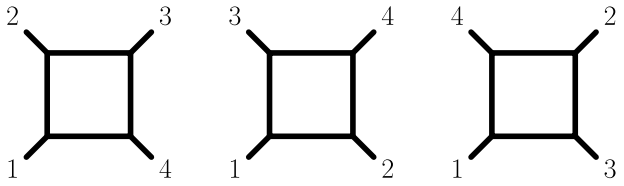

Figure 2.1: The three box diagrams contributing to the one-loop four-point amplitude of maximal $\mathcal{N} = 4$ super-Yang–Mills theory and half-maximal supergravity.

The one-loop four-point $\mathcal{N} = 4$ super-Yang–Mills amplitude was first obtained from the low-energy limit of a Type I superstring amplitude [41]. This amplitude is particularly simple and the only nonzero kinematic numerators are those of the box diagrams in Fig. 2.1,

$$n^{\text{box}}_{\mathcal{N}=4} = stA^{\text{tree}}_{\mathcal{N}=4}(1,2,3,4)\,, \tag{2.2.4}$$

where $s = (k_1{+}k_2)^2$ and $t = (k_2{+}k_3)^2$ are the usual Mandelstam invariants and $A^{\text{tree}}_{\mathcal{N}=4}(1,2,3,4)$ is the color-ordered tree superamplitude. The combination $stA^{\text{tree}}_{\mathcal{N}=4}(1,2,3,4)$ is crossing symmetric, so the three box diagrams have identical numerators. It is easy to check that this representation of the amplitude satisfies the color-kinematics duality (2.2.2).

Replacing the color factors in the pure Yang–Mills box contributions given in Ref. [42] with the $\mathcal{N} = 4$ super-Yang–Mills numerators (2.2.4), we obtain the $\mathcal{N} = 4$ supergravity amplitude as a sum over box diagrams,

$$\mathcal{M}^{\text{one-loop}}_{\mathcal{N}=4} = -\left(\frac{\kappa}{2}\right)^4 stA^{\text{tree}}_{\mathcal{N}=4}(1,2,3,4)\Big(I_{1234}[n_{1234,p}] + I_{1324}[n_{1324,p}] + I_{1423}[n_{1423,p}]\Big)\,, \tag{2.2.5}$$

where

$$I_{1234}[n_{1234,p}] \equiv \int \frac{d^Dp}{(2\pi)^D} \frac{n_{1234,p}}{p^2(p-k_1)^2(p-k_1-k_2)^2(p+k_4)^2}\,, \tag{2.2.6}$$

is the first box integral in Fig. 2.1 and $n_{1234,p}$ is the expression defined in Eq. (3.5) of Ref. [42]. The triangle and bubble contributions from the pure Yang–Mills amplitude are simply set to zero because the corresponding $\mathcal{N} = 4$ SYM numerators vanish. As dictated by the double-copy construction, the supergravity states are given by the tensor product of pure

Yang–Mills gluon states with the states of $\mathcal{N}=4$ super-Yang–Mills theory.

The case of $D=4$ is an example of enhanced cancellations because the three box diagrams are each logarithmically divergent, yet the sum over diagrams is finite. We can see this by finding power-counting divergent terms in each diagram that cannot be moved to other diagrams without introducing nonlocalities in the diagram numerators. An example is the term,

$$n_{1234,p} \sim p_{\mu_1} p_{\mu_2} p_{\mu_3} p_{\mu_4} \varepsilon_1^{\mu_1} \varepsilon_2^{\mu_2} \varepsilon_3^{\mu_3} \varepsilon_4^{\mu_4} + \cdots , \tag{2.2.7}$$

where $\varepsilon_i^{\mu_i}$ is the gluon polarization of leg i on the pure Yang–Mills side of the double copy.

The cancellations between the diagrams are nontrivial. To see the cancellation of the logarithmic divergences, we expand in large loop momentum or equivalently small external momenta k_i^μ. Because the integrals are only logarithmically divergent in $D=4$, this amounts to simply setting all k_i^μ to zero in the integrand (keeping the overall prefactor fixed). In this limit, the propagator of each graph become identical, and the resulting graph effectively becomes a scaleless vacuum integral. Such scaleless integrals vanish in dimensional regularization, but we can introduce a mass for each propagator to separate out the infrared divergences without affecting the ultraviolet divergence. Starting with the pure Yang–Mills numerators, keeping only the leading terms in all three box diagrams results in an integrand proportional to

$$\begin{aligned} -ist A^{\text{tree}}_{\mathcal{N}=4}(D_s-2) \frac{\varepsilon_1^{\mu_1}\varepsilon_2^{\mu_2}\varepsilon_3^{\mu_3}\varepsilon_4^{\mu_4}}{2(p^2-m^2)^4} \Big[& (p^2)^2 (\eta_{\mu_1\mu_4}\eta_{\mu_2\mu_3} + \eta_{\mu_1\mu_3}\eta_{\mu_2\mu_4} + \eta_{\mu_1\mu_2}\eta_{\mu_3\mu_4}) \\ & -4p^2 (\eta_{\mu_1\mu_2} p_{\mu_3} p_{\mu_4} + \eta_{\mu_1\mu_3} p_{\mu_2} p_{\mu_4} + \eta_{\mu_1\mu_4} p_{\mu_2} p_{\mu_3} + \eta_{\mu_2\mu_3} p_{\mu_1} p_{\mu_4} \\ & + \eta_{\mu_2\mu_4} p_{\mu_1} p_{\mu_3} + \eta_{\mu_3\mu_4} p_{\mu_1} p_{\mu_2}) + 24\, p_{\mu_1} p_{\mu_2} p_{\mu_3} p_{\mu_4} \Big] , \end{aligned} \tag{2.2.8}$$

where $A^{\text{tree}}_{\mathcal{N}=4} = A^{\text{tree}}_{\mathcal{N}=4}(1,2,3,4)$ and D_s is a state-counting parameter coming from contractions $\eta_\mu{}^\mu = D_s$. (In conventional dimensional regularization [43] $D_s = 4-2\epsilon$, but in other schemes, such as the four-dimensional helicity scheme [44], $D_s = 4$.) In the expression above we see explicitly that the amplitude is logarithmically divergent by power counting and

that no purely algebraic manipulations can expose the cancellation of the divergence. What makes this case particularly simple is that in the large loop-momentum limit all diagrams degenerate to a single vacuum integral, avoiding loop-momentum labeling ambiguities in different terms that plague higher loops.

This example provides a clear demonstration that even after summing over diagrams, enhanced cancellations are not visible prior to using properties of integrals. To expose the ultraviolet cancellation we use Lorentz invariance in the form of integration identities:

$$\int d^D p \, \frac{p_\mu p_\nu}{(p^2 - m^2)^4} = \int d^D p \, \frac{1}{D} \frac{\eta_{\mu\nu} p^2}{(p^2 - m^2)^4} \,, \tag{2.2.9}$$

$$\int d^D p \, \frac{p_\mu p_\nu p_\rho p_\sigma}{(p^2 - m^2)^4} = \int d^D p \, \frac{1}{D(D+2)} \frac{(\eta_{\mu\nu}\eta_{\rho\sigma} + \eta_{\mu\rho}\eta_{\nu\sigma} + \eta_{\mu\sigma}\eta_{\rho\nu})(p^2)^2}{(p^2 - m^2)^4} \,. \tag{2.2.10}$$

With these identities, we find that the integral of Eq. (2.2.8) is equal to the integral of

$$\begin{aligned} -ist A^{\text{tree}}_{\mathcal{N}=4}(D_s - 2) \frac{(p^2)^2}{2(p^2 - m^2)^4} \frac{(D-2)(D-4)}{D(D+2)} \\ \times \varepsilon_1^{\mu_1} \varepsilon_2^{\mu_2} \varepsilon_3^{\mu_3} \varepsilon_4^{\mu_4} (\eta_{\mu_1\mu_2}\eta_{\mu_3\mu_4} + \eta_{\mu_1\mu_3}\eta_{\mu_2\mu_4} + \eta_{\mu_1\mu_4}\eta_{\mu_2\mu_3}) \,, \end{aligned} \tag{2.2.11}$$

which vanishes in $D = 4$. While in this case, the cancellation is understood to be a consequence of supersymmetry [37], it does provide a robust example illustrating that enhanced cancellations become visible in the amplitudes only after making use of integral identities.

2.2.2 Two-loop example

Enhanced cancellations become more interesting beyond one loop where they correspond to a variety of ultraviolet cancellations for which standard-symmetry explanations are not known [17–19]. We therefore turn to half-maximal supergravity at two loops. In $D = 4$ the cancellations are well understood to be a consequence of supersymmetry [45], but in $D = 5$ no such explanation is known [10].

In $D = 4$ we can enormously simplify the integrand by using helicity states. A sim-

ple trick that helps us simplify the analysis in higher dimensions as well is to start with the higher-dimensional theory but to restrict the external states and momenta to live in a four-dimensional subspace. In this way we can use four-dimensional helicity methods to enormously simplify higher-dimensional integrands as well. This trick, of course, does not work for all states in the higher-dimensional theory, but is sufficient for our purpose of illustrating the difficulty of exposing enhanced cancellations at the integrand level.

Consider the four-point two-loop amplitude of $\mathcal{N} = 4$ supergravity. This amplitude has already been discussed in some detail in Ref. [29]. The double-copy construction of the two-loop integrand is rather straightforward. We start from the dimensionally-regularized $D = 4$ all-plus helicity $(+ + ++)$ pure Yang–Mills amplitude in the form given in Ref. [42]. (An earlier form of the integrand may be found in Ref. [46].) In this representation the kinematic numerators of the planar and nonplanar double-box diagrams shown in Fig. 2.2 are

$$\begin{aligned} n_{1234}^{\text{P YM}} = \mathcal{T}\Big(&(D_s-2)s\left(\lambda_p^2\lambda_q^2 + \lambda_p^2\lambda_{p+q}^2 + \lambda_q^2\lambda_{p+q}^2\right) + 16s\left((\lambda_p\cdot\lambda_q)^2 - \lambda_p^2\lambda_q^2\right) \\ &+ \frac{1}{2}(D_s-2)(p+q)^2\left((D_s-2)\lambda_p^2\lambda_q^2 + 8\left(\lambda_p^2+\lambda_q^2\right)(\lambda_p\cdot\lambda_q)\right)\Big)\,, \end{aligned} \tag{2.2.12}$$

$$n_{1234}^{\text{NP YM}} = \mathcal{T}\Big((D_s-2)s\left(\lambda_p^2\lambda_q^2 + \lambda_p^2\lambda_{p+q}^2 + \lambda_q^2\lambda_{p+q}^2\right) + 16s\left((\lambda_p\cdot\lambda_q)^2 - \lambda_p^2\lambda_q^2\right)\Big)\,, \tag{2.2.13}$$

where D_s is the state-counting parameter similar to that at one loop and the subscript '1234' refers to the diagram external leg labeling as in Fig. 2.2. The momenta p and q are the momenta carried by the propagators indicated in Fig. 2.2, while λ_p and λ_q are their (-2ϵ) components, where $\epsilon = (4-D)/2$. We use λ_{p+q} as a shorthand for $\lambda_p + \lambda_q$. The crossing symmetric prefactor

$$\mathcal{T} = \frac{[12][34]}{\langle 12\rangle\langle 34\rangle}\,, \tag{2.2.14}$$

is defined in terms of spinor inner products, following the notation of Ref. [47]. The remaining planar and nonplanar double-box numerators are given by relabeling these. There are contributions to the Yang–Mills integrand from other types of diagrams as well, but we will not need them for the double-copy procedure.

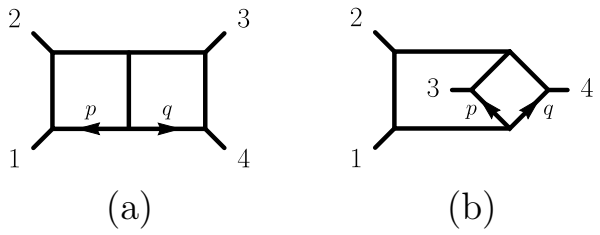

Figure 2.2: The planar and nonplanar double-box diagrams that contribute to the four-point amplitudes of $\mathcal{N} = 4$ supergravity.

To obtain half-maximal supergravity we then take the pure-Yang–Mills amplitude and replace the color factors with $\mathcal{N} = 4$ super-Yang–Mills numerators that satisfy BCJ duality using Eq. (2.2.2). For the two-loop four-point amplitude of $\mathcal{N} = 4$ SYM a representation that satisfies the duality happens to match the original construction [48]. The only nonvanishing diagrams are the planar and nonplanar double boxes shown in Fig. 2.2. The substitution (2.2.3) is simply

$$\begin{aligned} c^{\rm P}_{1234} &\to n^{{\rm P}\,\mathcal{N}=4}_{1234} = s^2 t A^{\rm tree}_{\mathcal{N}=4}(1,2,3,4)\,, \\ c^{\rm NP}_{1234} &\to n^{{\rm NP}\,\mathcal{N}=4}_{1234} = s^2 t A^{\rm tree}_{\mathcal{N}=4}(1,2,3,4)\,, \end{aligned} \tag{2.2.15}$$

where numerators other than the planar and nonplanar ones vanish. As for the one-loop case, we package the $\mathcal{N} = 4$ super-Yang–Mills tree amplitude for all states into a single superamplitude. The half-maximal supergravity amplitude is then obtained by summing over the planar and nonplanar double boxes in Fig. 2.2, with kinematics numerators given by the product of pure Yang–Mills and $\mathcal{N} = 4$ super-Yang–Mills numerators,

$$\begin{aligned} N^{{\rm P\,half\text{-}max.\,sugra}}_{1234} &= s^2 t A^{\rm tree}_{\mathcal{N}=4}(1,2,3,4) \times n^{\rm P\,YM}_{1234}\,, \\ N^{{\rm NP\,half\text{-}max.\,sugra}}_{1234} &= s^2 t A^{\rm tree}_{\mathcal{N}=4}(1,2,3,4) \times n^{\rm NP\,YM}_{1234}\,. \end{aligned} \tag{2.2.16}$$

The remaining supergravity planar and nonplanar double-box numerators are given by simple relabelings. Diagrams other than the planar and nonplanar double boxes vanish.

This construction is also valid for the $D = 5$ theory with the external states restricted to a $D = 4$ subspace. We simply take $\epsilon \to -1/2 + \epsilon$ and accordingly the λ_p and λ_q become one dimensional up to $\mathcal{O}(\epsilon)$ corrections. Similarly the state-counting parameter should be shifted, $D_s \to D_s + 1$. With these modifications, the simple integrand in Eq. (2.2.16) is valid for the $D = 5$ theory as well.

As terminology for the rest of the chapter, when we label an amplitude by its external helicity, we are not referring to the helicities of the supergravity theory, but to the helicities of the pure Yang–Mills theory comprising one side of the double-copy supergravity theory.

Cuts and labels for nonplanar amplitudes

Enhanced cancellations generally occur between diagrams of different topologies. A difficulty for exposing the cancellations at the integrand level beyond one loop is that there is no unique and well-defined notion of an integrand involving nonplanar diagrams. Nor is it clear in general how one should choose momentum labels in each diagram that would allow cancellations between diagrams of various topologies to occur. For planar diagrams there is a canonical choice of global variables for all diagrams based on dual variables [113], but no analogous notion is known in the nonplanar case. As a simple example consider the planar and nonplanar double-box diagrams in Fig. 2.2. Fundamentally, the propagator structure is different, making it unclear how one might be able show the cancellation without integration.

A way to sidestep the labeling issue is to focus on unitarity cuts. Generalized unitarity cuts that place at least one line on-shell in every loop impose global momentum labels on the cut. We can then ask whether we can find nontrivial cancellations in the cut linked to enhanced cancellations. If such cancellations happen at the level of the integrand, one should expect an improvement in the overall power counting after summing over all contributions to the cuts compared to individual terms. Some care is required because cuts can also obscure cancellations by restricting the diagrams that appear. The more legs that are cut, the fewer diagrams are included, since only those diagrams that contain propagators corresponding to

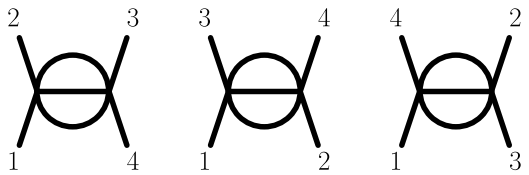

Figure 2.3: The three sunset integrals. These are ultraviolet divergent in $D = 4$ and $D = 5$.

the cut ones will be included. Because of this, it is best to focus on cuts where only a few legs are placed on shell.

Absence of cancellations in a three-particle cut

The three-particle cut in Fig. 2.4 is useful for studying enhanced cancellations. In the following section, using integration-by-parts technology we describe an arrangement of the integrand where potential divergences are pushed into sunset diagrams, illustrated in Fig. 2.3. This suggests that the three-particle cut, where the cut lines correspond to the three propagators of a sunset diagram, is a natural one for studying enhanced cancellations. In addition, this cut fixes all loop momentum labels in this amplitude in terms of the momenta of the cut lines. An obvious guess is that if we apply the three-particle cut corresponding to the internal lines of the sunset diagram, we should find improved power counting in the full sum over terms compared to individual contributions.

The $(++++)$ amplitude has a number of special features that simplify the analysis of the cut, making it easier to find ultraviolet cancellations if they exist. On the three-particle cut, the terms in the numerator proportional to $(p+q)^2$ in Eq. (2.2.12) are set to zero because they corresponds to one of the on-shell inverse propagators ℓ_1^2, ℓ_2^2 or ℓ_3^2, as can be seen in Fig. 2.4, making the form of the planar and nonplanar numerators identical in the three-particle cut. A useful feature of the remaining numerator terms that we exploit is that they are invariant under relabelings: the expression is the same under any mapping of the p and q propagator labels to any two of the three ℓ_1, ℓ_2 and ℓ_3. In addition, up to prefactors depending on external momenta, the dependence of the numerators is only on the components outside the

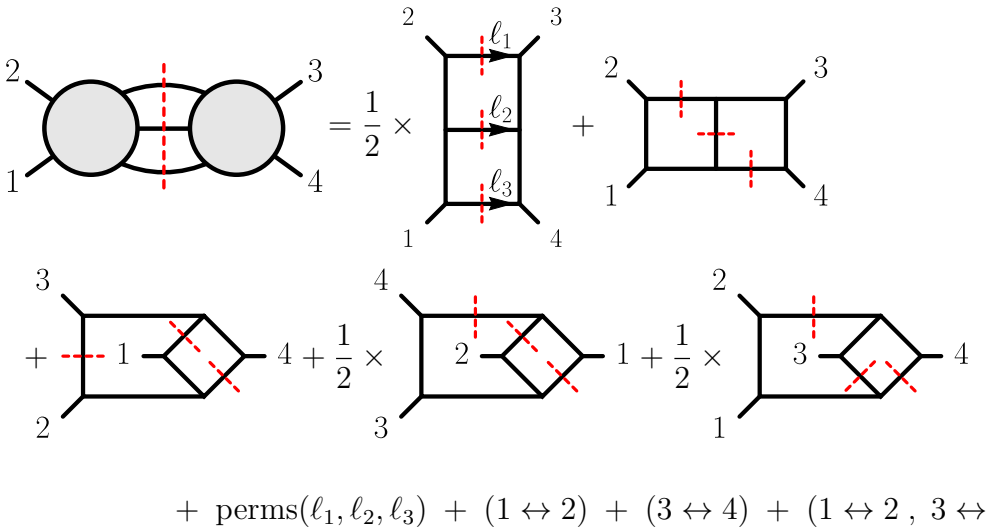

Figure 2.4: The contributing diagrams of the three-particle cut of the half-maximal supergravity two-loop four-point amplitude. The shaded (red) dashed lines indicated the legs which are cut.

four-dimensional subspace where the external momenta and helicities live. These features enormously simplify the analysis of the cut because most of the numerator factors out and is independent of permutations of external or internal legs.

Using these observations, after inserting the numerators into the planar and nonplanar double-box diagrams and taking the three-particle cut shown in Fig. 2.4, we obtain the expression:

$$
\begin{aligned}
\mathcal{I}^{\text{cut}} &= \mathcal{P}(\ell_1, \ell_2, \ell_3) \\
&\times \Bigg[\Bigg(\frac{1}{2} \frac{t^2}{(\ell_1 + k_1)^2 (\ell_3 + k_2)^2 (\ell_3 - k_3)^2 (\ell_1 - k_4)^2} + \frac{t^2}{(\ell_2 + k_1)^2 (\ell_3 + k_2)^2 (\ell_3 - k_3)^2 (\ell_1 - k_4)^2} \\
&\quad + \frac{s^2}{(\ell_1 + \ell_2)^2 (\ell_2 + \ell_3)^2 (\ell_3 + k_2)^2 (\ell_1 - k_4)^2} + \frac{1}{2} \frac{s^2}{(\ell_2 + \ell_3)^2 (\ell_3 + k_1)^2 (\ell_2 + k_2)^2 (\ell_1 - k_4)^2} \\
&\quad + \frac{1}{2} \frac{s^2}{(\ell_1 + \ell_2)^2 (\ell_3 + k_2)^2 (\ell_2 - k_3)^2 (\ell_1 - k_4)^2} \Bigg) + \text{perms}(\ell_1, \ell_2, \ell_3) \\
&\qquad + (1 \leftrightarrow 2) + (3 \leftrightarrow 4) + (1 \leftrightarrow 2,\ 3 \leftrightarrow 4) \Bigg] , \qquad (2.2.17)
\end{aligned}
$$

where the on-shell conditions $\ell_1^2 = \ell_2^2 = \ell_3^2 = 0$ are imposed. The prefactor $\mathcal{P}(\ell_1, \ell_2, \ell_3)$ is

$$\begin{aligned}\mathcal{P}(\ell_1, \ell_2, \ell_3) = &- i(D_s - 2) stA^{\text{tree}}_{\mathcal{N}=4}(1,2,3,4)\,\mathcal{T} \\ &\times \Big(\big(\lambda_{\ell_1}^2 \lambda_{\ell_2}^2 + \lambda_{\ell_1}^2 \lambda_{\ell_3}^2 + \lambda_{\ell_2}^2 \lambda_{\ell_3}^2\big) + 16s \left((\lambda_{\ell_1} \cdot \lambda_{\ell_2})^2 - \lambda_{\ell_1}^2 \lambda_{\ell_2}^2 \right) \Big) \,, \end{aligned} \tag{2.2.18}$$

which is invariant under the permutations of external and internal cut legs indicated in Eq. (2.2.17). We have analyzed Eq. (2.2.17) both analytically and numerically and we find that for $\ell_i \to \infty$ there is no improvement in the large loop-momentum behavior after summing over all terms, compared to the behavior of a single term. In fact, this is no surprise because other than the overall prefactor (2.2.18), this sum over terms is *precisely* the same one that appears in the three-particle cut of the two-loop four-point amplitude of $\mathcal{N} = 8$ supergravity given in Eq. (5.15) of Ref. [49]. In $\mathcal{N} = 8$ supergravity we know there are no further cancellations arising from the sum over diagrams. This can be seen as follows: the only nonvanishing diagrams in $\mathcal{N} = 8$ supergravity are the planar and nonplanar double boxes of Fig. 2.2, but with no loop momenta in the numerators [49]. Simple power counting shows that each diagram of $\mathcal{N} = 8$ supergravity is ultraviolet divergent in dimensions $D \geq 7$. This divergence does not cancel in the sum over diagrams, leading to a divergence of the four-point amplitude of $\mathcal{N} = 8$ supergravity [49]:

$$\mathcal{M}_4^{\text{two-loop},D=7-2\epsilon}\Big|_{\text{UV div.}} = \frac{1}{2\epsilon(4\pi)^7} \frac{\pi}{3} (s^2 + t^2 + u^2) \times \left(\frac{\kappa}{2}\right)^6 stu M^{\text{tree}}_{\mathcal{N}=8}(1,2,3,4)\,, \tag{2.2.19}$$

where we have stripped the coupling constant and $M^{\text{tree}}_{\mathcal{N}=8}$ is the supergravity tree amplitude. The fact that there are no further cancellations in $\mathcal{N} = 8$ supergravity implies that no integrand-level cancellation is possible in our $\mathcal{N} = 4$ supergravity three-particle cut (2.2.17). One might imagine trying to include relabelings $\ell_i \to -\ell_i$ in the spirit of Ref. [50] or other relabelings in order to try to expose cancellations. However, because of the link to the $\mathcal{N} = 8$ supergravity cut, it is clear there are no further cancellations to be found.

In summary, we see no evidence of cancellations at the integrand level. The usual su-

pergraph Feynman rules or amplitudes-based proofs of ultraviolet finiteness in gauge theory (see for example, Ref. [21]) rely on the ability to make the integrand manifestly ultraviolet finite by power counting. The difficulty in finding a standard-symmetry based explanation for enhanced cancellations [17–19] in gravity theories is presumably tied to our difficulty in identifying the cancellations at the integrand level. This greatly complicates any all-order understanding of the divergence properties of supergravity theories. If we are to unravel enhanced cancellations, we need to turn to the systematics of cancellations from integral identities.

2.3 Rearranging the integrand to show finiteness

As discussed in the previous section, it does not appear possible to expose enhanced cancellations purely at the integrand level. In this section we show how one can rearrange integrands into a form where all terms are manifestly finite by power counting, except those that integrate to zero. We do so using modern integration-by-parts (IBP) technology [30–34, 73, 98]. In our discussion we will be using the language of integrands and integrals interchangeably. This is because the modern approaches to integration by parts can be used to track terms in the integrand that integrate to zero, in a manner analogous to the one-loop technology of Refs. [51, 65].

We first outline how IBP relations can be used to reorganize integrands with enhanced cancellations so that all terms that are naively ultraviolet divergent by power counting integrate to zero. We start from a given integrand that has the schematic structure

$$\mathcal{I}^{\text{total}} = \sum_i \mathcal{I}_i^{\text{fin.}} + \sum_j \mathcal{I}_j^{\text{div.}} \,. \tag{2.3.1}$$

The sum runs over the various pieces of the integrand, denoted by $\mathcal{I}_i^{\text{fin.}}$, which are finite by power counting, and $\mathcal{I}_i^{\text{div.}}$ which are divergent by power counting. After integration, however,

the total may be finite. The idea is to reorganize this integrand into the form

$$\mathcal{I}^{\text{total}} = \sum_i \tilde{\mathcal{I}}_i^{\text{fin.}} + \sum_j \tilde{\mathcal{I}}_j^{\text{van.}}\,, \tag{2.3.2}$$

where $\tilde{\mathcal{I}}_i^{\text{fin.}}$ is another set of integrands that are finite after integration and $\tilde{\mathcal{I}}_j^{\text{van.}}$ can be divergent by power counting but integrate to zero,

$$\int \tilde{\mathcal{I}}_j^{\text{van.}} = 0\,, \tag{2.3.3}$$

thus making the finiteness manifest. The reorganization is accomplished by writing the sum over power-counting divergent integrals as

$$\sum_j \mathcal{I}_j^{\text{div.}} = \sum_j \mathcal{I}'^{\text{fin.}}_j + \sum_j (\mathcal{I}_j^{\text{div.}} - \mathcal{I}'^{\text{fin.}}_j)\,, \tag{2.3.4}$$

where the terms in parentheses integrates to zero and the finite integrals $\mathcal{I}'^{\text{fin.}}_j$ are included with the finite ones in Eq. (2.3.2).

IBP technology offers a systematic means for accomplishing this. We briefly review this. The IBP method [30] takes advantage of the fact that in dimensional regularization a total derivative vanishes:

$$\int \prod_i d^D\ell_i \, \frac{\partial}{\partial \ell_j^\mu} \left(\frac{v_j^\mu}{\prod_k D_k} \right) = 0\,, \tag{2.3.5}$$

where $1/D_k$ are propagators and v_j^μ are arbitrary functions of loop momenta as well as external kinematics or other vectors in the problem. Evaluating the derivatives gives a sum of terms, and the vanishing of the integral therefore implies a relation amongst the integrals corresponding to each term. By exhausting all such independent relations one can choose a basis of integrals in terms of which to express a given amplitude. The standard basis choice at one loop is a combination of boxes, triangles, and bubbles [52], but at higher loops there is no canonical choice. In general, different bases might be used to manifest different aspects

of the amplitude, such as its symmetries and/or behavior on certain unitarity cuts.

Generically, when applying integration-by-parts identities, there is no natural separation of the type in Eq. (2.3.2). In general, the coefficients of individual terms can develop $1/\epsilon$ singularities, and divergences cancel in complicated ways, making the finiteness unclear. To avoid this, some care is required to pick integral bases that (a) do not introduce divergences in integral coefficients and (b) contain a minimal number of divergent integrals. Usually, one picks a linearly independent set of integrals, because this minimizes the number of objects that need to be computed. But, even for an ultraviolet finite amplitude, a general choice of basis will likely have explicit ultraviolet divergences either in basis integrals or in their coefficients. The finiteness is thus obscured because the divergence cancels only in the full sum over contributions. A way to avoid this problem and express the amplitude in the form of Eq. (2.3.2) is to use an overcomplete set of integrals. The overcompleteness gives sufficient freedom that we can exploit to make the finiteness manifest.

We illustrate this procedure with a simple example. Suppose our expression is given as the sum of integrals:

$$A = \frac{1}{70}$$ 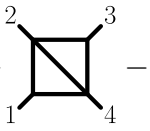

$$- \frac{1}{2s^2}$$ 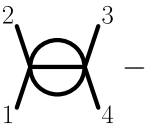

$$- \frac{1}{2t^2}$$ 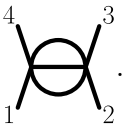

$$. \tag{2.3.6}$$

Each of these integrals are ultraviolet divergent in five dimensions with the following leading divergences (omitting an overall $\pi/32$):

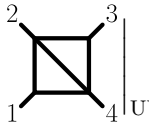

$$= \frac{1}{3\epsilon}\,,$$ 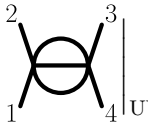

$$= \frac{s^2}{210\epsilon}\,,$$ 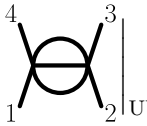

$$= \frac{t^2}{210\epsilon}\,. \tag{2.3.7}$$

Evaluating the divergence shows that Eq. (2.3.6) is finite, but this is not manifest in the

above representation. Now consider the following IBP identities

$$d\omega_1 = \quad - \frac{70}{s^2} \quad - \frac{1}{3s^2} \quad ,$$

$$d\omega_2 = \quad + \frac{70}{su} \quad + \frac{70}{tu} \quad - \frac{st}{3u} \quad , \tag{2.3.8}$$

where $d\omega_1$ and $d\omega_2$ are appropriate total derivatives; their precise form is not important for our purposes. The dot placed on a propagator indicates that the propagator is doubled, i.e., squared. This choice is convenient because the two integrals with doubled propagators are both ultraviolet finite in $D = 5$.

For this simple example, one can solve this system of equations for two of the three ultraviolet-divergent integrals. Plugging in the solution leaves only a single ultraviolet-divergent integral whose coefficient must vanish, if the amplitude is finite. However, the ability to express A in Eq. (2.3.6) in terms of a basis of manifestly finite integrals is a consequence of the simplicity of this example, and for more complicated amplitudes this straightforward approach will not suffice. We will therefore take a more general approach for this example. In particular, we can use Eq. (2.3.8) to rewrite the crossed box integral as

$$= \alpha\Big(- \frac{70}{su} \quad - \frac{70}{tu} \quad + \frac{st}{3u} \quad \Big)$$

$$+ (1-\alpha)\Big(\frac{70}{s^2} \quad + \frac{1}{3s^2} \quad \Big) + d\Big(\left(1-\alpha\right)\omega_1 + \alpha\,\omega_2\Big)\,, \tag{2.3.9}$$

where α is a free parameter. In this way we traded one ultraviolet-divergent integral for two

ultraviolet-divergent sunset integrals which were already in the basis, plus two other finite integrals and a collection of integrals that vanish (i.e., are total derivatives). Plugging this back into the original expression for A gives

$$A = \Big(\frac{1-\alpha}{s^2} - \frac{\alpha}{su} - \frac{1}{2s^2}\Big) \quad - \Big(\frac{\alpha}{tu} + \frac{1}{2t^2}\Big) \quad + \text{finite} + \frac{1}{70} d\Big((1-\alpha)\,\omega_1 + \alpha\,\omega_2\Big)\,, \tag{2.3.10}$$

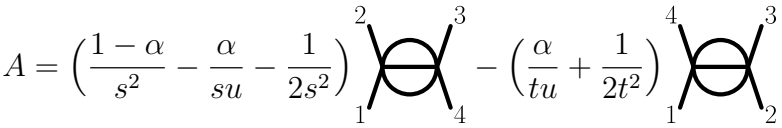

where "finite" corresponds to integrals that are manifestly ultraviolet finite with finite coefficients and the term $\frac{1}{70}d(...)$ vanishes upon integration. For general α this form of A is still not manifestly finite, but since α is arbitrary we can take it to be $\alpha = -u/2t$, in which case the coefficients to the two sunsets both vanish and A is then manifestly a sum of finite integrals and integrals that vanish. In general, one free parameter will not be enough to tune away two coefficients of ultraviolet-divergent integrals. For more complicated examples one needs to generate more IBP relations and introduce more tunable parameters, and in general each parameter can be used to set one coefficient to an ultraviolet-divergent integral to zero.

As a nontrivial example, we carried out this procedure for the $(-++{+}{+})$ two-loop amplitude of half-maximal supergravity in $D = 5$. (Recall that the helicity labels refer to the helicities of the pure Yang–Mills side of the double copy, with the external states restricted to live in a four-dimensional subspace.) The structure of this amplitude is much more complicated than the $(+++{+}{+})$ case and more representative of generic cases. In the first step we reduce the full integrand to a basis of master integrals using Larsen and Zhang's method [34]. After this procedure the only contributing ultraviolet-divergent integrals are the three different labels of the sunsets and a few others. We then used these types of overcomplete relations to express all of the (non-sunset) ultraviolet-divergent integrals in terms of ultraviolet-divergent sunset integrals, finite integrals and total derivatives that integrate

to zero. The tunable parameters are solved so that coefficients of the three sunsets vanish separately, while maintaining finiteness of the coefficients of all finite integrals. Therefore, by allowing for an over-complete basis and tuning the parameters that keep track of this over-completeness, we are able to write the amplitude in the desired form, Eq. (2.3.2).

We note that unless special care is taken, an IBP identity in general involves doubled propagators, as in Eq. (2.3.9). This has the unwanted side effect of introducing spurious infrared singularities even in $D = 5$. With more modern approaches [31–34, 73, 98] we can avoid the appearance of such integrals. This is achieved by imposing

$$\sum_j v_j^\mu \frac{\partial}{\partial \ell_j^\mu} D_k = f_k \, D_k \,, \tag{2.3.11}$$

on the v_j^μ and where f_k has polynomial dependence on Lorentz-invariant dot products of momenta. We have also applied the more modern approach and find similar results.

The procedure sketched above shows that the $D = 5$ two-loop four-point integrand of half-maximal supergravity can be rewritten in a form that is manifestly finite, up to terms that integrate to zero. However, this procedure relies on the specific details of the integrand and corresponding IBP relations. It is also computationally difficult to extend to higher loops. Clearly, we need an approach where the necessary identities can be derived from generic properties of loop integrals. We will describe such an approach in the next section.

2.4 Vacuum expansion and systematics of ultraviolet cancellations

In this section we describe a systematic approach to understanding enhanced cancellations, in a manner that appears to have an all-loop generalization. We continue to focus on the two-loop amplitudes of half-maximal supergravity. The ultraviolet behavior is determined at the integrand level by large values of loop momenta, or equivalently small external momenta. It is therefore natural to series expand the integrand in this limit. Although this expansion has the unwanted effect of losing contact with the unitarity cuts and introducing spurious

singularities, such as doubled propagators, it does have the important advantage of focusing on the term directly relevant for the ultraviolet behavior. In general, we are interested in the logarithmic divergences, so we series expand to the appropriate order where the integrals become logarithmically divergent in ultraviolet [19, 53]. (We note that while dimensional regularization does not have direct access to power divergences, such divergences become logarithmic simply by lowering the dimension.) This expansion generates a set of vacuum integrals. For example, at two loops these integrals have the form

$$\int d^D p \, d^D q \, \frac{\mathcal{N}(p, q, k_i)}{(p^2)^A (q^2)^B ((p+q)^2)^C} \,, \tag{2.4.1}$$

where A, B and C denote the powers of the propagators. In addition to being ultraviolet divergent, these vacuum integrals also are infrared divergent. This complicates the extraction of the ultraviolet divergences. For example, in dimensional regularization these integrals are scaleless, and the infrared singularities exactly cancel the ultraviolet ones. This is usually dealt with by introducing a mass regulator or by injecting external momentum into the diagram. (See, for example, Refs. [19,35,53].) We will avoid this complication by systematically finding relations between the divergences of the integrals using integration by parts.

As noted in the previous section, the simplest example to analyze is the case where the external gluons in the pure Yang–Mills side of the double-copy are restricted to live in four dimensions, and correspond to all-plus helicity $(+\,+\,+\,+)$. For this helicity configuration on the pure Yang–Mills side of the double copy, we use the spinor-helicity integrands in Eqs. (2.2.12) and (2.2.13). For the remaining helicity configurations we used the pure Yang–Mills integrand from Ref. [54]. The only contributions needed are those whose color structure matches those of the planar and nonplanar double-box diagrams. For other helicities we used the gauge-invariant projection method to be described in Ref. [55].

In four-dimensions these integrals do not have overall ultraviolet divergences because they are suppressed by the numerators; they are proportional to the (-2ϵ)-dimensional

components of loop momenta. (They do however contain subdivergences which cancel.) To have a nontrivial example, we turn to the same integrand but with the internal states in $D = 5$. In this case the numerator is not suppressed because λ_p and λ_q are one-dimensional. (In the context of dimensional regularization in $D = 5 - 2\epsilon$, they are actually $(1 - 2\epsilon)$ dimensional.) Using $D = 5$ properties the integrand simplifies: In $D = 5$ the λ_p and λ_q become one-dimensional so that

$$(\lambda_p \cdot \lambda_q)^2 - \lambda_p^2 \lambda_q^2 \to \mathcal{O}(\epsilon)\,, \tag{2.4.2}$$

in Eqs. (2.2.12) and (2.2.13).

In the large loop-momentum limit, the logarithmically divergent terms in $D = 5$ are given by

$$I^{\mathrm{P,\,NP}} = (D_s - 2)s \int d^D p\, d^D q\, \frac{\left(\lambda_p^2 \lambda_q^2 + \lambda_p^2 \lambda_{p+q}^2 + \lambda_q^2 \lambda_{p+q}^2\right)}{(p^2)^A (q^2)^B [(p+q)^2]^C} + \text{UV finite}\,, \tag{2.4.3}$$

where

$$(A, B, C) = \begin{cases} (3, 3, 1)\,, & \text{P: planar double box}\,, \\ (3, 2, 2)\,, & \text{NP: nonplanar double box}\,. \end{cases} \tag{2.4.4}$$

In the planar case there are power divergences coming from terms proportional to $(p+q)^2$, which removes the middle propagator generating a product of one-loop integrals. Such terms do not give rise to logarithmic divergences. (This is consistent with finiteness of such integrals in dimensional regularization, which is sensitive only to logarithmic divergences.) We may then ignore such terms for the purposes of trying to understand overall two-loop logarithmic divergence.

One way to evaluate Eq. (2.4.3) is to consider vacuum integrals with numerators that are polynomial in $v_j \cdot p$ and $v_j \cdot q$, where the v_j's are a set of orthonormal basis vectors for the

five-dimensional momentum space. We have

$$v_5 \cdot p = \lambda_p \,, \qquad v_5 \cdot q = \lambda_q \,, \qquad \sum_j (v_j \cdot p)(v_j \cdot p) = p^2, \qquad \sum_j (v_j \cdot q)(v_j \cdot q) = q^2 \,, \tag{2.4.5}$$

with appropriate factors of i inserted for the metric signature. Lorentz invariance then implies

$$\text{UV finite } = \int d^D p \, d^D q \, v_i^{[\mu} v_j^{\nu]} \left(p_\mu \frac{\partial}{\partial p^\nu} + q_\mu \frac{\partial}{\partial q^\nu} \right) \frac{\mathcal{N}(v_k \cdot p, v_k \cdot q)}{(p^2)^A (q^2)^B [(p+q)^2]^C} \,, \tag{2.4.6}$$

where the Lorentz indices μ and ν are antisymmetrized. By replacing $\mathcal{N}$ in the above equation by all possible monomials in $v_i \cdot p$ and $v_i \cdot q$ up to degree four, we generate linear relations between vacuum integrals with different numerators, allowing us to reduce Eq. (2.4.3) to scalar vacuum integrals. The result of this procedure is

$$\begin{aligned} I^{\mathrm{P,\,NP}} &= \frac{3}{70}(D_s - 2)s \int d^D p \, d^D q \, \frac{[(p^2)^2 + (q^2)^2 + ((p+q)^2)^2]}{(p^2)^A (q^2)^B [(p+q)^2]^C} \\ &= \frac{3}{70} \, (D_s - 2)s (I_{A-2,B,C} + I_{A,B-2,C} + I_{A,B,C-2}) \,, \end{aligned} \tag{2.4.7}$$

where the scalar vacuum integrals are defined as

$$I_{A,B,C} = \int d^D p \, d^D q \frac{1}{(p^2)^A (q^2)^B [(p+q)^2]^C} \,, \tag{2.4.8}$$

which is invariant under the six permutations of $\{A, B, C\}$. One can also obtain this equation by reducing the implicit tensor integrals in Eq. (2.4.3), using Lorentz invariance in the more traditional way following for example Eq. (4.18) of Ref. [35]. Alternatively, Mastrolia et. al. recently proposed an efficient algorithm to integrate away loop momentum components orthogonal to all external momenta [56].

For the particular cases of Eq. (2.4.7) we obtain

$$\begin{aligned} I^{\rm P} &= \frac{3s}{70}(D_s-2)\left(I_{1,3,1}+I_{3,1,1}+I_{3,3,-1}\right)+\text{UV finite} \\ &= \frac{3s}{70}(D_s-2)(2I_{3,1,1}+I_{3,3,-1})+\text{UV finite}, \qquad (2.4.9) \\ I^{\rm NP} &= \frac{3s}{70}(D_s-2)(I_{1,2,2}+I_{3,0,2}+I_{3,2,0})+\text{UV finite}\,, \qquad (2.4.10) \end{aligned}$$

where we used the fact that the integrals are invariant under the exchange of p and q in the second equality in Eq. (2.4.9). Summing the planar and nonplanar contributions, we conclude that the logarithmic UV divergence is given by

$$(I^{\rm P}+I^{\rm NP})\big|_{\log\ \rm UV}=\frac{3s}{70}(D_s-2)\left(2I_{3,1,1}+I_{1,2,2}\right)\big|_{\log\ \rm UV}\,. \qquad (2.4.11)$$

As explained above, the terms with "one-loop squared" propagator structures (e.g., $I_{3,2,0}$ or $I_{3,3,-1}$) do not contain logarithmic UV divergences. Also, it is not surprising that the final result is a linear combination of $I_{3,1,1}$ and $I_{1,2,2}$, as these are the only two possible logarithmically divergent vacuum integrals in $D=5$.

By explicit evaluation using a uniform internal mass m as an infrared regulator and dimensional regularization in $5-2\epsilon$ dimensions as an ultraviolet regulator, we find

$$\begin{aligned} I_{3,1,1}\Big|_{\rm UV\ div.} &= -\frac{\pi}{192\epsilon}\,, \\ I_{1,2,2}\Big|_{\rm UV\ div.} &= \frac{\pi}{96\epsilon}\,, \qquad (2.4.12) \end{aligned}$$

so the combination of integrals in Eq. (2.4.11) is ultraviolet finite in $D=5$. However, in order to understand the general structure of the cancellations, it is illuminating to instead show this using IBP identities.

2.4.1 Extracting divergences using IBP identities

We recall that the fundamental assumption of the IBP method is that the integral of a total derivative vanishes in dimensional regularization, as shown in Eq. (2.3.5). Obviously, integrals of total derivatives only vanish when boundary contributions vanish. In dimensional regularization however, we can consider the integral in a dimension where the boundary contribution is vanishing and then analytically continue the result (zero) to the original dimension. But in an another regularization scheme one has to consider the behavior of boundary terms. In particular, if the boundary term contains ultraviolet or infrared divergences itself, the corresponding IBP identity cannot be used to relate the divergences of the integrals.

On the other hand, dimensional regularization is known to regulate the ultraviolet and infrared simultaneously. In general this is very convenient, but this fact might obstruct the use of certain IBPs in this scheme for extracting ultraviolet divergences. The reason for this is that IBP identities in dimensional regularization can mix up ultraviolet and infrared poles. To illustrate this consider the following identity that relates bubble and triangle integrals in $D = 4$:

$$d\omega = s\,\epsilon \times$$ 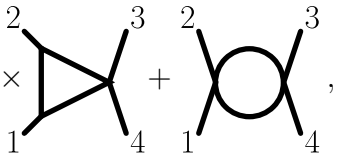

$$, \tag{2.4.13}$$

where ω is not relevant for the discussion. The internal propagators are all massless. The triangle integral has only an infrared divergence with a $1/\epsilon^2$ pole and the bubble has only an ultraviolet divergence with a $1/\epsilon$ pole. The ϵ dependence in the coefficient of the triangle allows the infrared and ultraviolet divergences to mix. In order to directly extract ultraviolet divergences without introducing an explicit infrared cutoff (such as a mass) we must make sure that the IBPs being used do not mix infrared and ultraviolet poles. These subtleties

are pertinent to our discussion since our aim is to extract ultraviolet divergences by focusing on scaleless vacuum integrals, which vanish in dimensional regularization.

However, IBP identities that avoid both of the above complications can be directly used to give relations between the ultraviolet divergences of different dimensionally-regularized vacuum integrals without introducing an additional explicit infrared cutoff. In this way we can demonstrate ultraviolet cancellations without explicitly evaluating any integrals. The situation in the presence of subdivergences is more subtle and outside the scope of our present discussion. We note that our principal aim is to examine the loop order where ultraviolet divergences might first occur, so subdivergences are not of primary concern.

Consider the following identities between two-loop vacuum integrals

$$\begin{aligned}
\text{UV finite} &= \int d^D p\, d^D q\, \left(p^\mu \frac{\partial}{\partial p^\mu} - q^\mu \frac{\partial}{\partial q^\mu} \right) \frac{1}{(p^2)^A (q^2)^B ((p+q)^2)^C} \\
&= (-2A + 2B)\, I_{A,B,C} - 2C\, I_{A-1,B,C+1} + 2C\, I_{A,B-1,C+1}\,, \\
\text{UV finite} &= \int d^D p\, d^D q\, \left(p^\mu \frac{\partial}{\partial q^\mu} \right) \frac{1}{(p^2)^A (q^2)^B ((p+q)^2)^C} \\
&= (-B + C)\, I_{A,B,C} - B\, I_{A-1,B+1,C} + B\, I_{A,B+1,C-1} \\
&\quad + C\, I_{A-1,B,C+1} - C\, I_{A,B-1,C+1}\,, \\
\text{UV finite} &= \int d^D p\, d^D q\, \left(q^\mu \frac{\partial}{\partial p^\mu} \right) \frac{1}{(p^2)^A (q^2)^B ((p+q)^2)^C} \\
&= (-A + C)\, I_{A,B,C} - A\, I_{A+1,B-1,C} + A\, I_{A+1,B,C-1} \\
&\quad + C\, I_{A,B-1,C+1} - C\, I_{A-1,B,C+1}\,.
\end{aligned} \tag{2.4.14}$$

In any of the three above identities, we can easily write the integrand as a total derivative because the contributions arising from commuting the loop momenta past the derivatives vanish. As desired there is no explicit dependence on the dimension D. With $A+B+C=5$, the above IBP identities relate logarithmically divergent integrals in $D=5$.

With dimensional regularization (and a mass as infrared cutoff) there are no boundary terms, but here we allow more general regularization schemes, in which case there may be

a ultraviolet finite boundary term on the left hand side of Eqs. (2.4.14). As elaborated in the appendix, even in such schemes, boundary terms do not contain divergences and do not modify the relations. We therefore use Eq. (2.4.14) as a direct relationship between the ultraviolet divergences of the vacuum integrals.

With $A = 1, B = C = 2$, the first equation in Eqs. (2.4.14) provides the following relation between the leading overall divergences of the integrals

$$(I_{1,2,2} + 2I_{1,1,3} - 2I_{0,2,3})\,\big|_{\log\ \mathrm{UV}} = (I_{1,2,2} + 2I_{1,1,3})\,\big|_{\log\ \mathrm{UV}} = 0\,, \tag{2.4.15}$$

where we used the fact that $I_{0,2,3}$ is a "one-loop squared" integral with power divergences and no logarithmic divergence. This is consistent with the explicit results in Eq. (2.4.12), while allowing us to expose cancellations in Eq. (2.4.11) without computing divergences of individual integrals or using identities that depend on details of the integrand.

In addition, by starting with the Yang–Mills integrand from Ref. [54] to construct the half-maximal supergravity integrand via Eq. (2.2.16), we have checked that for *any* external state, the log divergences in $D = 5$ are always proportional to the same combination as above,

$$(I_{1,2,2} + 2I_{3,1,1})\,, \tag{2.4.16}$$

whose leading log divergence vanishes.

While dimensional regularization is not sensitive to the potential quadratic divergences in $D = 5$, we can study these divergences by lowering the dimension to $D = 4$. In $D = 4$ one finds that for any helicity configuration h the expanded amplitude is

$$\mathcal{A}_h = C_h\,(2I_{3,3,-2} - 11I_{3,2,-1} + 7I_{3,1,0} + 5I_{2,2,0}) + \text{UV finite}\,, \tag{2.4.17}$$

for some coefficient C_h depending on the external states and on choices made for reference momenta when choosing external polarizations. We constructed the required integrand by

starting from two-loop four-point Feynman diagrams for pure-Yang-Mills and then applied to double-copy procedure to generate the diagrams of half-maximal supergravity. These are then expanded large loop momentum and simplified using Lorentz symmetry to obtained Eq. (2.4.17). We apply the identities (2.4.14) to the $D = 4$ case, under the logarithmic power-counting requirement $A + B + C = 4$, with A, B, C chosen to be all possible combinations of integers (some of which may be negative) with some cutoff on their absolute values. Dozens of IBP identities are generated, and the resulting linear system relates all integrals to $I_{1,2,2}$. In this way, we obtain cancellation of the divergences of Eq. (2.4.17) for the vacuum expansion of the $\mathcal{N} = 4$ supergravity amplitude.

Thus, we see that the two-loop cancellations in $D = 4$ and $D = 5$ can be understood entirely and systematically using IBP identities.

2.4.2 Generalizations and an all-loop conjecture

In general, the structure of IBP equations can be rather opaque. Might there be a simple organizing principle that applies to all loop orders? A strong hint is that the subset of IBP identities given in Eq. (2.4.6) follows from Lorentz symmetry. We also saw the key role that Lorentz symmetry played at one loop in Section 2.2. The obvious L-loop extension is

$$\text{UV finite } = \int \left(\prod_{a=1}^{L} d^D \ell_a \right) v_i^{[\mu} v_j^{\nu]} \sum_{a=1}^{L} \ell_{a\mu} \frac{\partial}{\partial \ell_a^\nu} \frac{\mathcal{N}(\ell_a \cdot v_b, \ell_a \cdot \ell_b)}{\prod_j D_j^{A_j}} \,, \tag{2.4.18}$$

where the ℓ_a are an independent set of loop momenta to be integrated, the v_a a set of external vectors in the problem and the $1/D_j$ the propagators in the diagram. As noted earlier, we can equivalently apply Lorentz invariance following the methods in Refs. [35, 56].

What about the identities in Eq. (2.4.14)? These can be understood as belonging to a special class of IBP identities generated by SL(2) transformations of the loop momenta of

the form

$$\begin{pmatrix} p \\ q \end{pmatrix} \to e^{\omega} \begin{pmatrix} p \\ q \end{pmatrix}, \tag{2.4.19}$$

with some traceless 2×2 matrix ω. Since such an SL(2) transformation leaves the integration measure $d^D p \, d^D q$ invariant, we have

$$\text{UV finite} = \int d^D p \, d^D q \, \omega_{ab} \, \ell_a^\mu \frac{\partial}{\partial \ell_b^\mu} \frac{1}{(p^2)^A (q^2)^B [(p+q)^2]^C}, \tag{2.4.20}$$

where we used the notation $(\ell_1, \ell_2) = (p, q)$. We can rewrite this as an IBP relation,

$$\text{UV finite} = \int d^D p \, d^D q \, \frac{\partial}{\partial \ell_b^\mu} \frac{\omega_{ab} \, \ell_a^\mu}{(p^2)^A (q^2)^B [(p+q)^2]^C}, \tag{2.4.21}$$

due to ω_{ab} being traceless. This also shows that these relations do not have explicit dependence on the spacetime dimension D.

In particular, the IBP identity which come from the first equation in (2.4.14) used to exhibit the cancellation of the logarithmic divergence in $D = 5$ is given by the SL(2) generator,

$$\omega_{ab} = \begin{pmatrix} 1 & 0 \\ 0 & -1 \end{pmatrix}. \tag{2.4.22}$$

In fact, the above ideas generalize trivially to the L-loop case by considering generators of SL(L). In more generality, the combination of Lorentz invariance and SL(L) transformations gives rise to some subset of SL(DL) transformations. As a nontrivial check that these ideas provide the key relations between the ultraviolet divergences of vacuum integrals, we have reproduced the relations between ultraviolet divergences of four-loop vacuum integrals in Appendix C of Ref. [35] in the context of obtaining the four-loop ultraviolet divergence for $\mathcal{N} = 8$ supergravity in the critical dimension, $D = 11/2$. One example of such a relation is given graphically in Fig. 2.5. This shows that Lorentz and SL(4) symmetry generates

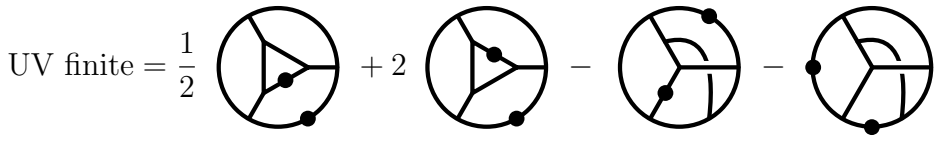

Figure 2.5: A four-loop relation between ultraviolet divergences of vacuum integrals in $D = 11/2$ dimensions, matching identity 22 from Table I in Appendix C of Ref. [35]. Where a black dot appears, the propagator is raised to a squared power.

a complete set of IBP identities necessary for reducing the vacuum integrals encoding the ultraviolet divergence to an independent set. (We know the set is independent from Eq. (4.15) of Ref. [35].) In this case there were no enhanced cancellations, but had they been present they would have been found after applying the identities.

This brings us to a conjecture:

- Given a loop integrand, homogeneous linear transformations of the loop momentum variables with unit Jacobian are sufficient for revealing enhanced cancellations of potential ultraviolet divergences in gravity theories.

Generally, we are interested in the first divergence of a theory in a given dimension so we do not need to concern ourselves with complications due to subdivergences or divergences beyond the logarithmic ones. Even if the cancellation are not complete and an ultraviolet divergence remains we expect these symmetries to generate a complete set of IBP identities for studying logarithmic divergences.

If this conjecture were to hold in general, it would shed light on the mysterious enhanced cancellations that have been observed in various supergravity theories. Furthermore, these transformations can be connected to the labeling difficulty of nonplanar integrands. Remarkably, even though there does not seem to be a single "discrete" relabeling of the integration variables for each diagram that allows us to construct an integrand that would manifest the cancellations, the freedom to change integration variables appears to be at the root of the cancellations.

2.5 Conclusions

In this chapter we took initial steps towards systematically understanding enhanced ultraviolet cancellations in supergravity theories [8–10]. These cancellations go beyond those presently understood from standard-symmetry argumentation [17–19] and therefore appear to require novel explanations.

While a different avenue for understanding enhanced cancellations based on exploiting the double-copy structure of gravity theories has been successful for the special case of half-maximal supergravity in $D = 5$ [10], it is unclear how to extend that argument beyond two loops. In contrast, our large loop-momentum analysis here relies only on generic properties of the integrands and integrals.

In nonabelian gauge theories, standard methods including superspace techniques can be used expose ultraviolet cancellations at the integrand level. One might have thought that it is possible to similarly find organizations of multi-loop integrands of supergravity theory. However, as we showed via one- and two-loop examples, it does not seem possible to do this without relying also on integration properties.

The simplest example of an enhanced cancellation in a supergravity theory is probably the vanishing of one-loop divergences in pure $\mathcal{N} = 4$ supergravity in four dimensions. While the cancellation of the divergence in $D = 4$ is well understood as a consequence of supersymmetry [37], the pattern of cancellation amongst the diagrams serves as a prototype for enhanced cancellations. The double-copy construction [26] allowed us to obtain the $\mathcal{N} = 4$ supergravity integrand very easily from the corresponding ones of pure-Yang–Mills and $\mathcal{N} = 4$ super-Yang–Mills theory. Even in this relatively simple case where there are no labeling ambiguities, we found that the cancellations cannot be exposed at purely the integrand level. After using integral identities that follow from Lorentz invariance, the cancellations become visible.

We also investigated the more interesting case of half-maximal supergravity at two loops.

In $D = 5$, no standard symmetry explanation is known for the cancellation that removes the logarithmic divergence [10,17]. We showed that the three-particle cuts display no integrand-level cancellations, even though the final integrated expression does display the cancellations. Based on our considerations, purely integrand-based proofs of the observed enhanced cancellations do not appear to be possible.

In order to systematize ultraviolet cancellations after integration, we used integration-by-parts identities [30]. This gives a systematic means for finding all relations between the different integrals. While the machinery of doing so is generally difficult to apply at high loop orders, at two-loops we made use of various advances for controlling the complexity of the identities [31–34,73,98]. As an example we showed that one can use these ideas to rearrange the full integrands of amplitudes so that they consist of terms that are manifestly finite as well as terms that integrate to zero. While this construction is a proof of principle and gives some insight into how the cancellations happen, it is too dependent on details of the integrands and the associated identities to be useful for developing an all-orders understanding.

To develop such an understanding, we instead focused on the large loop-momentum behavior of the integrands. For the two-loop $\mathcal{N} = 4$ supergravity amplitude, by series expanding at large loop momentum, we demonstrated that the only identities needed to expose the cancellation are those that follow from Lorentz and an SL(2) symmetry. Using these principles we also reproduced the necessary four-loop identities [35] for extracting the ultraviolet divergence of $\mathcal{N} = 8$ in the critical dimension where it first appears, suggesting that we have identified the key identities.

This led us to conjecture that at L loop order the integral identities generated by Lorentz and SL(L) symmetry are sufficient for exposing the enhanced cancellations of ultraviolet divergences, when they happen. If generally true, it would point towards a symmetry explanation of enhanced cancellations.

There are a number of avenues for further exploration. It would be important to first explicitly confirm our conjecture for the known three- and four-loop examples of enhanced

ultraviolet cancellations [8, 9], and to develop an all-loop understanding. It would also be interesting to study whether this set of integral identities is also applicable to more general problems in QCD and other theories that involve extracting ultraviolet divergences. It may also turn out to be helpful for efficiently obtaining the required integration-by-parts identities for analyzing divergences in $\mathcal{N} = 8$ supergravity at five loops and beyond, once the integrands become available [57].

We expect that in the coming years, as new theoretical tools are developed, a complete and satisfactory understanding of enhanced ultraviolet cancellations in gravity theories will follow.

2.6 Boundary terms in logarithmically divergent IBPs

In section 2.4 we claimed that for logarithmically divergent integrals even in schemes other than dimensional regularization, the boundary contributions of the IBP relations do not alter the relation between the divergences. Here we demonstrate this. This is relevant to our discussion because it supports the notion that the required IBP relations to obtain the cancellations of the studied logarithmic divergences are robust and do not depend on details of the scheme.

First, recall that the vacuum expansion to logarithmically divergent integrals, the IBPs are of the form,

$$\int \prod_i d^D \ell_i \, \frac{\partial}{\partial \ell_j^\mu} \left(\frac{\ell_k^\mu \prod_a N_a^{B_a}}{\prod_b D_b^{A_b}} \right) , \tag{2.6.1}$$

where the powers A_b and B_a of the propagators $1/D_b$ and irreducible numerators N_a are such that the integrals are logarithmically divergent. Consider ultraviolet regularization after Wick rotation using a physical cut off Λ, under which the right-hand-side of Eq. (2.6.1), as a total divergence, is turned into a boundary integral at the compact cutoff surface by Stokes' theorem. Since the number of propagators makes the integral logarithmically divergent, the boundary integral also has mass dimension 0. In Wilson's floating cutoff picture, a

change in the cutoff Λ does not change the boundary integral, which precludes it from having an ultraviolet divergence. Note that the above argument breaks down if we consider, e.g. quadratically divergent IBP relations. This argument is equivalent to the textbook explanation of the finiteness of anomalies in one-loop diagrams given by a boundary term of a linearly divergent integral [58].

However, there is an extra subtlety at higher loops that does not arise in the study of anomalies. The argument cannot be trivially extended to the case where there are subdivergences because there is no longer just one UV divergence coefficient to be fixed by a single floating cutoff. However, this is of secondary concern because usually we are interested in studying the very first potential divergence of a supergravity theory. (There are some subtleties with evanescent effects feeding into divergences which require some care [13].) The most interesting cases, such as $\mathcal{N} = 8$ supergravity at five loops in $D = 24/5$, automatically have no subdivergences because of a lack of lower-loop divergences. It would be nevertheless interesting to understand the behavior of boundary terms in general and study whether the relations generated by Lorentz and SL(L) symmetry can be applied to more general problems of extracting divergences from vacuum integrals in the presence of subdivergences.

We also comment on the dimensional regularization, which requires a mass regulator to separate out infrared singularities. One might worry that this mass regulator might interfere with the IBP identities. However, it is easy to argue that when there are no subdivergences the mass regulator does not cause any issues. To prevent IBP identities from mixing up ultraviolet and infrared poles, infrared divergences can be regulated by introducing a uniform mass m to every propagator on the right-hand-side of Eq. (2.6.1). It is best to introduce the mass prior to vacuum expansion to retain cancellations of subdivergences [53]. After series expanding in small external momentum, we again obtain a sum of logarithmically divergent vacuum integrals (whose internal propagators are regulated by the uniform mass), but we also obtain additional vacuum integrals multiplied by factors of m^2. To have the correct dimensions, these additional integrals must have negative mass dimension and are power-

counting finite in the ultraviolet. Assuming there are no one-loop subdivergences, a naive power counting is sufficient for establishing the lack of ultraviolet divergence. Therefore we obtain relations between logarithmic ultraviolet divergences of massive vacuum integrals. Furthermore, there is a smooth limit when the dimension D tends to a fixed integer (or a fractional number in more exotic cases), while the mass m tends to zero, because our special IBP identities have no D dependence and because leading logarithmic ultraviolet divergences are mass-independent. So we end up with relations between logarithmic ultraviolet divergences of massless vacuum integrals. This argument is applicable whenever dimensional regularization rules out lower-loop subdivergences, for example for supergravity calculations in fractional dimensions (see e.g., Ref. [35]). We note that Ref. [59] also investigated well-defined limits of IBP identities as the dimension tends to an integer, in the different context of studying finite integrals.

Chapter 3

Dual Conformal Symmetry, Integration-by-Parts Reduction, Differential Equations and the Nonplanar Sector

We show that dual conformal symmetry, mainly studied in planar $\mathcal{N} = 4$ super-Yang–Mills theory, has interesting consequences for Feynman integrals in nonsupersymmetric theories such as QCD, including the nonplanar sector. A simple observation is that dual conformal transformations preserve unitarity cut conditions for any planar integrals, including those without dual conformal symmetry. Such transformations generate differential equations without raised propagator powers, often with the right-hand side of the system proportional to the dimensional regularization parameter ϵ. A nontrivial subgroup of dual conformal transformations, which leaves all external momenta invariant, generates integration-by-parts relations without raised propagator powers, reproducing, in a simpler form, previous results from computational algebraic geometry for several examples with up to two loops and five legs. By opening up the two-loop three- and four-point nonplanar diagrams into planar ones,

we find a nonplanar analog of dual conformal symmetry. As for the planar case this is used to generate integration-by-parts relations and differential equations. This implies that the symmetry is tied to the analytic properties of the nonplanar sector of the two-loop four-point amplitude of $\mathcal{N} = 4$ super-Yang–Mills theory.

3.1 Introduction

Dual conformal symmetry is a hidden symmetry of planar $\mathcal{N} = 4$ super-Yang-Mills theory [60–64] which puts strong constraints on the analytic structure of its scattering amplitudes. In this chapter we will discuss applications of this symmetry towards questions of practical interest in generic theories, such as finding useful and compact integration-by-parts (IBP) relations and differential equations (DEs) for loop integrals. We also use these ideas to extend the symmetry to the nonplanar sector by explicitly constructing it for the full two-loop four-point amplitude of $\mathcal{N} = 4$ super-Yang–Mills theory. As for the planar case, the symmetry leads to useful IBP relations and DEs.

An important feature of the IBP relations and DEs generated by dual conformal transformations is that they are naturally compatible with generalized unitarity [24], which is a powerful method for computing multi-loop scattering amplitudes. Generalized unitarity helps to overcome the fast growth of complexity as the loop order and the number of legs increase. At one loop, unitarity-compatible integrand-based reduction [51, 65, 66] simplifies loop amplitudes to a linear combination of master integrals, with coefficients determined from generalized unitarity cuts. This has led to tremendous progress, including the "NLO revolution" for computing NLO QCD corrections for collider processes (see e.g. Refs. [67]). To extend the reach of generalized unitarity to generic theories at higher loops, it is natural to retain the following two important properties: (i) the parametrization is minimal without redundant parameters, leading to invertible linear systems which can be solved to determine the integrand; (ii) the integrand is decomposed into master integrands and spurious integrands that vanish upon integration, so only the coefficients of the master integrands are

needed to evaluate the amplitudes.

These methods for evaluating scattering amplitudes offer great promise to tackle general problems at two loops and beyond (see e.g. Ref. [68]). For dimensionally regularized integrals beyond one loop, it is in fact easy to write down a parametrization that satisfies property (i) by identifying a minimal set of "irreducible numerators" that cannot be expressed as linear combinations of inverse propagators. For integrals in integer (most often four) dimensions, the problem is more intricate, as Gram determinant identities further reduce the number of independent terms in the integrand. But a complete and computationally efficient solution has been found using polynomial division algorithms [56, 69, 70]. To construct a parametrization to satisfy the above property (ii), a first step has been developed in the mentioned papers exploiting the rotation symmetry in the "transverse" directions orthogonal to all external momenta. This is in direct analogy with the one-loop case [71]. A second step, which is substantially more nontrivial, is to identify all remaining contributions that integrate to zero. At higher loops the only known practical means to accomplish this [33] is to exploit IBP relations [30] without increasing propagator powers [31], to not only simplify the problem, but to make it naturally compatible with generalized unitarity. Our approach based on exploiting dual conformal transformations automatically generates IBP relations with these properties.

In the study of scattering amplitudes, theories with more symmetries have often led to unexpected simplifications for theories with fewer symmetries. For example tree-level gluon amplitudes in pure Yang-Mills have hidden supersymmetry because they coincide with the same amplitudes in super-Yang–Mills theory [75]. A one-loop example is that supersymmetric decompositions can be applied to nonsupersymmetric theories [24, 76]. Following this philosophy, we aim to develop a relatively simple analytic understanding of IBP-generating vectors for a variety of one- and two-loop Feynman integrals with vanishing or degenerate masses, using dual conformal symmetry of planar $\mathcal{N} = 4$ super-Yang–Mills theory as a guiding principle. The use of dual conformal symmetry also extends to a large class of

planar Feynman integrals in even integer dimensions, with an appropriate number of propagators [59–63, 77]. This is easiest to implement for planar diagrams where dual conformal symmetry is defined, but as we shall see by opening up nonplanar diagrams into planar diagrams [78], we identify a symmetry that is analogous to dual conformal symmetry.

When we consider integrals in arbitrary dimensions, generic numerators or integrals with too few propagators, the symmetries are lost because the numerators cannot balance the conformal weights from the denominators and the integration measure. However, for our purpose of finding IBP-generating vectors, only the geometry of the unitarity cut surface, fixed by the propagators not the numerators, is relevant. Therefore we can still find insights from dual conformal symmetry in order to analyze the loop integrals of any theory more generally. It turns out that a subgroup of dual conformal transformations, which leaves external momenta unchanged, generates infinitesimal shifts in the loop momenta to produce IBP relations without higher-power propagators. This is connected to the fact that under dual conformal transformations and their nonplanar generalization, the infinitesimal variations of inverse propagators are proportional to the inverse propagators themselves.

To illustrate the ideas in a simple context, we first present a number of one-loop examples. As a toy example we illustrate the case of the one-loop triangle diagram with a single external mass. While standard integral reductions [51, 52, 65] reduce tensor triangle integrals to the scalar triangle integral, we show that dual conformal transformations can be directly applied to reduce the scalar triangle integral to bubble integrals. Then we use this example to illustrate the embedding formalism [59, 80] which reduces conformal transformations in an $\mathrm{SO}(d-1,1)$ dual spacetime to linear Lorentz transformations in an $\mathrm{SO}(d,2)$ embedding space. The latter treatment will involve a general algorithm that can be applied to all one-loop integrals. Finally, we turn to two-loop examples, including nonplanar cases. We adopt a level-by-level approach to IBP reduction. For each topology, we only identify IBP relations which reduce all tensor integrals to top-level master integrals and lower-level integrals with fewer propagators. One can descend into the lower-level topologies recursively to accomplish

the complete IBP reduction.

We also use dual conformal symmetries to generate DEs for integrals [81, 96]. This has proven to be a powerful means for evaluating integrals. The DEs we generate are in terms of integrals without propagators raised to higher powers, along the lines of Ref. [82]. For the integrands that would be invariant in four dimensions under dual conformal transformations or their nonplanar analogs, the right-hand side of the DEs are automatically proportional to the dimensional regularization parameter $\epsilon = (4-d)/2$. If there were no infrared singularities, we could take $\epsilon \to 0$, and the right side of the DEs would vanish. This property is already known for such integrals, after reducing to a carefully chosen basis of integrals [83–85]. In our case, it follows from the existence of a symmetry.

Besides the practical utility of IBP relations and DEs, our considerations point to a nontrivial generalization of dual conformal symmetry to the full nonplanar sector of $\mathcal{N} = 4$ super-Yang–Mills theory. Refs. [86, 87, 116] found in a variety of nontrivial examples that the analytic properties implied by dual conformal symmetry such as having only logarithmic singularities, no poles at infinity and other properties carry over to the nonplanar sector. What symmetries might be behind this? In this chapter we take initial steps toward understanding the symmetries behind these properties, by building on the connection between dual conformal transformations and polynomial tangent vectors of unitarity cut surfaces. For the case of the nonplanar sector of the two-loop four-point amplitude [48, 49] based on our analysis of symmetries of integrals we show that there is indeed a symmetry analogous to dual conformal symmetry.

This chapter is organized as follows. In Section 3.2, we review unitarity-compatible IBP relations, dual conformal transformations and the embedding formalism which linearizes the transformations. In Section 3.3, we illustrate the application of dual conformal transformations, starting from the simple toy example of the one-loop triangle with massless propagators and one massive external leg. Two parallel treatments are presented, one based directly on dual conformal transformations in d dimensions and the other based on the $\mathrm{SO}(d, 2)$ em-

bedding space. The latter part of the section will present two more complicated examples at one loop, namely the triangle diagram with two external masses, and the massive triangle diagram involved in QCD corrections of the $H \to b\bar{b}$ decay. Section 3.4 gives two-loop planar examples, reproducing nontrivial IBP-generating vectors previously obtained from computational algebraic geometry. Section 3.5 outlines applications to obtain DEs using transformations that act nontrivially on the external momenta. Section 3.6 formulates a nonplanar analog of dual conformal symmetry. Applications to IBP and differential equations for dimensionally-regularized nonplanar integrals are also worked out. In Section 3.7, we show the invariance of the two-loop four-point amplitude of $\mathcal{N} = 4$ super-Yang–Mills theory under this symmetry. Our conclusions and outlook are presented in Section 3.8. An appendix giving matrices describing the dual conformal transformations of the two-loop pentabox integrals is also included.

3.2 Basic concepts

In this section we give an overview of basic concepts that will be useful for the remainder of the chapter. We first review the notion of unitarity-compatible IBP relations that do not increase the propagator powers, which generically occurs whenever derivatives hit propagators. Then we discuss using dual conformal transformations as a means for generating IBP relations that are compatible with unitarity cuts and do not increase the powers of the propagators. We will also review the embedding formalism for dual conformal transformations. This will be useful in subsequent sections, since it reduces conformal transformations to simpler Lorentz transformations in two higher dimensions.

3.2.1 Unitarity-compatible IBP relations

Consider an L-loop Feynman integral with L independent loop momenta, $l_1, l_2, \ldots, l_L$, M external legs with momenta p_i, $1 \leq i \leq M$, and N propagators, $1/\Delta_j$, $1 \leq j \leq N$,

$$\int \prod_{A=1}^{L} d^d l_A \frac{\mathcal{N}}{\prod_j \Delta_j} \,. \tag{3.2.1}$$

where $\mathcal{N}$ is a numerator that has polynomial dependence on all possible Lorentz-invariant dot products amongst loop and external momenta.

Integration-by-parts relations [30] arise because total derivatives integrate to zero in dimensional regularization,

$$0 = \int \prod_{A=1}^{L} d^d l_A \, \frac{\partial}{\partial l_B^\mu} \frac{v_B^\mu \mathcal{N}}{\prod_j \Delta_j} \,, \tag{3.2.2}$$

where there is implicit summation over the loop momentum label B, and v_B^μ is built out of all possible Lorentz vectors p_i^μ and l_A^μ, each multiplied by polynomials in Lorentz-invariant dot products. The identity amongst integrals comes from explicitly applying the derivative. We will refer to

$$v_B^\mu \frac{\partial}{\partial l_B^\mu} \,, \tag{3.2.3}$$

as an IBP-generating vector or IBP vector.

If the vector satisfies the condition [31]

$$v_B^\mu \frac{\partial}{\partial l_B^\mu} \Delta_j = \mathcal{W}_j \Delta_j \,, \tag{3.2.4}$$

where there is an implicit sum over B and μ, for each $1 \leq j \leq N$, with the $\mathcal{W}_j$ being polynomials in Lorentz-invariant dot products, then the IBP relation Eq. (3.2.2) will not lead to propagators raised to two or more powers. More generally speaking, if we start with some propagator raised to a power, the power of that propagator will not be increased further in the IBP relation [68]. This will be called a "unitarity-compatible" IBP relation,

as unitarity cut conditions are easily imposed when there are no raised propagator powers. The standard ways to find IBP vectors that satisfy Eq. (3.2.4) are based on solving syzygy equations [31, 34, 68, 74], often using software for computational algebraic geometry [88].

This is natural with the unitarity approach. If a certain inverse propagator Δ_j is set to zero by a unitarity cut, then for that case the right-hand side of Eq. (3.2.4) is zero, which means the IBP-generating vector is a tangent vector to the unitarity cut surface of *any* cut, maximal or non-maximal [33]. It should be emphasized that it is a polynomial (rather than rational) tangent vector.

3.2.2 Unitarity-compatible differential equations

A powerful method for evaluating Feynman integrals is differential equations with respect to external momenta [81, 96]. In this method, one computes derivatives

$$\chi_i^\mu \frac{\partial}{\partial p_i^\mu} \int \prod_{A=1}^{L} d^d l_A \frac{\mathcal{N}}{\prod_j \Delta_j}\,, \tag{3.2.5}$$

where there is implicit summation of i over every external momentum, and χ_i^μ generates an infinitesimal change in the kinematic invariants (i.e. Lorentz-invariant dot products between external momenta). We require χ_i^μ to have no dependence on loop momenta. Since total derivatives vanish upon integration, Eq. (3.2.5) is equivalent to

$$\begin{aligned}\int \prod_{A=1}^{L} d^d l_A \left[\chi_i^\mu \frac{\partial}{\partial p_i^\mu}\frac{\mathcal{N}}{\prod_j \Delta_j} + \frac{\partial}{\partial l_B^\mu}\frac{v_B^\mu \mathcal{N}}{\prod_j \Delta_j}\right] \\ = \int \prod_{A=1}^{L} d^d l_A \left[\frac{\partial v_B^\mu}{\partial l_B^\mu} + \left(\chi_i^\mu \frac{\partial}{\partial p_i^\mu} + v_B^\mu \frac{\partial}{\partial l_B^\mu}\right)\right] \frac{\mathcal{N}}{\prod_j \Delta_j}\,.\end{aligned} \tag{3.2.6}$$

We will refer to

$$\chi_i^\mu \frac{\partial}{\partial p_i^\mu} + v_B^\mu \frac{\partial}{\partial l_B^\mu} \tag{3.2.7}$$

as the DE-generating vector. Under the condition [82]

$$\left(\chi_i^\mu \frac{\partial}{\partial p_i^\mu} + v_B^\mu \frac{\partial}{\partial l_B^\mu}\right) \Delta_j = \mathcal{W}_j \Delta_j \,, \tag{3.2.8}$$

for some polynomial $\mathcal{W}_j$ for each $1 \leq j \leq N$, Eq. (3.2.6) has no propagators raised to higher powers, i.e. is unitarity compatible. In our framework, IBP-generating vectors are special cases of DE-generating vectors without external momentum derivatives. Similarly, IBP relations are regarded as special cases of differential equations whose left-hand side is zero rather than an external momentum derivative of the integral. Similar to the interpretation of Eq. (3.2.4), Eq. (3.2.8) implies that the DE-generating vector is a tangent vector to unitarity cut surfaces, considered as solutions to unitarity cut conditions in the space of *both* external and loop momenta.

We will refer to $\mathcal{W}_j$ as the weight of the inverse propagator ρ_j under the infinitesimal transformation of p_i and l_B generated by the vector (3.2.7). The total divergence term $\partial v_B^\mu / \partial l_B^\mu$ in Eq. (3.2.6) may be regarded as the weight $\mathcal{W}_{\text{measure}}$ of the integration measure, coming from an infinitesimal deviation of the Jacobian from unity (see a later discussion around Eq. (3.2.23)), under the same transformation. In addition, in some cases of interest, the numerator $\mathcal{N}$ also has a well-defined weight $\mathcal{W}_\mathcal{N}$ with polynomial dependence on external and loop momenta. In this case Eq. (3.2.6) is rewritten as

$$\begin{aligned} &\int \prod_{A=1}^{L} d^d l_A \left[\frac{\partial v_B^\mu}{\partial l_B^\mu} + \left(\chi_i^\mu \frac{\partial}{\partial p_i^\mu} + v_B^\mu \frac{\partial}{\partial l_B^\mu}\right)\right] \frac{\mathcal{N}}{\prod_j \Delta_j} \\ &\qquad = \int \prod_{A=1}^{L} d^d l_A \left(\mathcal{W}_{\text{measure}} + \mathcal{W}_\mathcal{N} - \sum_k \mathcal{W}_k\right) \frac{\mathcal{N}}{\prod_j \Delta_j} \,. \end{aligned} \tag{3.2.9}$$

If in the above equation,

$$\mathcal{W}_{\text{measure}} + \mathcal{W}_\mathcal{N} - \sum_k \mathcal{W}_k = 0 \,, \tag{3.2.10}$$

then the integral is formally invariant under the infinitesimal transformation generated by the vector (3.2.7). A trivial example is a Lorentz transformation (in both external and loop

momenta), under which the integration measure, propagators, and the numerator are separately invariant. In most cases the integrals are infrared singular and an infrared regulator is needed. This shifts the weight of the measure factor by terms proportional to ϵ, making the symmetry anomalous.

3.2.3 Properties of IBP- and DE-generating vectors

IBP-generating vectors defined by Eq. (3.2.4) and DE-generating vectors defined by Eq. (3.2.8) satisfy the following properties:

First, if an IBP-generating vector (or DE-generating vector) is multiplied by a polynomial in Lorentz-invariant dot products of external and loop momenta, it is still a valid IBP-generating vector (or DE-generating vector). Furthermore, the linear combination of two IBP-generating vectors (or DE-generating vectors) is still a valid vector. Therefore, IBP- and DE-generating vectors form *modules* over the ring of polynomials.

Second, by applying Eq. (3.2.8) twice, it can be seen that the composition of two DE-generating vectors still does not raise the power of any propagator. Furthermore, the components χ_i^μ remain independent of the loop momenta. This can be used to compute higher-order differential equations [89, 90] without generating doubled propagators.

Third, it follows from the second property above that IBP- and DE-generating vectors form a closed Lie algebra. The action of the DE vector (3.2.7) in Eq. (3.2.6) is, in the language of differential geometry, the Lie derivative action on the form

$$\prod_{A=1}^{L} d^d l_A \, \frac{\mathcal{N}}{\prod_j \Delta_j} \,. \tag{3.2.11}$$

It is well known that the Lie derivative action of vectors commutes with the Lie bracket of vectors, i.e. the Lie algebra structure extends to the action of IBP- and DE-generating vectors. This is essentially the observation of Ref. [91] in the slightly different context of IBP reduction with doubled propagators. As in the aforementioned reference, the Lie

algebra structure allows us to reduce the redundancy of IBP relations—all the necessary IBP relations arise from the action of a minimal generating set of IBP vectors on the possible tensor integrals.

Fourth, given the unitarity-compatible conditions in Eqs. (3.2.4) and (3.2.8), the IBP- and DE-generating vectors are valid on unitarity cuts and can be used to generate relations between cut integrals [92, 93].

3.2.4 Dual conformal symmetry

If the Feynman integral Eq. (3.2.1) is planar and only has massless propagators, we can write each inverse propagator as either

$$(y_A - y_B)^2, \qquad (A \neq B)\,, \tag{3.2.12}$$

or

$$(y_A - x_j)^2\,, \tag{3.2.13}$$

where A and B are loop-momentum labels, and x_j are the vertices of a coordinate-space polygon whose edge $(x_{i+1} - x_i)$ is equal to the external momenta p_i. We will refer to x_j as external momentum points and y_A as loop-momentum points. This is known as the dual-space version of planar Feynman integrals, as each y_A and x_j may be considered as coordinate-space points in a dual $\mathrm{SO}(d-1,1)$ "spacetime" (not to be confused with ordinary spacetime).

As a simple example, consider the two-loop planar double-box integral,

$$I^{(2)} = \int d^d l_1\, d^d l_2 \frac{1}{l_1^2 (l_1 - p_1)^2 (l_1 - p_1 - p_2)^2 l_2^2 (l_2 + p_4)^2 (l_2 + p_3 + p_4)^2 (l_1 - l_2)^2}\,, \tag{3.2.14}$$

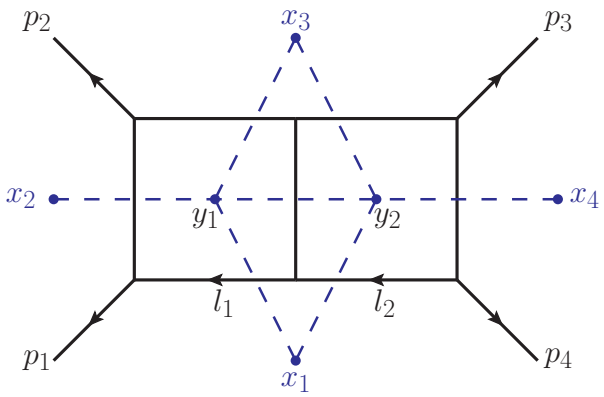

Figure 3.1: The double-box integrals. Differences of the dual points give momenta flowing in the diagram. The x_i and y_i are dual coordinates of the double box integral. The dual diagram is given by the dashed (blue) diagram.

illustrated in Fig. 3.1. We define the dual points implicitly, via

$$p_1 = x_2 - x_1\,, \qquad p_2 = x_3 - x_2\,, \qquad p_3 = x_4 - x_3\,, \qquad p_4 = x_1 - x_4\,,$$
$$l_1 = y_1 - x_1\,, \qquad l_2 = y_2 - x_1\,. \tag{3.2.15}$$

These variables automatically enforce momentum conservation on the p_i. Performing the change of variables (3.2.15) in the double box, gives

$$I^{(2)} = \int d^d y_1\, d^d y_2\, \frac{1}{(y_1-x_1)^2(y_1-x_2)^2(y_1-x_3)^2(y_1-y_2)^2(y_2-x_1)^2(y_2-x_3)^2(y_2-x_4)^2}\,. \tag{3.2.16}$$

The dual conformal transformations include scalings $z_i \to a z_i$ and inversions $z_i^\mu \to z_i^\mu / z_i^2$, where z_i may be either an external x_i or internal y_A dual point. Under the inversion, we have

$$(x_i - x_j)^2 \to \frac{(x_i - x_j)^2}{x_i^2 x_j^2}\,, \qquad (y_A - x_j)^2 \to \frac{(y_A - x_j)^2}{y_A^2 x_j^2}\,, \qquad (y_A - y_B)^2 \to \frac{(y_A - y_B)^2}{y_A^2 y_B^2}\,. \tag{3.2.17}$$

From the perspective of planar $\mathcal{N} = 4$ super-Yang-Mills theory, dual conformal transformations are interesting because they formally leave the amplitude invariant, ignoring regulator

issues. From our perspective, what makes them interesting is that they leave the unitarity cut surface $(y_A - x_j)^2 = 0$ invariant. These considerations suggest that we can generate IBP relations and differential equations that are automatically compatible with unitarity. This is true whether or not the integrals are invariant. Indeed, the noninvariance is precisely what we will use to generate nontrivial IBP relations and differential equations.

To generate IBP relations and differential equations we should phrase the conformal transformation as infinitesimal transformations. Under an infinitesimal conformal boost defined by an $\mathrm{SO}(d-1,1)$ vector b^μ, a dual coordinate z^μ transforms as

$$\Delta z^\mu = \frac{1}{2} b^\mu z^2 - (b \cdot z) z^\mu \,. \tag{3.2.18}$$

Under an infinitesimal scaling (i.e. dilatation) transformation with parameter β,

$$\Delta z^\mu = \beta z^\mu \,. \tag{3.2.19}$$

(Throughout this chapter, Δ will be understood as a differential operator or a symmetry generator, so the right-hand side of the above equation is not multiplied by an explicit infinitesimal parameter.) Finally, under Lorentz transformations parametrized by an antisymmetric $\Omega^{\mu\nu}$,

$$\Delta z^\mu = \Omega^{\mu\rho} \eta_{\rho\nu} z^\nu = \Omega^\mu{}_\nu \, z^\nu \,, \tag{3.2.20}$$

where $\eta_{\rho\nu}$ is the metric. Combining the conformal boost, scaling, and Lorentz transformations, we have

$$\Delta z^\mu = \frac{1}{2} b^\mu z^2 + (\beta - b \cdot z) z^\mu + \Omega^\mu{}_\nu \, z^\nu \,. \tag{3.2.21}$$

In terms of the infinitesimal transformations, if two points z_1^μ and z_2^μ both transform according to Eq. (3.2.21), then a simple calculation gives

$$\Delta (z_1 - z_2)^2 = \left[2\beta - b \cdot (z_1 + z_2) \right] (z_1 - z_2)^2 \,, \tag{3.2.22}$$

which is proportional to $(z_1 - z_2)^2$. Therefore, under an infinitesimal dual conformal transformation for y_A^μ and x_j^μ, the variation of any inverse propagator is proportional to the inverse propagator itself. This immediately echoes the condition (3.2.8) for the lack of propagators raised to higher powers, and implies that dual conformal transformations generate unitarity-compatible differential equations [82]. The dual-spacetime integration measure transforms as the trace of the infinitesimal deviation of the Jacobian matrix from the identity matrix,

$$\Delta\left(d^d z\right) = d^d z \frac{\partial \Delta z^\mu}{\partial z^\mu} = d^d z \, \left(\beta - b \cdot z\right) d\,. \tag{3.2.23}$$

As discussed in Section 3.2.2, IBP-generating vectors arise if we impose the further condition that the infinitesimal dual conformal transformations do not shift the external points,

$$\Delta x_j = 0\,, \tag{3.2.24}$$

for each external point x_j. We will give examples in subsequent sections for explicitly solving this constraint.

3.2.5 Embedding formalism

A convenient means for carrying out conformal transformations is via the embedding formalism of Refs. [59, 80]. In this construction, the system is embedded in a space with two extra dimensions. This allows us to reformulate dual conformal transformations as Lorentz transformations in the higher-dimensional space.

The embedding formalism maps each dual point z^μ in the $\mathrm{SO}(d-1,1)$ dual space to a point in $\mathrm{SO}(d,2)$ invariant space. Following the conventions of Ref. [59], we introduce

$$Z^a = \begin{pmatrix} Z^\mu \\ Z^- \\ Z^+ \end{pmatrix} = \begin{pmatrix} z^\mu \\ -z^2 \\ 1 \end{pmatrix}. \tag{3.2.25}$$

These vectors are defined modulo the identification

$$Z \cong \alpha Z, \quad \alpha \neq 0\,, \tag{3.2.26}$$

which is referred to as a GL(1) "gauge freedom". The inverse map is

$$z^\mu = \frac{Z^\mu}{Z^+}\,. \tag{3.2.27}$$

The SO$(d,2)$ invariant contraction is defined by the inner product

$$(XY) = X^a X_a \equiv 2X^\mu Y_\mu + X^+Y^- + X^-Y^+\,. \tag{3.2.28}$$

Thus the point defined in Eq. (3.2.25) is on the light cone,

$$(ZZ) = 0\,. \tag{3.2.29}$$

We introduce the point at infinity, I, which is the limit of Eq. (3.2.25) with all components of x^μ uniformly tending to infinity, with an appropriate scaling using the gauge freedom in Eq. (3.2.26),

$$I^a = \lim_{|z|\to\infty} \left(-\frac{1}{z^2}\right) \begin{pmatrix} z^\mu \\ -z^2 \\ 1 \end{pmatrix} = \begin{pmatrix} 0 \\ 1 \\ 0 \end{pmatrix}. \tag{3.2.30}$$

This has the effect of compactifying the loop-momentum space [93]. Using Eq. (3.2.25), we map the loop-momentum points y_A^μ to

$$Y_A^a = \begin{pmatrix} y_A^\mu \\ -y_A^2 \\ 1 \end{pmatrix}, \tag{3.2.31}$$

and map the dual kinematic points x_j^μ to

$$X_j^a = \begin{pmatrix} x_j^\mu \\ -x_j^2 \\ 1 \end{pmatrix} . \tag{3.2.32}$$

The inverse propagators are now represented by $\mathrm{SO}(d,2)$ inner products between these points,

$$(y_A - y_B)^2 = -\frac{(Y_A Y_B)}{(Y_A I)(Y_B I)} , \tag{3.2.33}$$

$$(y_A - x_j)^2 = -\frac{(Y_A X_j)}{(Y_A I)(X_j I)} , \tag{3.2.34}$$

where GL(1) invariance is ensured by the denominators involving the point at infinity. The denominators are unity in the gauge of Eq. (3.2.31). The factor $(X_j I)$ in the denominator of the right-hand side of the second line can be omitted, because we will always choose the gauge $(X_j I) = 1$, as in Eq. (3.2.32).

The integration measure for each loop becomes, suppressing the loop label,

$$d^d y \to \frac{d^{d+2} Y \, \delta(Y^2/2)}{(YI)^d \, \mathrm{Vol}(\mathrm{GL}(1))} , \tag{3.2.35}$$

where Y^2 is a shorthand for $(YY) = Y^a Y_a$ and the expression is formally divided by the volume of the GL(1) gauge orbit.

We define $\mathrm{SO}(d,2)$ Lorentz transformations acting on some function $f(Z)$ using two reference vectors Z_i and Z_j, as

$$\begin{aligned} \Delta f(Z) &= (Z_{[i} \, Z) \left(Z_{j]} \frac{\partial}{\partial Z} \right) f(Z) = Z^a_{[i} \, Z_a \, Z^b_{j]} \frac{\partial}{\partial Z^b} f(Z) \\ &= \left(Z_i^a \, Z_a \, Z_j^b \frac{\partial}{\partial Z^b} - Z_j^a \, Z_a \, Z_i^b \frac{\partial}{\partial Z^b} \right) f(Z) , \end{aligned} \tag{3.2.36}$$

where a and b are $\mathrm{SO}(d,2)$ indices. Notice that the factor $\delta(Y^2/2)$ in Eq. (3.2.35) is in-

variant under these transformations. The square-bracket notation in the first line indicates antisymmetrization over i and j, as explicitly implemented in the second line.

Integration-by-parts relations follow from Lorentz invariance identities [59],

$$0 = \int \frac{d^{d+2}Y\,\delta(Y^2/2)}{\mathrm{Vol}(\mathrm{GL}(1))}\, u(Z_i, Z_j)\mathcal{I}\,, \tag{3.2.37}$$

where

$$u(Z_i, Z_j) \equiv (Z_{[i}\,Y)\left(Z_{j]}\,\frac{\partial}{\partial Y}\right) = (Z_i^b Y_b Z_j^a - Z_j^b Y_b Z_i^a)\frac{\partial}{\partial Y^a}\,, \tag{3.2.38}$$

is a one-loop IBP-generating vector. In Eq. (3.2.37) it acts on some general loop integrand $\mathcal{I}$. The factor $1/(YI)^d$ from the integration measure in Eq. (3.2.35) is absorbed into $\mathcal{I}$. Concrete examples of such IBP relations will be given in subsequent sections.

The $\mathrm{SO}(d,2)$ Lorentz transformations exactly correspond to conformal transformations in Minkowski space with the $\mathrm{SO}(d-1,1)$ invariant metric, which can be checked using the inverse map formula (3.2.27). For example, in Eq. (3.2.38), a d-dimensional translation $\Delta z^\mu = e^\mu$ is equivalent to setting

$$Z_i = I = \begin{pmatrix} 0 \\ 1 \\ 0 \end{pmatrix}, \qquad Z_j = \begin{pmatrix} e^\mu \\ 0 \\ 0 \end{pmatrix}. \tag{3.2.39}$$

A d-dimensional conformal boost (3.2.18) with parameter b^μ is equivalent to setting

$$Z_i = -\frac{1}{2}\begin{pmatrix} 0 \\ 0 \\ 1 \end{pmatrix}, \qquad Z_j = \begin{pmatrix} b^\mu \\ 0 \\ 0 \end{pmatrix}. \tag{3.2.40}$$

Finally, a scaling transformation (3.2.19) is equivalent to setting

$$Z_i = I = \begin{pmatrix} 0 \\ 1 \\ 0 \end{pmatrix}, \qquad Z_j = - \begin{pmatrix} 0 \\ 0 \\ \beta \end{pmatrix}. \tag{3.2.41}$$

Therefore the IBP relations from $\mathrm{SO}(d,2)$ Lorentz invariance arise from infinitesimal conformal transformations of the d-dimensional loop momenta. Following the logic of the previous subsection, such IBP relations will not have propagators raised to higher powers if the $\mathrm{SO}(d,2)$ Lorentz transformations in Eq. (3.2.36) leave the external momenta invariant, i.e. leave the X_j points invariant up to $GL(1)$ gauge scaling.

More generally, we can consider any IBP-generating vector in the embedding space,

$$V^a \frac{\partial}{\partial Y^a}\,. \tag{3.2.42}$$

The above expression can be identified with an IBP-generating vector $v^\mu \partial_\mu$ in ordinary $\mathrm{SO}(d-1,1)$ space if it satisfies the following two conditions: (i) it must be GL(1) gauge invariant, and (ii) it must commute with the measure factor $\delta(Y^2/2)$, i.e.,

$$V^a Y_a = 0\,. \tag{3.2.43}$$

The resulting IBP relation is, again showing the one-loop case for illustration,

$$\begin{aligned} 0 &= \int \frac{d^{d+2}Y\,\delta(Y^2/2)}{\mathrm{Vol}(\mathrm{GL}(1))} \frac{\partial}{\partial Y^a}\left(V^a \mathcal{I}\right) \\ &= \int \frac{d^{d+2}Y\,\delta(Y^2/2)}{\mathrm{Vol}(\mathrm{GL}(1))} \left(\mathcal{I}\,\frac{\partial V^a}{\partial Y^a} + V^a \frac{\partial \mathcal{I}}{\partial Y^a}\right), \end{aligned} \tag{3.2.44}$$

consisting of a divergence term proportional to an integrand $\mathcal{I}$ and a second term involving derivatives of $\mathcal{I}$. For an IBP-generating vector as in Eq. (3.2.38) from Lorentz invariance, the divergence term vanishes, so Eq. (3.2.37) only involves derivatives of $\mathcal{I}$.

We can extend the above discussion to include internal masses [93, 94] by modifying Eq. (3.2.32) to map the external momentum point x_j^μ to

$$X_j^a = \begin{pmatrix} x_j^\mu \\ -x_j^2 + m_j^2 \\ 1 \end{pmatrix} . \tag{3.2.45}$$

This changes Eq. (3.2.34) to

$$(x_j - y_A)^2 - m_j^2 = -\frac{(Y_A X_j)}{(Y_A I)} . \tag{3.2.46}$$

Since Eq. (3.2.46) contains a mass m_j that is independent of the loop label A, the formula only allows arbitrary masses at the one-loop level, and at higher loops, the masses of some propagators must be correlated or vanishing.

3.3 IBP for one-loop triangle integrals

To illustrate the ideas of the previous section, we present some simple one-loop examples. It is well known that by Passarino-Veltman or OPP reduction [51, 52, 65], triangle tensor integrals can all be reduced to triangle scalar integrals and daughter integrals (i.e. bubble and tadpole integrals from collapsing certain propagators of the triangle diagram). In the language of unitarity-compatible IBP reduction, this is accomplished by IBP-generating vectors which are rotation generators in the spacetime directions orthogonal to all external momenta [33]. However, under special kinematic configurations, scalar triangle integrals can be further reduced to bubble integrals using IBP reduction. The necessary IBP-generating vectors will be the main topic of this section.

First we show directly how dual conformal transformations can be used to generate unitarity-compatible IBP relations without higher-power propagators. We then streamline the procedure using the embedding formalism [59,80] that reduces conformal transformations

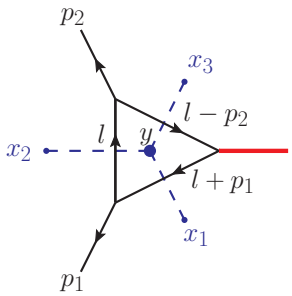

Figure 3.2: The one-loop triangle with outgoing external momenta p_1, p_2, $-p_1 - p_2$ and dual points x_1, x_2, x_3. All internal propagators are massless, and the single massive external leg has mass $(p_1 + p_2)^2 = s$, shown as a thick (red) line. The dashed (blue) lines indicate the dual diagram.

to simpler Lorentz transformations in higher dimensions.

3.3.1 One-external-mass triangle: direct treatment

Consider the one-loop triangle shown in Fig. 3.2. For illustrative purposes, we specialize to the simple case of all internal and external legs being massless, with the exception of the right-most leg of the figure. The three inverse propagators are

$$\Delta_1 = (l + p_1)^2, \qquad \Delta_2 = l^2, \qquad \Delta_3 = (l - p_2)^2 \,. \tag{3.3.1}$$

The external kinematic invariants are

$$p_1^2 = p_2^2 = 0, \qquad (p_1 + p_2)^2 = s \,. \tag{3.3.2}$$

We introduce dual coordinates x_j, $1 \leq j \leq 3$ and y, such that

$$p_1 = x_2 - x_1, \qquad p_2 = x_3 - x_2, \qquad l = y - x_2 \,. \tag{3.3.3}$$

The external points x_j completely fix the external momenta, while y is an internal point corresponding to shifted loop momentum. Since p_j and l are expressed as differences between

dual coordinates x_j and y in Eq. (3.3.3), we are free to apply the same translation to all the dual coordinates. We choose to fix the translation "gauge freedom" by taking,

$$x_2 = 0\,, \tag{3.3.4}$$

so the explicit expressions for the dual coordinates are

$$x_1 = -p_1\,, \qquad x_2 = 0\,, \qquad x_3 = p_2\,, \qquad y = l\,. \tag{3.3.5}$$

With this gauge choice, in terms of these dual coordinates, Eqs. (3.3.1) and (3.3.2) become

$$\Delta_1 = (y - x_1)^2\,, \qquad \Delta_2 = y^2\,, \qquad \Delta_3 = (y - x_3)^2\,, \tag{3.3.6}$$

and

$$x_1^2 = x_2^2 = x_3^2 = 0, \qquad (x_2 - x_1)^2 = (x_3 - x_2)^2 = 0, \qquad (x_3 - x_1)^2 = s\,. \tag{3.3.7}$$

Eqs. (3.3.6) and (3.3.7) imply that

$$y \cdot x_1 = \frac{1}{2}(\Delta_2 - \Delta_1), \qquad y \cdot x_2 = 0\,, \qquad y \cdot x_3 = \frac{1}{2}(\Delta_2 - \Delta_3)\,. \tag{3.3.8}$$

As discussed in Section 3.2, the key property of the dual conformal transformations (3.2.21) is that when acting on inverse propagators, they return results proportional to the inverse propagator itself, as shown in Eq. (3.2.22). In order to use dual conformal transformations to generate IBP relations, we restrict to the subset (3.2.24) where the transformations do not shift the external points.

The shift under the transformation of the loop momentum gives an IBP-generating vector

$$\Delta y^\mu \frac{\partial}{\partial y^\mu} \; = \Delta l^\mu \frac{\partial}{\partial l^\mu} = v^\mu \frac{\partial}{\partial l^\mu}\,, \tag{3.3.9}$$

that satisfies the key condition of Eq. (3.2.4) that it does not raise the power of propagators in the IBP identity. Applying Eq. (3.2.21) to x_j^μ, and using $x_j^2 = 0$ from Eq. (3.3.7), Eq. (3.2.24) becomes

$$0 = (\beta - b \cdot x_j) x_j, \quad j = 1, 2, 3\,. \tag{3.3.10}$$

One solution to Eq. (3.3.10) is

$$\beta = s\,, \qquad\qquad b = -2(x_1 + x_3)\,, \tag{3.3.11}$$

where we used Eq. (3.2.3). This gives, using Eq. (3.2.21),

$$\Delta l = v = -l^2(x_1 + x_3) + [s + 2\, l \cdot (x_1 + x_3)]\, l\,. \tag{3.3.12}$$

The IBP-generating vector $v^\mu \partial_\mu$ satisfies

$$v^\mu \frac{\partial}{\partial l^\mu} \rho_i = \mathcal{W}_i \rho_i, \quad 1 \le i \le 3\,, \tag{3.3.13}$$

where $\mathcal{W}_i$ follows from Eq. (3.2.22),

$$\mathcal{W}_i = 2\beta - b \cdot (l + x_i)\,. \tag{3.3.14}$$

The divergence of the vector follows from Eq. (3.2.23),

$$\mathcal{W}_{\text{measure}} = \frac{\partial v^\mu}{\partial l^\mu} = (\beta - b \cdot l) d\,. \tag{3.3.15}$$

We obtain the IBP relation

$$\begin{aligned}
0 &= \int d^d l \, \frac{\partial}{\partial l^\mu} \frac{v^\mu}{\Delta_1 \Delta_2 \Delta_3} \\
&= \int d^d l \, \left(\mathcal{W}_{\text{measure}} - \mathcal{W}_1 - \mathcal{W}_2 - \mathcal{W}_3 \right) \frac{1}{\Delta_1 \Delta_2 \Delta_3} \\
&= \int d^d l \, \big[(d-6)\beta + b \cdot (x_1 + x_2 + x_3) - (d-3) b \cdot l \big] \frac{1}{\Delta_1 \Delta_2 \Delta_3} \\
&= \int d^d l \, \big[(d-4) s + 2(d-3)(x_1 + x_3) \cdot l \big] \frac{1}{\Delta_1 \Delta_2 \Delta_3} \, .
\end{aligned} \tag{3.3.16}$$

In the last line above, we have used the explicit solution for β and b^μ in Eq. (3.3.11). Simplifying the result using Eqs. (3.3.5) and (3.3.8), the final IBP relation is

$$\begin{aligned}
0 &= \int d^d l \big[(d-4) s + (d-3)(2\rho_2 - \rho_1 - \rho_3) \big] \frac{1}{\Delta_1 \Delta_2 \Delta_3} \\
&= (d-4) s I_{\text{tri}} + 2(d-3) I^{(s)}_{\text{bub}} \, ,
\end{aligned} \tag{3.3.17}$$

where I_{tri} is the scalar triangle integral in Fig. 3.2 and $I^{(s)}_{\text{bub}}$ is the scalar bubble integral obtained from the term proportional to Δ_2 which cancels the propagator $1/\Delta_2 = 1/l^2$, so that the mass of both external legs is s. The terms proportional to Δ_1 and Δ_3 in the second line of Eq. (3.3.17) give bubble integrals with massless external legs, which vanish in dimensional regularization and are discarded in the last line. Eq. (3.3.17) corresponds to a well-known relation between the one-external-mass triangle and the bubble integral (see e.g. the fourth appendix of Ref. [95]). The coefficient of the triangle integral in Eq. (3.3.17) vanishes as $d \to 4$ while the coefficient of the bubble integral does not. This is due to infrared singularities of the triangle integral. This simple example illustrates the basic principle behind using dual conformal symmetry to generate useful IBP relations.

3.3.2 Embedding-space treatment of one- and two-external-mass triangles

To streamline dual conformal transformations and the construction of IBP-generating vectors we use the embedding formalism [59, 80] summarized in Section 3.2.5. This reduces d-dimensional conformal transformations to simpler $(d+2)$-dimensional Lorentz transformations. The algorithm involves solving for all $(d+2)$-dimensional Lorentz transformations that leave the external momenta invariant. This is used to construct a matrix that encodes the action of the IBP vector, so that the IBP relations can be conveniently constructed. We will use the above one-external-mass triangle as an example, before explaining the generalization. Here we apply Lorentz rotations that act in the subspace of external points. One can also consider Lorentz rotations in the embedding space that only act in the space orthogonal to the external points, as we do in Section 3.4.2.

Using Eqs. (3.2.34) and (3.2.35), the scalar triangle integral in Fig. 3.2 is written in the $\mathrm{SO}(d,2)$ embedding space,

$$I_{\text{tri}} = \int \frac{d^{d+2}Y\,\delta(Y^2/2)}{(YI)^{d-3}\,\mathrm{Vol}(\mathrm{GL}(1))}\,\frac{(-1)^3}{(YX_1)(YX_2)(YX_3)}\,, \tag{3.3.18}$$

where Y and X_j are as defined in Eqs. (3.2.31) and (3.2.32) and as in Eq. (3.2.35) Y^2 is a shorthand for $(YY) = Y^a Y_a$. The factor $(-1)^3$ comes from the minus sign on the right-hand side of Eq. (3.2.34).

We define a subset of infinitesimal $(d+2)$-dimensional Lorentz transformations Δ_ω by an antisymmetric 4×4 matrix ω^{ij}, acting on a $(d+2)$ dimensional point Z^a as

$$\Delta_\omega Z^a = \sum_{1\le i,j\le 4} (ZX_i)\omega^{ij}X_j^a\,, \tag{3.3.19}$$

where X_1, X_2, X_3 are the three external points in Eq. (3.3.18) and $X_4 = I$, where I is defined in Eq. (3.2.30). We will choose the ω^{ij} such that the above Lorentz transformation leaves

X_1, X_2, X_3 invariant up to a GL(1) gauge scaling. This means that under the transformations only the loop-momentum shifts by an infinitesimal amount, captured by the IBP vector,

$$\frac{1}{2}\omega^{ij}u(X_i, X_j) = \omega^{ij}(X_i Y)X_j^a \frac{\partial}{\partial Y^a}\,. \tag{3.3.20}$$

The summation over $1 \leq i, j \leq 4$ is implicit, and we have used the definition of $u(X_i, X_j)$ in Eq. (3.2.38).

The Lorentz transformations in Eq. (3.3.19) acts on X_k as

$$\begin{aligned}\Delta_\omega X_k^a &= g_{ki}\,\omega^{ij}X_j^a \\ &\equiv \bar{\omega}_k{}^j X_j^a\,,\end{aligned} \tag{3.3.21}$$

where we defined the "embedding-space gram matrix" as,

$$g_{ij} = (X_i X_j) = \begin{pmatrix} 0 & 0 & -s & 1 \\ 0 & 0 & 0 & 1 \\ -s & 0 & 0 & 1 \\ 1 & 1 & 1 & 0 \end{pmatrix}, \tag{3.3.22}$$

where we identify X_4 with I and the last row and column contain entries of unity due to the gauge choice $(X_j I) = 1$ in Eq. (3.2.32). We then impose the condition that X_1, X_2, X_3 but not $X_4 = I$, are left invariant by the Lorentz transformation:

$$\Delta_\omega X_k^a = \alpha_k\, X_k^a\,, \qquad \text{if } k = 1, 2, 3, \tag{3.3.23}$$

where α_k can be absorbed into the $GL(1)$ invariance of the integrand (3.2.26) which takes $(d+2)$-dimensional vectors to be equivalent if they are scaled. The second line in Eq. (3.3.21)

defines the "IBP matrix", and depends on the free parameters ω^{ij} which we determine below,

$$\bar{\omega} \equiv g\,\omega = \begin{pmatrix} s\omega_{13} - \omega_{14} & s\omega_{23} - \omega_{24} & -\omega_{34} & -s\omega_{34} \\ -\omega_{14} & -\omega_{24} & -\omega_{34} & 0 \\ -\omega_{14} & -s\omega_{12} - \omega_{24} & -s\omega_{13} - \omega_{34} & -s\omega_{14} \\ -\omega_{12} - \omega_{13} & \omega_{12} - \omega_{23} & \omega_{13} + \omega_{23} & \omega_{14} + \omega_{24} + \omega_{34} \end{pmatrix}. \tag{3.3.24}$$

Eq. (3.3.23) implies

$$\bar{\omega}_k{}^j = 0 \quad \text{if } k = 1, 2, 3,\ j \neq k, 1 \leq j \leq 4\,, \tag{3.3.25}$$

i.e., the non-diagonal entries have to vanish in all but the last rows. This gives four independent homogeneous linear constraints on the six possible components of the antisymmetric matrix ω,

$$\begin{aligned} \omega_{14} = \omega_{34} &= 0\,, \\ -s\omega_{12} - \omega_{24} &= 0\,, \\ s\omega_{23} - \omega_{24} &= 0\,. \end{aligned} \tag{3.3.26}$$

The two independent solutions are

$$\omega^{(1)} = \begin{pmatrix} 0 & -1 & 0 & 0 \\ 1 & 0 & 1 & s \\ 0 & -1 & 0 & 0 \\ 0 & -s & 0 & 0 \end{pmatrix}, \qquad \omega^{(2)} = \begin{pmatrix} 0 & 0 & 1 & 0 \\ 0 & 0 & 0 & 0 \\ -1 & 0 & 0 & 0 \\ 0 & 0 & 0 & 0 \end{pmatrix}, \tag{3.3.27}$$

under which the IBP matrix in Eq. (3.3.24) becomes

$$\bar{\omega}^{(1)} = \begin{pmatrix} 0 & 0 & 0 & 0 \\ 0 & -s & 0 & 0 \\ 0 & 0 & 0 & 0 \\ 1 & -2 & 1 & s \end{pmatrix}, \qquad \bar{\omega}^{(2)} = \begin{pmatrix} s & 0 & 0 & 0 \\ 0 & 0 & 0 & 0 \\ 0 & 0 & -s & 0 \\ -1 & 0 & 1 & 0 \end{pmatrix}, \tag{3.3.28}$$

respectively. To compute IBP relations, the IBP vector (3.3.20) acts on (YX_k) as

$$\begin{aligned} \Delta_\omega(YX_k) &= \frac{1}{2}\omega^{ij}u(X_i,X_j)(YX_k) = \omega^{ij}(X_iY)(X_jX_k) = -g_{kj}\omega^{ji}(YX_i) \\ &= -\bar{\omega}_k{}^i(YX_i), \end{aligned} \tag{3.3.29}$$

where we used the antisymmetry of ω, and $u(X_i, X_j)$ is defined in Eq. (3.2.38). In terms of matrix components $\bar{\omega}_i{}^j$ that are nonvanishing for either solution, the resulting IBP relation is,

$$\begin{aligned} 0 &= \int \frac{d^{d+2}Y\,\delta(Y^2/2)}{\mathrm{Vol}(\mathrm{GL}(1))}\,\Delta_\omega\left(\frac{(-1)^3}{(YI)^{d-3}(YX_1)(YX_2)(YX_3)}\right) \\ &= \int \frac{d^{d+2}Y\,\delta(Y^2/2)}{\mathrm{Vol}(\mathrm{GL}(1))}\,\frac{(-1)^3}{(YI)^{d-3}(YX_1)(YX_2)(YX_3)}\left\{\left[\left(\sum_{i=1}^{3}\bar{\omega}_i{}^i\right)+(d-3)\bar{\omega}_4{}^4\right]\right. \\ &\qquad\qquad \left. +\frac{1}{(YI)}\left[(d-3)\sum_{i=1}^{3}\bar{\omega}_4{}^i(YX_i)\right]\right\} \\ &= \int d^dl\,\frac{1}{\Delta_1\Delta_2\Delta_3}\left\{\left[\left(\sum_{i=1}^{3}\bar{\omega}_i{}^i\right)+(d-3)\bar{\omega}_4{}^4\right]-(d-3)(\bar{\omega}_4{}^1\Delta_1+\bar{\omega}_4{}^2\Delta_2+\bar{\omega}_4{}^3\Delta_3)\right\} \\ &= \int d^dl\,\frac{1}{\Delta_1\Delta_2\Delta_3}\left\{\left[\left(\sum_{i=1}^{3}\bar{\omega}_i{}^i\right)+(d-3)\bar{\omega}_4{}^4\right]-(d-3)\bar{\omega}_4{}^2\Delta_2\right\}, \end{aligned} \tag{3.3.30}$$

where on the last line we dropped the contributions proportional to Δ_1 and Δ_3 because those generate scaleless bubble integrals that vanish in dimensional regularization.

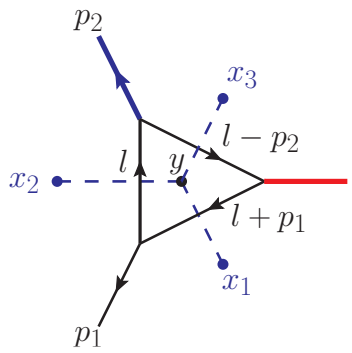

Figure 3.3: The one-loop triangle with outgoing external momenta p_1, p_2, $-p_1 - p_2$. All internal propagators are massless, and the massive external legs, shown as thick lines, have masses $p_2^2 = t$ and $(-p_1 - p_2)^2 = s$. The dashed (blue) line indicates the dual diagram.

Substituting the first solution for $\bar{\omega}$ in Eq. (3.3.28) ,

$$\bar{\omega}_1^{(1)1} = \bar{\omega}_3^{(1)3} = 0\,, \qquad \bar{\omega}_4^{(1)4} = -\bar{\omega}_2^{(1)2} = s, \qquad \bar{\omega}_4^{(1)2} = -2\,, \tag{3.3.31}$$

into Eq. (3.3.30) yields,

$$0 = s(d-4)I_{\text{tri}} + 2(d-3)I_{\text{bub}}^{(s)}\,, \tag{3.3.32}$$

reproducing Eq. (3.3.17).

For the second solution in Eq. (3.3.27), we have

$$\bar{\omega}_1^{(2)1} = -\bar{\omega}_3^{(2)3} = s\,, \qquad \bar{\omega}_2^{(1)2} = \bar{\omega}_4^{(1)4} = 0\,, \qquad \bar{\omega}_4^{(1)2} = 0\,, \tag{3.3.33}$$

so the IBP relation (3.3.30) is trivial because it involves only integrals that vanish in dimensional regularization.

As another example, consider the triangle with two external masses shown in Fig. 3.3. Following the same procedure as in the one-external-mass case, we introduce dual coordinates as usual

$$p_1 = x_2 - x_1\,, \qquad p_2 = x_3 - x_2\,, \qquad l = y - x_2\,. \tag{3.3.34}$$

Following a similar analysis as for the single-external-mass case, we find only a single solution

that leaves all the external momenta invariant. The associated IBP matrix is

$$\bar{\omega} = \begin{pmatrix} -(s-t) & 0 & 0 & 0 \\ 0 & -(s-t) & 0 & 0 \\ 0 & 0 & s-t & 0 \\ 2 & -2 & 0 & s-t \end{pmatrix}, \tag{3.3.35}$$

which encodes the action of the IBP-generating vector through Eq. (3.3.29). The resulting IBP relation, expressed in terms of the non-vanishing matrix components $\bar{\omega}_i{}^j$, is

$$\begin{aligned} 0 &= \int d^d l \frac{1}{\Delta_1 \Delta_2 \Delta_3} \left\{ \left[\sum_{i=1}^{3} \bar{\omega}_i{}^i + (d-3)\bar{\omega}_4{}^4 \right] - (d-3)\bar{\omega}_4{}^1 \Delta_1 - (d-3)\bar{\omega}_4{}^2 \Delta_2 - (d-3)\bar{\omega}_4{}^3 \Delta_3 \right\} \\ &= (d-4)(s-t) I^{(s,t)}_{\text{tri}} - 2(d-3) I^{(t)}_{\text{bub}} + 2(d-3) I^{(s)}_{\text{bub}} \,, \end{aligned} \tag{3.3.36}$$

where $I^{(s)}_{\text{bub}}$ is the bubble diagram obtained by canceling the propagator $l - q_2$, and $I^{(s)}_{\text{bub}}$ is the bubble diagram obtained by canceling the propagator $l - q_1$. When $t = 0$, $I^{(t)}_{\text{bub}}$ is a scaleless integral which vanishes in dimensional regularization, so the above IBP relation Eq. (3.3.36) becomes the same as the previous IBP relation Eq. (3.3.32) found for the triangle with only one massive external leg.

3.3.3 The Higgs to $b\bar{b}$ decay triangle

As a more sophisticated example to illustrate the use of dual conformal transformations in the presence of a mass, consider the one-loop triangle integral involved in the decay of the Higgs to a $b\bar{b}$ quark pair, with the bottom quark mass appearing in both internal and external lines, as depicted in Fig. 3.4. Internal masses are included in the embedding formalism, as described at the end of Section 3.2.5.

Introducing dual coordinates as usual, the three propagators are written as squared

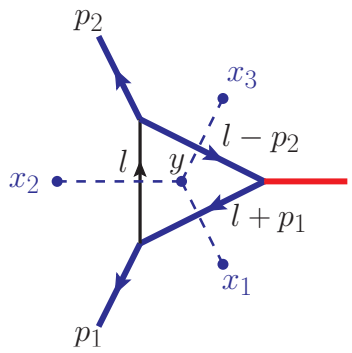

Figure 3.4: The one-loop triangle that appears in the decay of a Higgs boson to a $b\bar{b}$ quark pair. The outgoing external momenta are p_1, p_2, $-p_1 - p_2$. The Higgs leg, shown as a thick (red) line on the right-most part of the figure, has squared mass $(-p_1 - p_2)^2 = m_H^2$. The bottom-quark lines, appearing in both external legs and internal propagators, are shown as thick (blue) lines with squared mass m_b^2.

differences between dual coordinates,

$$\Delta_1 = (y - x_1)^2, \qquad \Delta_2 = (y - x_2)^2, \qquad \Delta_3 = (y - x_3)^2\,, \tag{3.3.37}$$

with gauge choice $x_2 = 0$, while the kinematic invariants are written as

$$x_2^2 = 0, \qquad x_1^2 = x_3^2 = m_b^2, \qquad (x_2 - x_1)^2 = (x_3 - x_2)^2 = m_b^2, \qquad (x_1 - x_3)^2 = m_H^2\,, \tag{3.3.38}$$

involving three massive external legs and two massive internal propagators. Eqs. (3.3.37) and (3.3.38) imply that

$$y \cdot x_1 = \frac{1}{2}(\Delta_2 - \Delta_1 + m_b^2)\,, \qquad y \cdot x_2 = 0\,, \qquad y \cdot x_3 = \frac{1}{2}(\Delta_2 - \Delta_3 + m_b^2)\,. \tag{3.3.39}$$

The embedding-space Gram matrix is, using the mapping Eq. (3.2.45) for the massive case

and identifying I with X_4,

$$g_{ij} = (X_i X_j) = \begin{pmatrix} 2m_b^2 & 0 & 2m_b^2 - m_H^2 & 1 \\ 0 & 0 & 0 & 1 \\ 2m_b^2 - m_H^2 & 0 & 2m_b^2 & 1 \\ 1 & 1 & 1 & 0 \end{pmatrix}. \tag{3.3.40}$$

Using the general algorithm illustrated in Subsection 3.3.2, there is only one solution to the antisymmetric matrix ω^{ij} such that the IBP vector

$$\frac{1}{2}\omega^{ij} u(X_i, X_j)\,, \tag{3.3.41}$$

leaves all external momenta invariant. The solution is

$$\omega = \begin{pmatrix} 0 & -1 & 0 & 0 \\ 1 & 0 & 1 & m_H^2 - 4m_b^2 \\ 0 & -1 & 0 & 0 \\ 0 & -(m_H^2 - 4m_b^2) & 0 & 0 \end{pmatrix}, \tag{3.3.42}$$

which gives the IBP matrix,

$$\bar{\omega} = \begin{pmatrix} 0 & 0 & 0 & 0 \\ 0 & -(m_H^2 - 4m_b^2) & 0 & 0 \\ 0 & 0 & 0 & 0 \\ 1 & -2 & 1 & (m_H^2 - 4m_b^2) \end{pmatrix}, \tag{3.3.43}$$

which encodes the action of the IBP-generating vector through Eq. (3.3.29). The resulting

IBP relation, expressed in terms of the matrix components $\bar{\omega}_i{}^j$, is

$$
\begin{aligned}
0 &= \int d^d l \, \frac{1}{\Delta_1 \Delta_2 \Delta_3} \left\{ \left[\left(\sum_{i=1}^{3} \bar{\omega}_i{}^i \right) + (d-3) \bar{\omega}_4{}^4 \right] - (d-3) \bar{\omega}_4{}^1 \Delta_1 - (d-3) \bar{\omega}_4{}^2 \Delta_2 - (d-3) \bar{\omega}_4{}^3 \Delta_3 \right\} \\
&= (d-4)(m_H^2 - 4m_b^2) I_{\text{tri}}^{H b \bar{b}} + 2(d-3) I_{\text{bub}}^{(H)} - 2(d-3) I_{\text{bub}}^{(b)} \,, \qquad (3.3.44)
\end{aligned}
$$

where $I_{\text{tri}}^{H b \bar{b}}$ is the scalar triangle diagram, $I_{\text{bub}}^{(H)}$ is the bubble sub-diagram obtained by canceling the propagator with momentum l, and $I_{\text{bub}}^{(b)}$ is the bubble sub-diagram obtained by canceling either the propagator with momentum $l + p_1$ or the one with momentum $l - p_2$. The IBP relation for the one-external-mass triangle (3.3.32) can be reproduced from the above IBP relation (3.3.44) by setting $m_H^2 = s$, $m_b^2 = 0$.

For higher-loop planar integrals with up to four external legs of any topology, the algorithm presented above can be adapted to find nontrivial dual conformal transformations that leave all the external momenta invariant. We start with the embedding-space Gram matrix for the specific integral topology as in Eq. (3.3.22), with X_{N+1} defined to be equal to I. Then we repeat the subsequent calculations to produce the IBP matrix as in Eq. (3.3.24), leading to homogeneous linear constraints as in Eq. (3.3.25). Solving the linear constraints gives the IBP vectors and relations. As discussed in the previous subsection, for any solution of the antisymmetric matrix ω that has a vanishing last column, we will obtain IBP relations that only involve integrals with canceled propagators. Therefore such solutions may be discarded if we are interested in the IBP reduction of top-level integrals. In the next section we will describe another class of useful dual conformal transformations orthogonal to all external momenta, which will be useful at higher loops.

3.4 IBP for planar two-loop integrals

In this section we discuss the more interesting case of higher-loop integrals. With generic mass configurations (e.g. with all external and internal masses being different from each

other), a complete set of IBP-generating vectors is tabulated in Ref. [33]. Here we apply dual conformal symmetry to uncover extra IBP-generating vectors for planar two-loop integrals with massless lines. In Section 3.6 we will extend this to the nonplanar case.

3.4.1 Conformal transformations in transverse dimensions

In the direct treatment of Section 3.3.1, the parameter of the conformal boost in Eq. (3.3.11), with x_i^μ given in Eq. (3.3.5), is a linear combination of external momenta. However, another interesting possibility is a conformal boost in a direction orthogonal to all external momenta, which gives unitarity-compatible IBP-generating vectors for *every* planar integral at any loop order.

Consider a general L-loop N-point diagram. For a planar N-point diagram at L loops, we take the dual coordinates to be $x_1, x_2, \ldots, x_N$. It is easy to fix the translation gauge freedom such that every x_i^μ is written as a linear combination of the external momenta p_i^μ. (For example, if we fix $x_1 = 0$, then $x_i = \sum_{j=1}^{i-1} p_j$.) In Eq. (3.2.22), we choose the conformal-boost parameter b^μ to be any vector that is orthogonal to all external momenta, and do not include a scaling transformation (i.e. setting $\beta = 0$). This gives $\Delta(x_i - x_j)^2 = 0$ for all pairs of i, j, which means all Mandelstam variables are left invariant. Therefore it is always possible to keep each individual external momentum invariant by adding a compensating Lorentz transformation.

In the planar case, the $\mathrm{SO}(d, 2)$ embedding formalism gives a convenient way of proceeding. This eliminates the need to fix a gauge for the translation degrees of freedom of the dual coordinates. For illustration, we focus on $d = 4 - 2\epsilon$ dimensional loop integrals with N external momenta, where $N \leq 5$. Generally, the embedding-space reference points $X_1, X_2, \ldots, X_N$ and the point at infinity I together span $N + 1$ "physical" dimensions, leaving an orthogonal "transverse" space of dimension $(d + 2) - (N + 1) = d - (N - 1)$. This directly corresponds to the subspace of ordinary $\mathrm{SO}(d - 1, 1)$ spacetime orthogonal to the

$N-1$ dimensions spanned by the external momenta.[1] In addition, in the $(N+1)$-dimensional "physical" space spanned by $X_1, X_2, \ldots, X_N, I$, one can always find one vector $\tilde{I}$ that satisfies the N conditions,

$$(\tilde{I} X_i) = 0, \quad 1 \leq i \leq N\,. \tag{3.4.1}$$

In particular, if the top-left $N \times N$ sub-block $\tilde{g}_{ij} = (X_i X_j)$ of the embedding-space Gram matrix is non-singular, then the above $\tilde{I}$ can be found by projecting I onto the space orthogonal $X_1, X_2, \ldots X_N$,

$$\tilde{I}^a = I^a - (I X_i)(\tilde{g}^{-1})_{ij} X_j^a\,. \tag{3.4.2}$$

We can also define a set of vectors that span the transverse space. Let N_k, with $1 \leq k \leq d+1-N$, be an orthonormal basis of this orthogonal space. The $\mathrm{SO}(d,2)$ Lorentz transformations in Eq. (3.2.36), with $Z_i = \tilde{I}$ and $Z_j = N_k$ for any $1 \leq k \leq d+1-N$, leave all $X_j\,(1 \leq j \leq N)$ invariant, since it only acts in the transverse space. So we obtain a valid unitarity-compatible IBP-generating vector

$$u(\tilde{I}, N_k) = \sum_A \left[(\tilde{I}\, Y_A) \left(N_k \frac{\partial}{\partial Y_A} \right) - (N_k\, Y_A) \left(\tilde{I} \frac{\partial}{\partial Y_A} \right) \right], \tag{3.4.3}$$

following the notation of the one-loop version in Eq. (3.2.38). However, the IBP relation from the multi-loop version of Eq. (3.2.37),

$$0 = \int \left(\prod_A \frac{d^{d+2} Y_A\, \delta(Y_A^2/2)}{\mathrm{Vol}(\mathrm{GL}(1))} \right) u(\tilde{I}, N_k)\, \mathcal{I}\,, \tag{3.4.4}$$

breaks the Lorentz symmetry in the $d-(N+1)$-dimensional transverse space, since it introduces vectors N_k not present in the original problem, so it is not ideal. A remedy is to contract the Lorentz indices to give IBP-generating vectors that are invariant under the Lorentz symmetry of the transverse directions. We can write down the following L different

[1] For example, for a five-point diagram, with dimensional regularization the transverse space has dimension $4 - 2\epsilon - (5-1) = -2\epsilon$.

vectors,

$$\frac{1}{(-Y_B I)}(N_k Y_B) u(\tilde{I}, N_k) = u\left(\tilde{I}, \frac{\tilde{Y}_{B\perp}}{(-Y_B I)}\right), \tag{3.4.5}$$

where the index k is summed and $1 \leq B \leq L$ specifies one of the independent loop momentum. The label B is not summed in Eq. (3.4.5). The contraction over the index k ensures Lorentz invariance in the transverse directions, while the normalization factor $1/(-Y_B I)$ ensures GL(1) gauge invariance. $Y_{B\perp}$ is the projection of Y_B onto the transverse space, using the inverse of the $(N+1)\times(N+1)$ Gram matrix $g_{ij} = (X_i X_j)$ with $X_{N+1} \equiv I$,

$$Y^a_{B\perp} = (N_k Y_B) N^a_k = Y^a_B - (Y_B X_i) g^{-1}_{ij} X^a_j \,. \tag{3.4.6}$$

This results in the IBP relations (see Eq. (3.2.44) for the one-loop analog),

$$0 = \int \left(\prod_A \frac{d^{d+2} Y_A \, \delta(Y_A^2/2)}{\mathrm{Vol}(\mathrm{GL}(1))}\right) \sum_A \left[(\tilde{I}\, Y_A)\, \left(N_k \frac{\partial}{\partial Y_A}\right) - (N_k\, Y_A) \left(\tilde{I}\, \frac{\partial}{\partial Y_A}\right)\right] \left(\frac{(N_k Y_B)}{(-Y_B I)} \mathcal{I}\right), \tag{3.4.7}$$

where there is implicit summation over k, and B is a fixed loop label $1, 2, \ldots, L$.

The right-hand side of Eq. (3.4.5) is an example of an IBP-generating vector defined using reference vectors with dependence on loop momenta. The IBP relation from such a vector is a superposition of familiar $\mathrm{SO}(d,2)$ Lorentz symmetry identities, as in Eq. (3.4.7). IBP relations are obtained from the vector in explicit components,

$$u\left(\tilde{I}, \frac{\tilde{Y}_{B\perp}}{(-Y_B I)}\right) = \left(\frac{(\tilde{I} Y_A)}{(-Y_B I)} \tilde{Y}^a_{B\perp} - \frac{(\tilde{Y}_{B\perp} Y_A)}{(-Y_B I)} \tilde{I}^a\right) \frac{\partial}{\partial Y^a_A} \,, \tag{3.4.8}$$

then calculating the total divergence, as in Eq. (3.2.44). As before, in this expression A is summed over but B is not.

Since the IBP relations we derived earlier already suffice to reduce the triangle integrals to bubble integrals, we do not need the additional IBP relations coming from the transverse space.[2] But these relations are needed at the two-loop level.

[2] These additional IBP relations in fact vanish on the maximal cut, for the three different triangle integrals

3.4.2 Global and loop-by-loop conformal transformations

Now consider Lorentz transformations in the embedding space that affect the external momenta. To simplify the discussion we focus on two loops. We trivially extend the definition of the infinitesimal Lorentz transformation in Eq. (3.2.38) to simultaneously transform both Y_1 and Y_2,

$$u_{12}(Z_i, Z_j) = \sum_{A=1}^{2} u_A(Z_i, Z_j) = \sum_{A=1}^{2} (Z_{[i}\, Y_A) \left(Z_{j]}\, \frac{\partial}{\partial Y_A} \right). \tag{3.4.9}$$

Similarly, we will define loop-by-loop Lorentz transformations, namely

$$u_1(Z_i, Z_j), \quad u_2(Z_i, Z_j) \tag{3.4.10}$$

acting only on Y_1 and only on Y_2, respectively. For appropriate Z_i and Z_j, $u_{12}(Z_i, Z_j)$ can be considered a global $\mathrm{SO}(d, 2)$ transformation (instead of acting only on the loop momentum points) that leaves all the external momenta invariant, so that Eq. (3.4.9) is a two-loop IBP-generating vector that does not lead to propagators raised to higher powers. The situation is entirely analogous to the one-loop case, and allows one-loop IBP-generating vectors to be reused at higher loops. A difference from the one-loop case is that we need the IBP-generating vectors arising from transverse directions, as explained in Section 3.4.1, which may be considered as loop-momentum-dependent global conformal transformations.

For some of the more complicated two-loop integral topologies such as the penta-box discussed in Subsection 3.4.5, IBP-generating vectors from global conformal transformations are *not* sufficient. To deal with this, we construct a class of loop-by-loop unitarity-compatible IBP-generating vectors. Consider the inverse propagators,

$$-\frac{(Y_1 X_i)}{(Y_1 I)}, \quad -\frac{(Y_2 X_j)}{(Y_2 I)}, \quad \frac{(Y_1 Y_2)}{(Y_1 I)(Y_2 I)}, \quad \text{with } i \in \sigma_1, \quad j \in \sigma_2\,, \tag{3.4.11}$$

where σ_1 and σ_2 are both subsets of $\{1, 2, \ldots, N\}$. If an $\mathrm{SO}(d, 2)$ transformation parametrized

considered in the previous section.

by the antisymmetric matrix $\omega^{ij}_{(1)}$ leaves all the X_i points ($i \in \sigma_1$) invariant, the action of the transformation on Y_1 alone gives the IBP-generating vector

$$V_1^a \frac{\partial}{\partial Y_1^a} = \frac{1}{2}\omega^{ij}_{(1)} u_1(X_i, X_j)\,, \tag{3.4.12}$$

which does not raise the power of any propagator denominator of the form $-(Y_1 X_i)/(Y_1 I)$. The vector also does not raise the power of any propagator denominator of the form $-(Y_2 X_j)/(Y_2 I)$ because the vector does not involve derivatives with respect to the second loop momentum. However, the vector may double the power of the propagator denominator $\Delta_c \equiv -(Y_1 Y_2)/(Y_1 I)(Y_2 I)$, so this is not yet a valid unitarity-compatible vector.

Similarly, if a conformal transformation parametrized by $\omega^{ij}_{(2)}$ leaves all the X_j points with $j \in \sigma_2$ invariant, we can write down an IBP-generating vector

$$V_2^a \frac{\partial}{\partial Y_2^a} = \frac{1}{2}\omega^{ij}_{(2)} u_2(X_i, X_j)\,, \tag{3.4.13}$$

which again does not increase the power of any propagator denominator except for Δ_c. Our final IBP-generating vector, to be denoted by $\mathrm{cross}(V_1, V_2)$, is

$$\begin{aligned}\mathrm{cross}(V_1^a \partial_{1\,a}, V_2^a \partial_{2\,a}) &= \frac{1}{(Y_1 I)(Y_2 I)} \left\{ \left[V_1^b \frac{\partial}{\partial Y_1^b}(Y_1 Y_2) \right] V_2^a \frac{\partial}{\partial Y_2^a} - \left[V_2^b \frac{\partial}{\partial Y_2^b}(Y_1 Y_2) \right] V_1^a \frac{\partial}{\partial Y_1^a} \right\} \\ &= \frac{1}{(Y_1 I)(Y_2 I)} \left\{ (V_1 Y_2) V_2^a \frac{\partial}{\partial Y_2^a} - (V_2 Y_1) V_1^a \frac{\partial}{\partial Y_1^a} \right\}, \end{aligned} \tag{3.4.14}$$

where the overall prefactor $1/((Y_1 I)(Y_2 I))$ is needed for GL(1) gauge invariance. This is designed to annihilate $(Y_1 Y_2)$. As a result, this IBP-generating vector does not raise the power of the propagator denominator Δ_c. To see this, in Eq. (3.2.4) we have

$$\mathcal{W}_c = \frac{\mathrm{cross}(V_1^a \partial_{1\,a}, V_2^a \partial_{2\,a})\rho_c}{\rho_c} = -\frac{\mathrm{cross}(V_1^a \partial_{1\,a}, V_2^a \partial_{2\,a})\big((Y_1 I)(Y_2 I)\big)}{(Y_1 I)(Y_2 I)}\,, \tag{3.4.15}$$

which evaluates to an expression with polynomial dependence on loop momenta, because

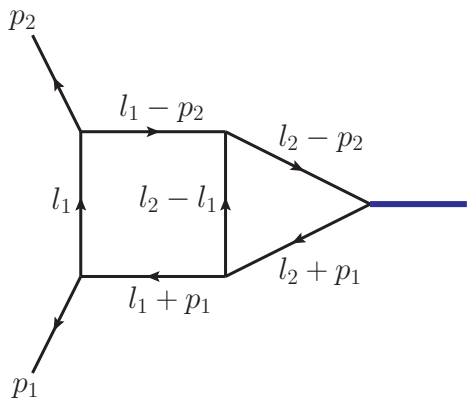

Figure 3.5: The triangle-box diagram.

the gauge $(Y_1 I) = (Y_2 I) = 1$ eliminates the denominators.

3.4.3 The triangle-box

As an explicit example, consider the two-loop triangle-box diagram shown in Fig. 3.5. The inverse propagators are

$$\begin{aligned} &\Delta_1 = (l_1 + p_1)^2, \qquad \Delta_2 = l_1^2, \qquad \Delta_3 = (l_1 - p_2)^2, \\ &\Delta_4 = (l_2 + p_1)^2, \qquad \Delta_5 = (l_2 - p_2)^2, \qquad \Delta_6 = (l_2 - l_1)^2 , \end{aligned} \tag{3.4.16}$$

while an "irreducible numerator", which cannot be written as a linear combination of inverse propagators, is

$$\Delta_7 = l_2^2 . \tag{3.4.17}$$

Notice that l_2 is not the momentum of any propagator, due to our choice of momentum routing. The external kinematic invariants are identical to those of the one-loop triangle with one external mass in Section 3.3,

$$p_1^2 = p_2^2 = 0, \quad (p_1 + p_2)^2 = s . \tag{3.4.18}$$

Introducing dual coordinates as usual, the six inverse propagators and one irreducible numerator become

$$\begin{aligned}
&\Delta_1 = (y_1 - x_1)^2, \quad \Delta_2 = (y_1 - x_2)^2, \quad \Delta_3 = (y_1 - x_2)^2, \\
&\Delta_4 = (y_2 - x_1)^2, \quad \Delta_5 = (y_2 - x_3)^2, \quad \Delta_6 = (y_2 - y_1)^2, \quad \Delta_7 = (y_2 - x_2)^2 \,,
\end{aligned} \tag{3.4.19}$$

with the kinematic invariants written as

$$(x_2 - x_1)^2 = (x_3 - x_2)^2 = 0, \quad (x_3 - x_1)^2 = -s \,. \tag{3.4.20}$$

The triangle-box integral, with the irreducible numerator Δ_7 raised to the m-th power, is written as

$$\begin{aligned}
I_m^{\text{tri-box}} &= \int d^d l_1 \int d^d l_2 \frac{\Delta_7^m}{\Delta_1 \Delta_2 \Delta_3 \Delta_4 \Delta_5 \Delta_6} \\
&= \int \frac{d^{d+2} Y_1 \, \delta(Y_1^2/2)}{\text{Vol}(\text{GL}(1))} \int \frac{d^{d+2} Y_2 \, \delta(Y_2^2/2)}{\text{Vol}(\text{GL}(1))} \\
&\quad \times \frac{(-1)^{6+m} (Y_2 X_2)^m}{(Y_1 I)^{d-4} (Y_2 I)^{d-3+m} (Y_1 X_1)(Y_1 X_2)(Y_1 X_3)(Y_2 X_1)(Y_2 X_3)(Y_1 Y_2)} \,.
\end{aligned} \tag{3.4.21}$$

Since the external momenta are identical to those for the one-loop triangle, the same subgroup of conformal transformations in dual space leaves the external momenta invariant. Therefore, we can reuse the IBP-generating vectors for the one-loop triangle. The IBP-generating vector is parametrized as

$$\frac{1}{2} \omega^{ij} u_{12}(X_i, X_j) = \sum_{A=1}^{2} \omega^{ij} (X_i Y_A) X_j^a \frac{\partial}{\partial Y_A^a} \,, \tag{3.4.22}$$

which differs from the corresponding one-loop expression (3.3.20) only by an additional summation over the loop label A. We reuse the first solution $\omega_{(1)}$ for the antisymmetric matrix ω^{ij} in Eq. (3.3.27) found at one loop. The action of the IBP-generating vector is a

straightforward generalization of the one-loop expression (3.3.29),

$$\begin{aligned}
&\Delta_{\omega(1)}(Y_A X_1) = \Delta_{\omega(1)}(Y_A X_3) = 0,\\
&\Delta_{\omega(1)}(Y_A X_2) = s(Y_A X_2),\\
&\Delta_{\omega(1)}(Y_A I) = -\left[(Y_A X_1) - 2(Y_A X_2) + (Y_A X_3)\right] - s(Y_A I),\\
&\Delta_{\omega(1)}(Y_1 Y_2) = 0\,.
\end{aligned} \tag{3.4.23}$$

Other than the appearance of the loop label A which may be either 1 or 2, the only difference from the one-loop expression is the last line, namely the trivial statement that $(Y_1 Y_2)$ is invariant under simultaneous Lorentz transformations of Y_1 and Y_2.

IBP relations can be computed in a way similar to how it is done at one loop in Eq. (3.3.32), in terms of the non-vanishing components of the first solution for $\bar{\omega}$ in Eq. (3.3.28),

$$\begin{aligned}
0 &= \int \frac{d^{d+2}Y_1\,\delta(Y_1^2/2)}{\mathrm{Vol}(\mathrm{GL}(1))} \int \frac{d^{d+2}Y_2\,\delta(Y_2^2/2)}{\mathrm{Vol}(\mathrm{GL}(1))}\\
&\quad \times \Delta_{\omega(1)} \frac{(-1)^{6+m}(Y_2X_2)^m}{(Y_1I)^{d-4}(Y_2I)^{d-3+m}(Y_1X_1)(Y_1X_2)(Y_1X_3)(Y_2X_1)(Y_2X_3)(Y_1Y_2)}\\
&= \int \frac{d^{d+2}Y_1\,\delta(Y_1^2/2)}{\mathrm{Vol}(\mathrm{GL}(1))} \int \frac{d^{d+2}Y_2\,\delta(Y_2^2/2)}{\mathrm{Vol}(\mathrm{GL}(1))}\\
&\quad \times \frac{(Y_2X_2)^m}{(Y_1I)^{d-4}(Y_2I)^{d-3+m}(Y_1X_1)(Y_1X_2)(Y_1X_3)(Y_2X_1)(Y_2X_3)(Y_1Y_2)}\\
&\quad \times \Bigg\{(-1)^{6+m}\left[-\bar{\omega}_2{}^2(m-1) + (d-4)\bar{\omega}_4{}^4 + (d-3+m)\bar{\omega}_4{}^4\right]\\
&\quad +(-1)^{5+m}\left[-\frac{(d-4)}{(Y_1I)}\left(\sum_{i=1}^{3}\bar{\omega}_4{}^i(Y_1X_i)\right) - \frac{(d-3+m)}{(Y_2I)}\left(\sum_{i=1}^{3}\bar{\omega}_4{}^i(Y_2X_i)\right)\right]\Bigg\}\,.
\end{aligned} \tag{3.4.24}$$

It is illuminating to look at Eq. (3.4.24) on the maximal cut of the triangle-box, which sets

$$(Y_1X_1) = (Y_1X_2) = (Y_1X_3) = (Y_2X_1) = (Y_2X_3) = (Y_1Y_2) = 0\,. \tag{3.4.25}$$

After translating Eq. (3.4.24) back to $\mathrm{SO}(d-1,1)$ loop-momentum space, imposing the

maximal cut, and substituting $\bar{\omega}_i{}^j$ for their explicit values, we obtain

$$0 = 2(d-4+m)s\, I_m^{\text{tri-box}} + 2(d-3+m) I_{m+1}^{\text{tri-box}} + \text{ daughter integrals}, \tag{3.4.26}$$

using the notation of Eq. (3.4.21) and "daughter integrals" refer to integrals where some of the triangle-box propagators are canceled. This is a recursion relation which reduces all the triangle-box integrals to the scalar integral $I_0^{\text{tri-box}}$ and integrals with canceled propagators.

We will further show that the scalar triangle-box integral is also reducible to integrals with canceled propagators, by constructing another IBP relation using transformations in the transverse directions as explained in Subsection 3.4.1. We define

$$\tilde{I} = X_2\,, \tag{3.4.27}$$

which satisfies Eq. (3.4.1) and also define $Y_{1\perp}$ according to Eq. (3.4.6) with B set to 1,

$$Y_{1\perp}^a = Y_1^a - (Y_1 X_i) g_{ij}^{-1} X_j^a\,, \tag{3.4.28}$$

which is the projection of Y_1 onto the transverse space orthogonal to X_1, X_2, X_3, I. Using the IBP-generating vector Eq. (3.4.5) with $B = 2$,

$$\frac{-1}{(Y_1 I)} u_{12}(\tilde{I}, \tilde{Y}_{1\perp})\,, \tag{3.4.29}$$

the IBP relations can be written down as a total divergence as in Eq. (3.2.44) (but generalized to more than one loop by trivially adding a summation over loop labels 1 and 2), with $\mathcal{I}$ set to

$$\mathcal{I} = \frac{(-1)^6 s}{(Y_1 I)^{d-4}(Y_2 I)^{d-3}(Y_1 X_1)(Y_1 X_2)(Y_1 X_3)(Y_2 X_1)(Y_2 X_3)(Y_1 Y_2)}\,. \tag{3.4.30}$$

Explicit calculation gives the IBP relation, again dropping terms that vanish on the maximal

cut for the purpose of illustration,

$$0 = -(d-3)s\, I_0^{\text{tri-box}} + \text{daughter integrals}\,. \tag{3.4.31}$$

Combined with the recursion relation Eq. (3.4.26), this shows that all triangle-box integrals can be reduced to zero on the maximal cut. In other words, all these integrals can be reduced to integrals with canceled propagators, if we retain all terms proportional to inverse propagators in the calculation of the IBP relations.

3.4.4 The double box

Consider now the two-loop double-box integral in Fig. 3.1. The inverse propagators with the assigned momentum labels are

$$\begin{aligned}
&\Delta_1 = l_1^2\,, \qquad \Delta_2 = (l_1 - p_1)^2\,, \qquad \Delta_3 = (l_1 - p_1 - p_2)^2\,, \qquad \Delta_4 = (l_2 - p_1 - p_2)^2\,, \\
&\Delta_5 = (l_2 + p_4)^2, \qquad \Delta_6 = l_2^2\,, \qquad \Delta_7 = (l_2 - l_1)^2\,,
\end{aligned} \tag{3.4.32}$$

while a choice of irreducible numerators is

$$\Delta_8 = (l_1 + p_4)^2\,, \qquad \Delta_9 = (l_2 - p_1)^2\,. \tag{3.4.33}$$

To write every inverse propagator in the dual-space form, as either $(y_1 - y_2)^2$ or $(y_A - x_j)^2$, we define the $\mathrm{SO}(d-1,1)$ dual coordinates x_j and y_A such that

$$\begin{aligned}
&x_2^\mu - x_1^\mu = p_1^\mu\,, \qquad x_3^\mu - x_2^\mu = p_2^\mu\,, \qquad x_4^\mu - x_3^\mu = p_3^\mu\,, \qquad x_1^\mu - x_4^\mu = p_4^\mu\,, \\
&y_1^\mu - x_1^\mu = l_1^\mu\,, \qquad y_2^\mu - x_1^\mu = l_2^\mu\,.
\end{aligned} \tag{3.4.34}$$

under which the seven inverse propagators become

$$\Delta_1 = (y_1 - x_1)^2\,, \qquad \Delta_2 = (y_1 - x_2)^2\,, \qquad \Delta_3 = (y_1 - x_3)^2\,, \qquad \Delta_4 = (y_2 - x_3)^2\,,$$
$$\Delta_5 = (y_2 - x_4)^2\,, \qquad \Delta_6 = (y_2 - x_1)^2\,, \qquad \Delta_7 = (y_2 - y_1)^2\,, \tag{3.4.35}$$

and the two irreducible numerators become

$$\Delta_8 = (y_1 - x_4)^2\,, \qquad \Delta_9 = (y_2 - x_2)^2\,. \tag{3.4.36}$$

A convenient visualization of the dual points is shown in Fig. 3.1. In terms of these quantities, we define the planar double-box integrand as

$$\Omega_1^{\rm P} = d^d l_1 d^d l_2 \frac{st}{\Delta_1 ... \Delta_7}\,. \tag{3.4.37}$$

where

$$s = (p_1 + p_2)^2 = (x_1 - x_3)^2\,, \qquad t = (p_2 + p_3)^2 = (x_2 - x_4)^2\,, \tag{3.4.38}$$

are Mandelstam invariants needed to cancel overall conformal weights.

As usual for planar integrals, we map the dual coordinates y_A^μ and x_j^μ to $\mathrm{SO}(d,2)$ embedding-space points Y_A and X_j, following Eqs. (3.2.31) and (3.2.32). If we use the algorithm presented in Section 3.3.2 to find infinitesimal $\mathrm{SO}(d,2)$ Lorentz transformations that leave all X_j invariant, we find two such transformations in the notation of Eq. (3.2.38):

$$u_{12}(X_1, X_3), \qquad u_{12}(X_2, X_4)\,, \tag{3.4.39}$$

following the notation of Eq. (3.4.9). For the one-loop box diagram, both transformations vanish on the maximal cut because $(YX_i) = 0$, $1 \le i \le 4$. But for the two-loop double-box topology, $(Y_1 X_4)$ and $(Y_2 X_2)$ are proportional to the irreducible numerators, so the

IBP-generating vector,

$$u_{12}(X_2, X_4)\,, \tag{3.4.40}$$

still gives an IBP-generating vector that does not vanish on the maximal cut. Eq. (3.4.40) is essentially the same as the first IBP-generating vector for the double box in Ref. [31] obtained using computational algebraic geometry. There is another IBP-generating vector for the double box following the discussion of Subsection 3.4.1. We define another $\mathrm{SO}(d,2)$ embedding-space point $Y_{1\perp}$,

$$Y_{1\perp}^a = Y_1^a - (Y_1 X_i) g_{ij}^{-1} X_j^a\,, \tag{3.4.41}$$

where as usual, $g_{ij} = (X_i X_j)$ is the embedding-space Gram matrix, with X_5 identified with I. We also define the $\mathrm{SO}(d,2)$ embedding-space point $\tilde{I}$,

$$\tilde{I}^a = s(X_2^a + X_4^a) + t(X_1^a + X_3^a) + st\, I^a\,, \tag{3.4.42}$$

which is the same as Eq. (3.4.2) but with an extra overall factor st, and satisfies Eq. (3.4.1). Using the IBP-generating vector (3.4.5) with $B = 1$, we have

$$u_{12}(\tilde{I}, Y_{1\perp})\,. \tag{3.4.43}$$

We have checked using computer algebra that the two IBP-generating vectors, Eqs. (3.4.40) and (3.4.43), with all possible choices of numerators in $\mathcal{I}$ in the two-loop generalization of Eq. (3.2.44), generate a complete set of IBP relations that reduce all double-box tensor integrals to two double=box master integrals and daughter integrals (i.e., integrals with canceled propagators). It is worth noting that the two vectors we found are written down in a very compact form, whereas in Ref. [31] nearly one page is needed to display the vectors found from computational algebraic geometry.

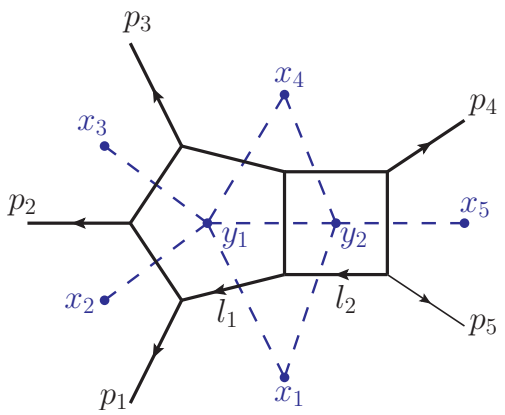

Figure 3.6: The penta-box integral.

3.4.5 The penta-box

As a more complex example consider the two-loop five-point penta-box shown in Fig. 3.6, along with dual coordinates x_i and y_A introduced as usual. There are five independent kinematic variables, which may be chosen as

$$s_{12}, s_{23}, s_{34}, s_{45}, s_{51}\,, \tag{3.4.44}$$

where $s_{ij} = (p_i + p_j)^2$. The embedding-space Gram matrix is, identifying I with X_6,

$$g_{ij} = (X_i X_j) = \begin{pmatrix} 0 & 0 & -s_{12} & -s_{45} & 0 & 1 \\ 0 & 0 & 0 & -s_{23} & -s_{51} & 1 \\ -s_{12} & 0 & 0 & 0 & -s_{34} & 1 \\ -s_{45} & -s_{23} & 0 & 0 & 0 & 1 \\ 0 & -s_{51} & -s_{34} & 0 & 0 & 1 \\ 1 & 1 & 1 & 1 & 1 & 0 \end{pmatrix}. \tag{3.4.45}$$

With $\tilde{I}$ defined as in Eq. (3.4.2), we obtain two IBP-generating vectors from conformal transformations in transverse directions, by setting $B = 1, 2$ in Eq. (3.4.5),

$$u\left(\tilde{I}, \frac{\tilde{Y}_{1\perp}}{(-Y_1 I)}\right), \tag{3.4.46}$$

$$u\left(\tilde{I}, \frac{\tilde{Y}_{2\perp}}{(-Y_2 I)}\right) . \tag{3.4.47}$$

Next, we examine conformal transformations which do not explicitly involve transverse directions. As in Eq. (3.3.19), we write down a conformal transformation parametrized as

$$\Delta_\omega Z^a = \sum_{1\le i,j\le 6} (ZX_i)\omega^{ij} X_j^a \,, \tag{3.4.48}$$

where ω is a 6×6 antisymmetric matrix. Unlike the previous three-point and four-point examples in this chapter, we are not able to find a solution for ω^{ij} which leaves all external momenta invariant. However, all is not lost. As discussed in the latter half of Subsection 3.4.2, we can look for two different conformal transformations for the two sub-loops, and combine the two to give a unitarity-compatible IBP-generating vector.

We find one solution $\omega^{ij}_{(1)}$ which leaves x_1, x_2, x_3, x_4, or equivalently p_1, p_2, p_3, invariant, and three solutions $\omega^{ij}_{(2a)}, \omega^{ij}_{(2b)}, \omega^{ij}_{(2c)}$ which leave x_1, x_4, x_5, or equivalently p_4, p_5 invariant. These solutions are tabulated in Appendix 3.9.[3] Therefore, the following IBP-generating vectors do not increase the power of any propagator except the vertical central propagator in Fig. 3.6,

$$\begin{aligned} &\frac{1}{2}\omega^{ij}_{(1)} u_1(X_i, X_j), \quad \frac{1}{2}\omega^{ij}_{(2a)} u_2(X_i, X_j), \\ &\frac{1}{2}\omega^{ij}_{(2b)} u_2(X_i, X_j), \quad \frac{1}{2}\omega^{ij}_{(2c)} u_2(X_i, X_j) \,. \end{aligned} \tag{3.4.49}$$

These vectors can be combined to give IBP-generating vectors that do not increase the

[3] In quoting the number of solutions, we have ignored the solutions which ultimately do not lead to independent new IBP relations.

power of any propagator. Using the notation of Eqs. (3.4.12), (3.4.13) and (3.4.14), these IBP-generating vectors are

$$\begin{aligned}
&\text{cross}\left(\frac{1}{2}\omega^{ij}_{(1)}u_1(X_i,X_j),\frac{1}{2}\omega^{ij}_{(2a)}u_2(X_i,X_j)\right),\\
&\text{cross}\left(\frac{1}{2}\omega^{ij}_{(1)}u_1(X_i,X_j),\frac{1}{2}\omega^{ij}_{(2b)}u_2(X_i,X_j)\right),\\
&\text{cross}\left(\frac{1}{2}\omega^{ij}_{(1)}u_1(X_i,X_j),\frac{1}{2}\omega^{ij}_{(2c)}u_2(X_i,X_j)\right).
\end{aligned} \tag{3.4.50}$$

We have checked, using computer algebra, that the five IBP-generating vectors in Eqs. (3.4.46), (3.4.47) and (3.4.50) are sufficient to reduce all penta-box integrals to three master integrals. Again, the five vectors are given by compact analytic expressions, in contrast to lengthy expressions one generally finds using computational algebraic geometry.

This formalism generalizes straightforwardly, e.g. to the six-point case, although one would need to check that the IBP relations are complete for each individual diagram topology, which is left to future work.

3.5 Differential equations for planar integrals

In this section we briefly comment on applications of the ideas described in previous sections to constructing differential equations for integrals. An infinitesimal dual conformal transformation produces differential equations when we remove the restriction to the sub-algebra that keeps external legs invariant. We present a treatment in the embedding space, which simplifies the transformations and has the advantage that there is no need to fix the translation gauge for the dual coordinates. In the nonplanar case, covered in Section 3.6, where the transformations for some kinematic invariants become less obvious it will be simpler to use a "direct" treatment.

Consider the one-loop box, shown in Fig. 3.7 which has the same external momenta and the $\mathrm{SO}(d,2)$ points X_i as the double box in Section 3.4.4. Consider an infinitesimal $\mathrm{SO}(d,2)$

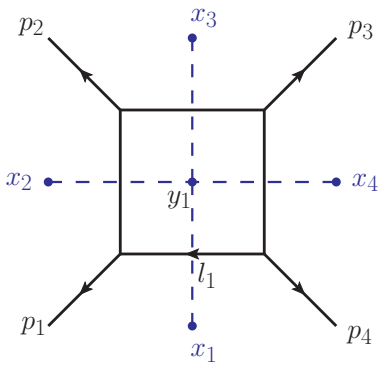

Figure 3.7: The one-loop box diagram and its dual diagram.

Lorentz transformation ΔZ given by

$$\Delta Z^a = (Z_1 Z) Z_2^a - (Z_2 Z) Z_1^a \,, \tag{3.5.1}$$

with parameters

$$Z_1 = X_2, \quad Z_2 = s\, I + (X_1 + X_3) \,, \tag{3.5.2}$$

which satisfies

$$\begin{aligned} &(Z_1 X_1) = (Z_1 X_2) = (Z_1 X_3) = 0, \quad (Z_1 X_4) = -t, \quad (Z_1 I) = 1 \\ &(Z_2 X_1) = (Z_2 X_3) = 0, \quad (Z_2 X_2) = (Z_2 X_4) = s, \quad (Z_2 I) = 2 \,. \end{aligned} \tag{3.5.3}$$

The transformation of the $\mathrm{SO}(d,2)$ points are

$$\begin{aligned} &\Delta X_1 = \Delta X_3 = 0, \quad \Delta X_2 = -s X_2 \,, \\ &\Delta X_4 = -t Z_2 - s Z_1 = -st\, I - t\, X_1 - t\, X_3 - s X_2 \,, \\ &\Delta Y = (Y X_2)(s\, I + X_1 + X_3) - s(Y I) X_2 - (Y X_1) X_2 - (Y X_3) X_2 \,, \end{aligned} \tag{3.5.4}$$

which shows X_1, X_2, and X_3 are invariant up to a GL(1) gauge scaling. In other words the d-dimensional dual coordinates x_1^μ, x_2^μ and x_3^μ are left invariant. The factor $(Y I)$, which

appears in the integration measure, transforms as

$$\Delta(YI) = (I\Delta Y) = 2(YX_2) - (YX_1) - (YX_3) - s(YI)\,. \tag{3.5.5}$$

As a result, $s = (x_1 - x_3)^2$ is invariant, while explicit calculation shows

$$\Delta t = 2(s+t)t\,. \tag{3.5.6}$$

So the transformation produces differential equations in the t variable,

$$\begin{aligned}
2(s+t)t\frac{\partial}{\partial t}\left(stI^{\text{box}}\right) &= \int \frac{d^{d+2}Y\delta(Y^2/2)}{\text{Vol}(\text{GL}(1))}\,\Delta\left(\frac{(X_1X_3)(X_2X_4)}{(YI)^{d-4}(YX_1)(YX_2)(YX_3)(YX_4)}\right) \\
&= \int \frac{d^{d+2}Y\delta(Y^2/2)}{\text{Vol}(\text{GL}(1))}\,\frac{(X_1X_3)(X_2X_4)}{(YX_1)(YX_2)(YX_3)(YX_4)}\,\Delta\left(\frac{1}{(YI)^{d-4}}\right) \\
&= \int \frac{d^{d+2}Y\delta(Y^2/2)}{\text{Vol}(\text{GL}(1))}\,\frac{(X_1X_3)(X_2X_4)}{(YX_1)(YX_2)(YX_3)(YX_4)}\,\frac{1}{(YI)^{d-4+1}} \\
&\qquad\qquad \times(-d+4)\left[2(YX_2) - (YX_1) - (YX_3) - s(YI)\right] \\
&= \epsilon\left[-2s\left(stI^{\text{box}}\right) + 4st\,I^{\text{tri},t} - 4st\,I^{\text{tri},s}\right],
\end{aligned} \tag{3.5.7}$$

where the last line consists of the box, the t-channel triangle, and the s-channel triangle integrals. After summing s- and t-channel versions of this equation it immediately reproduces Eq. (4.11) of Ref. [96].

It is noteworthy that the right-hand side of the differential equation so derived is proportional to ϵ [83,84]. It is perhaps not too surprising that this structure naturally arises in our approach. If we ignore the effect of the regulator, the combination stI^{box} is invariant under dual conformal transformations in four dimensions. However, the box integral is infrared singular so a regulator is required. Dimensional regularization breaks the invariance, so instead of finding zero on the right-hand side we find terms proportional to ϵ. Besides leading to simpler differential equations, integrals with such symmetries are expected to have interesting properties, including uniform transcendentality [103] and $d\log$ forms [107]. It would

be interesting to further explore these ideas at higher loops, not only for the planar case, but also for nonplanar integrals in the context of the approach of Section 3.6.

We end this section with some discussions about the applicability of this method to more complicated integral topologies. First, let us look at the number of legs allowed. In this simple example, a conformal boost changes the dimensionless ratio of Mandelstam variables, s/t, while a scaling transformation rescales both s and t. Together these two transformations allow the *whole phase space* of external kinematic invariants to be explored. For massless planar diagrams, this breaks down when there are six or more external legs, because nontrivial conformally invariant cross ratios exist [77], and conformal transformations only allow us to explore a subspace of the phase space with the same cross ratios.

Second, consider the ϵ factorization properties of the differential equations for more general integrals. For any integrand that is dual conformal invariant, our method automatically leads to differential equations where there is an explicit factor of ϵ on the right-hand side. For more complicated examples beyond the one-loop box, it is generally necessary to perform unitarity-compatible IBP reduction to bring the right-hand side into a linear combination of master integrals. Assuming that IBP reduction of the right-hand side does not introduce singularities, this gives a symmetry-based understanding of Henn's ϵ form of differential equations. For planar integrals that are not invariant, we still obtain differential equations without raised propagator powers. This allows unitarity-compatible IBP reduction to be used to simplify the differential equations, even though we no longer would have ϵ factorization prior to IBP reduction. Third, the applicability of our method to nonplanar topologies will be demonstrated in the next section, where differential equations are derived for the nonplanar double box by identifying a symmetry analogous to dual conformal symmetry.

3.6 Nonplanar analog of dual conformal symmetry

In this section we find a nonplanar analog of dual conformal transformations at two loops. We do so by working out the symmetries of two-loop integrals with three or four external

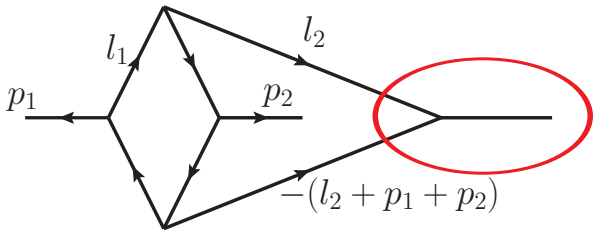

Figure 3.8: The crossed triangle-box, with two massless legs p_1 and p_2, and one massive leg shown as a thick line. We remove the right-most part of the diagram enclosed in a (red) ellipse, in order to open up the diagram into a one-loop planar diagram.

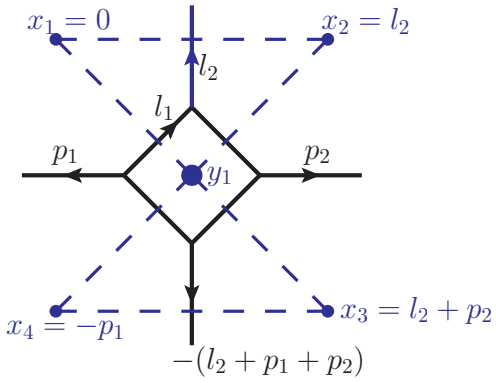

Figure 3.9: This figure is obtained from Fig. 3.8 by removing the right-most part enclosed in the (red) ellipse, including the massive leg. The result is a planar diagram, allowing dual coordinates x_i to be introduced. Each of the dashed (blue) lines corresponds to one of the six propagators in the integral.

legs.

3.6.1 Hidden symmetry of a two-loop nonplanar three-point integral

We start by deriving IBP-generating vectors for a two-loop nonplanar integral topology, the crossed triangle-box integral shown in Fig. 3.8, with two massless outgoing external momenta p_1 and p_2, and one outgoing massive external momentum $-(p_1+p_2)$ on the right. The kinematics is given by

$$p_1^2 = p_2^2 = 0, \quad (p_1+p_2)^2 = s\,. \tag{3.6.1}$$

Our strategy is to open up the nonplanar diagram by removing vertices in the graph. This strategy has been pursued in Ref. [78] to find symmetries of leading singularities of nonplanar integrands. Here we will find symmetries of the *complete off-shell* integrand, up to anomalies introduced by dimensional regularization of infrared singularities, similar to the situation in the planar case. A key hint comes from the fact that in the planar case, dual conformal transformations generate polynomial tangent vectors of unitarity cut surfaces, under which each propagator transforms with a polynomial weight as in Eq. (3.2.8). Therefore, we will first find transformations of nonplanar integrands with this property, before verifying that such transformations are in fact a symmetry of the integrand with appropriate numerators.

To open up the nonplanar diagram in Fig. 3.8 into a planar one, we remove the massive external leg and the vertex attached to it enclosed in the (red) circle, producing a planar one-loop diagram in Fig. 3.9, in which two "external" legs depend on the second loop momentum. Dual coordinates may be introduced for this planar one-loop diagram, as illustrated by the dashed lines in Fig. 3.9. In this case, we find it more convenient to directly work with conformal transformations in d dimensions rather than using the embedding formalism. The inverse propagators are expressed as squared differences between pairs of points in dual spacetime,

$$\begin{aligned}
&\Delta_1 = l_1^2 = (y_1 - x_1)^2\,, && \Delta_2 = (l_1 - l_2)^2 = (y_1 - x_2)^2\,,\\
&\Delta_3 = (l_1 - l_2 - p_2)^2 = (y_1 - x_3)^2\,, && \Delta_4 = (l_1 + p_1)^2 = (y_1 - x_4)^2\,,\\
&\Delta_5 = l_2^2 = (x_2 - x_1)^2\,, && \Delta_6 = [-(l_2 + p_1 + p_2)]^2 = (x_4 - x_3)^2\,,
\end{aligned} \tag{3.6.2}$$

while the only irreducible numerator can be chosen as

$$\Delta_7 = (l_2 + p_1)^2 = (x_2 - x_4)^2\,. \tag{3.6.3}$$

While the external momentum p_1 and p_2 each can be written as the difference between two dual coordinates, this is no longer true for the massive external momenta $-(p_1 + p_2)$,

in contrast to the planar case. Choosing a gauge $x_1 = 0$ to fix the translation degree of freedom, the dual coordinates are positioned at

$$x_1 = 0, \qquad x_2 = l_2, \qquad y_1 = l_1, \qquad x_3 = l_2 + p_2, \qquad x_4 = -p_1\,. \tag{3.6.4}$$

Using these variables, the crossed triangle-box integral in Fig. 3.8, with m powers of the irreducible numerator, is

$$\begin{aligned} I_m^{\text{ctb}} &= \int d^d y_1 \int d^d x_2 \frac{\Delta_7^m}{\Delta_1\Delta_2\Delta_3\Delta_4\Delta_5\Delta_6} \\ &= \int d^d y_1 \int d^d x_2 \frac{(x_2 - x_4)^{2m}}{(y_1 - x_1)^2 (y_1 - x_2)^2 (y_1 - x_3(x_2))^2 (y_1 - x_4)^2 (x_2 - x_1)^2 (x_4 - x_3(x_2))^2}\,, \end{aligned} \tag{3.6.5}$$

where x_3 is taken to be a function of $x_2 = l_2$.

The expression in Eq. (3.6.5) is in a form where we can conveniently apply conformal transformations. An infinitesimal transformation, consisting of a conformal boost with parameter b^μ, a scaling with parameter β, and a Lorentz transformation $\Omega^\mu{}_\nu$, is given by

$$\Delta z^\mu = \frac{1}{2} z^2\, b^\mu + (\beta - b \cdot z) z^\mu + \Omega^\mu{}_\nu z^\nu\,. \tag{3.6.6}$$

Under the transformation, each inverse propagator of the form $(z_1 - z_2)^2$ has a weight given by Eq. (3.2.22),

$$[2\beta - b \cdot (z_1 + z_2)]\,. \tag{3.6.7}$$

For a propagator given by $1/(z_1 - z_2)^2$, the weight has an opposite sign. Meanwhile, the integration measures $d^d y_1$ and $d^d x_2$ have a weight given by Eq. (3.2.23),

$$\frac{\partial \Delta y_1^\mu}{\partial y_1^\mu} = (\beta - b \cdot y_1)\, d\,, \qquad \frac{\partial \Delta x_2^\mu}{\partial x_2^\mu} = (\beta - b \cdot x_2)\, d\,. \tag{3.6.8}$$

For the nonplanar integral in Eq. (3.6.5), the total weight, from the integration measures,

irreducible numerators, and propagators, is

$$\begin{aligned}\mathcal{W}(m,b,\beta) =& d\,(\beta - b\cdot y_1) + d\,(\beta - b\cdot x_2) + m\,[2\beta - b\cdot(x_2+x_4)] \\ & - \left(\sum_{i=1}^{4}[2\beta - b\cdot(y_1+x_i)]\right) - [2\beta - b\cdot(x_1+x_2)] - [2\beta - b\cdot(x_3+x_4)]\,, \quad (3.6.9)\end{aligned}$$

which, using the explicit expression Eq. (3.6.4), becomes

$$\mathcal{W}(m,b,\beta) = 2\beta(d+m-6) + b\cdot[-(d-4)(l_1+l_2) + 2p_2 - 2p_1 - m(l_2-p_1)]\,. \quad (3.6.10)$$

We obtain IBP-generating vectors when the transformation Eq. (3.6.6) leaves both p_1 and p_2 invariant, i.e.

$$\Delta p_1 = \Delta x_1 - \Delta x_4 = 0\,, \qquad \Delta p_2 = \Delta x_3 - \Delta x_2 = 0\,. \quad (3.6.11)$$

A solution for such a transformation is

$$b = p_2\,, \qquad \beta = -\frac{p_1\cdot p_2}{2} = -\frac{s}{4}\,, \qquad \Omega^{\mu}{}_{\nu} = \frac{1}{2}p_{1\,\nu}p_2^{\mu} - \frac{1}{2}p_{2\,\nu}p_1^{\mu}\,. \quad (3.6.12)$$

The weight (3.6.10) is then (using $p_2^2 = 0$),

$$\begin{aligned}\mathcal{W}(m,p_2,-\frac{s}{4}) &= -\frac{s}{2}(d+m-6) + p_2\cdot[-(d-4)(l_1+l_2) - 2p_1 - m\,(l_2-p_1)] \\ &= \frac{1}{2}(d-4+m)s + \left(d-4+\frac{m}{2}\right)(\Delta_7-\Delta_6) + \frac{1}{2}(d-4)(\Delta_3-\Delta_2)\,. \quad (3.6.13)\end{aligned}$$

Remarkably, the above expression vanishes when $d = 4$ and $m = 0$. This shows the integrand of the scalar integral I_0^{ctb} is invariant under a nontrivial infinitesimal transformation.[4]

[4]By "nontrivial", we mean that the transformation is not a Lorentz transformation (of both external and loop momenta) which trivially leave the integral invariant.

The IBP relation obtained from Eq. (3.6.13) is

$$0 = \int d^d l_1 \int d^d l_2 \frac{\Delta_7^m \mathcal{W}(m, p_2, -\frac{s}{4})}{\Delta_1 \Delta_2 \Delta_3 \Delta_4 \Delta_5 \Delta_6} = \frac{1}{2}(d-4+m)s\, I_m^{\text{ctb}} + \left(d-4+\frac{m}{2}\right) I_{m+1}^{\text{ctb}} + \text{daughter integrals}\,, \tag{3.6.14}$$

which reduces all integrals of this topology to the scalar master integral I_0^{ctb} and daughter integrals with canceled propagators. We checked that Eq. (3.6.14) agrees with maximal-cut IBP relations obtained from computational algebraic geometry. Since this is a single scale integral, differential equations are not useful unless additional scales are introduced [85]; in any case its value is given in Ref. [97].

3.6.2 Hidden symmetry of two-loop four-point nonplanar integrals

Consider now the two-loop four-point nonplanar integral with massless external legs displayed in Fig. 3.10. In this case, if we follow the same procedure as for the nonplanar triangle-box, we find no solution for a generalized dual conformal transformation that leaves the external points invariant, so the construction does not generate IBP relations. However, by relaxing this condition, we have no difficulty finding an invariance of the integrals with appropriate numerators. We use it to construct differential equations along the lines of Section 3.5, implying that the symmetry determines the analytic structure. As we emphasize in the subsequent section, this implies that the nonplanar sector of the two-loop four-point $\mathcal{N} = 4$ super-Yang–Mills amplitude has a hidden symmetry analogous to dual conformal symmetry.

In order to define an analog of dual conformal symmetry we open the diagram by removing the part of the diagram in Fig. 3.10 enclosed by a red ellipse, including the leg with external momentum p_2. This opens up the two-loop diagram into a one-loop diagram with "fake", loop-momentum-dependent external legs as shown in Fig. 3.11. With this construction every propagator momentum is expressed as the difference between two dual-space points. Each

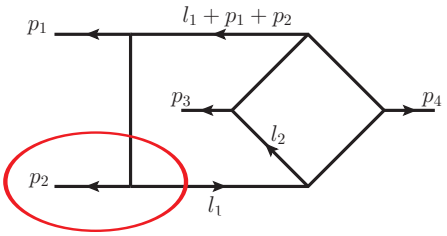

Figure 3.10: The two-loop nonplanar crossed box. The part of the diagram enclosed in a red ellipse will later be removed, so that the diagram is broken up into a one-loop planar diagram.

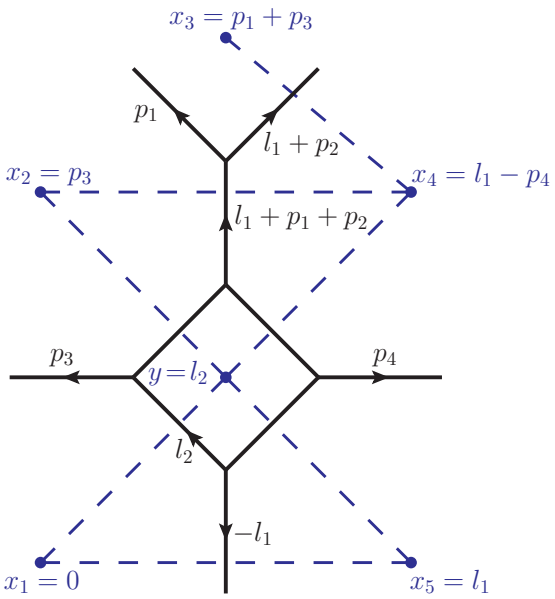

Figure 3.11: The planar one-loop diagram obtained by removing the bottom left part of Fig. 3.10. This allows one to introduce dual coordinates x_i. Each of the dashed lines corresponds to one of the six propagators in the integral.

of the external momenta p_1, p_3, and p_4 is also expressed as the difference between two dual coordinates, though the same is *not* true for p_2 (in contrast to the planar case). Although one might worry that this may cause problems with the construction, we shall see that it does not.

We take the inverse propagators as,

$$\Delta_1 = l_1^2 = (x_1 - x_5)^2, \qquad \Delta_2 = (l_1 + p_2)^2 = (x_4 - x_3)^2\,, \qquad \Delta_3 = (l_1 + p_1 + p_2)^2 = (x_4 - x_2)^2\,,$$
$$\Delta_4 = (l_1 - l_2)^2 = (y - x_5)^2\,, \qquad \Delta_5 = l_2^2 = (y - x_1)^2\,,$$
$$\Delta_6 = (l_2 - p_3)^2 = (y - x_2)^2\,, \qquad \Delta_7 = (l_2 - l_1 + p_4)^2 = (y - x_4)^2\,, \tag{3.6.15}$$

and we have chosen the gauge

$$x_1 = 0\,, \qquad x_2 = p_3\,, \qquad x_3 = p_1 + p_3\,, \qquad x_4 = l_1 - p_4\,, \qquad x_5 = l_1\,, \qquad y = l_2\,. \tag{3.6.16}$$

We can define two numerators (which are not independent irreducible numerators, but nevertheless are convenient for notational purposes),

$$\Delta_8 = (l_1 - p_3)^2 = (x_5 - x_2)^2, \quad \Delta_9 = (l_1 - p_4)^2 = (x_4 - x_1)^2\,. \tag{3.6.17}$$

We also note that

$$u = (p_1 + p_3)^2 = (x_3 - x_1)^2\,. \tag{3.6.18}$$

Refs. [86, 87, 116] express the two-loop four-point amplitude in terms of integrals that have only logarithmic singularities, reflecting a property of the full amplitude. In this representation the two nonplanar integrands that appear in the amplitude (up to relabelings) are,

$$\Omega_1^{\rm NP} = d^d l_1 d^d l_2 \frac{su\Delta_8}{\Delta_1 ... \Delta_7}\,, \tag{3.6.19}$$
$$\Omega_2^{\rm NP} = d^d l_1 d^d l_2 \frac{st\Delta_9}{\Delta_1 ... \Delta_7}\,. \tag{3.6.20}$$

The normalization of each is chosen so it has unit leading singularity [87]. Our task will be to find a hidden symmetry responsible for the simple analytic properties after integration.

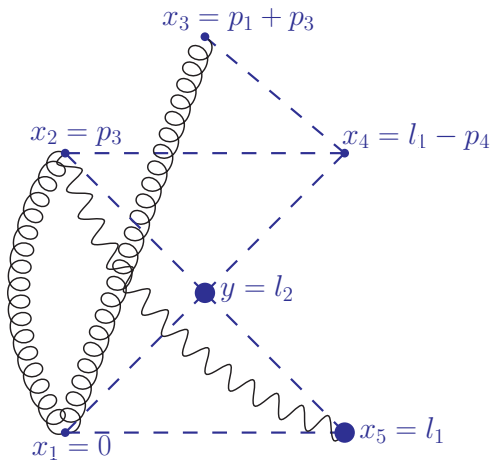

Figure 3.12: Weight diagram for the integrand (3.6.19) under the conformal boost (3.6.23).

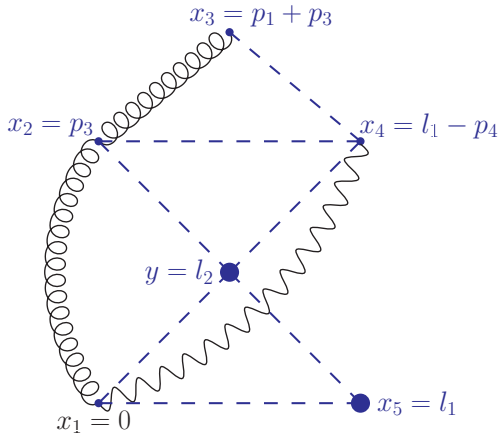

Figure 3.13: Weight diagram for the integrand (3.6.20) under the conformal boost (3.6.23).

A conformal boost on the x_i's and y with parameter b^μ gives

$$\Delta p_4 \equiv \Delta x_5 - \Delta x_4 \tag{3.6.21}$$

$$= (l_1 \cdot p_4)b - (p_4 \cdot b)l_1 - (l_1 \cdot b - p_4 \cdot b)p_4 \,. \tag{3.6.22}$$

The appearance of loop momentum in the transformation of external momentum is not surprising, given that once we cut a nonplanar diagram open internal momenta effectively become "external". This is, of course, not desirable if we wish to use the transformations to construct differential equations. To remove the loop-momentum dependence of this variation,

we simply choose

$$b = p_4 \,. \tag{3.6.23}$$

While this restricts the transformations to a subset of conformal transformations, we shall see that this is sufficient for constructing differential equations analogous to those of the planar case. Applying the conformal transformation gives

$$\begin{aligned}
\Delta p_1 &= \Delta x_3 - \Delta x_2 = \frac{1}{2}(u\, p_4 - t\, p_3 + u\, p_1)\,, \\
\Delta p_3 &= \Delta x_2 - \Delta x_1 = -\frac{1}{2} s\, p_3\,, \\
\Delta p_4 &= \Delta x_5 - \Delta x_4 = 0\,,
\end{aligned} \tag{3.6.24}$$

so that the masslessness of these three external legs is preserved. In fact, the masslessness of p_1, p_3, and p_4 are trivially preserved by the properties of conformal transformations, since each of these three momenta is the difference between two points in dual space. Remarkably, the same is nontrivially true of the second leg, as can be readily checked,

$$\Delta p_2^2 = 2p_2 \cdot \Delta p_2 = -2p_2 \cdot (\Delta p_1 + \Delta p_3 + \Delta p_4) = 0\,. \tag{3.6.25}$$

This ensures that the transformation preserves the masslessness of all external legs, which is essential for the construction to be useful. In addition we have,

$$\begin{aligned}
\Delta s &= \Delta(2p_3 \cdot p_4) = 2(p_3 \cdot \Delta p_4 + p_4 \cdot \Delta p_3) = -\frac{s}{2} s\,, \\
\Delta t &= \Delta(2p_1 \cdot p_4) = 2(p_1 \cdot \Delta p_4 + p_4 \cdot \Delta p_1) = -\frac{t+2s}{2} t\,.
\end{aligned} \tag{3.6.26}$$

Note that applying Eq. (3.2.22) directly gives,

$$\Delta u = -b \cdot (x_3 + x_1)u = -p_4 \cdot (p_1 + p_3)u = -\frac{u}{2}(t+s) = -\Delta s - \Delta t\,, \tag{3.6.27}$$

which is consistent with momentum conservation. It will be convenient for later purposes to write down the weights of s, t, and u under the transformation, as dot products between $(-p_4)$ and other momenta,

$$\begin{aligned}
\mathcal{W}_s &\equiv \frac{\Delta s}{s} = -p_4 \cdot p_3 \,, \\
\mathcal{W}_t &\equiv \frac{\Delta t}{t} = -p_4 \cdot (p_1 + 2p_3) \,, \\
\mathcal{W}_u &\equiv \frac{\Delta u}{u} = -p_4 \cdot (p_1 + p_3) \,.
\end{aligned} \tag{3.6.28}$$

Meanwhile, a numerator of the form $(z_i - z_j)^2$ has the weight $-p_4 \cdot (z_i + z_j)$, while an extra minus sign is present in the weight for a propagator of the form $1/(z_i - z_j)^2$. The weight of the integration measure is given by $-d\,p_4 \cdot (x_5 + y) = -d\,p_4 \cdot (l_1 + l_2)$. We can now straightforwardly prove that the nonplanar contributions to the $\mathcal{N} = 4$ super-Yang–Mills amplitudes are invariant under this transformation. Namely, in $d = 4$, the two integrands (3.6.19) and (3.6.20) in the amplitudes transform as,

$$\Delta\Omega_1^{\rm NP} = \Delta\Omega_2^{\rm NP} = 0 \,. \tag{3.6.29}$$

A pictorial way to derive the above equation is as follows. We have shown that the weights of the Mandelstam variables, numerators, propagators, and integration measures are each written in the form $-p_4 \cdot W$ for some "weight vector" W^μ. So it is convenient to represent the weight of the integrand diagrammatically as in Figs. 3.12 and 3.13. In the diagrams, the weight of a propagator of the form $1/(z_1 - z_2)^2$ is represented by a dashed line connecting two points z_1 and z_2, contributing $-(z_1^\mu + z_2^\mu)$ to the weight vector W^μ. The weight of a numerator of the form $(z_1 - z_2)^2$ is represented by a wiggly line connecting two points z_1 and z_2, contributing $z_1^\mu + z_2^\mu$ to the weight vector W^μ. The weight of the Mandelstam variables appearing in the numerator is represented by a coil-like line connecting two points z_1 and z_2, again contributing $z_1^\mu + z_2^\mu$ to the weight vector W^μ. To reproduce Eq. (3.6.28),

for $\mathcal{W}_s$ we choose $z_1 = 0 = x_1$ and $z_2 = p_3 = x_2$, for $\mathcal{W}_t$ we choose $z_1 = p_3 = x_2$ and $z_2 = p_1 + p_3 = x_3$, and for $\mathcal{W}_u$ we choose $z_1 = 0 = x_1$ and $z_2 = p_1 + p_3 = x_3$. Finally, the weight of the integration measure is indicated by large black dots at the two points x_5 and y. In our notation, a large black dot at any point z contributes $d\,z^\mu$ to the weight vector W^μ, with d being the spacetime dimension. The total weight vector $\sum W^\mu$ can now be read off from the diagram in the following manner: at each vertex (i.e. a dual-space point) z^μ, we count the number of wiggly lines and coil-like lines joining the vertex, subtract the number of dashed lines joining the vertex, and add the spacetime dimension d if a large black dot appears at the vertex. The final number is multiplied by z^μ and included in $\sum W^\mu$. For the first integrand $\Omega_1^{\rm NP}$ in Eq. (3.6.19), the weight diagram in Fig. 3.12 gives the weight vector

$$\begin{aligned}\sum W_1^\mu &= (2-2)x_1^\mu + (2-2)x_2^\mu + (1-1)x_3^\mu - 3x_4^\mu + (1-2+d)x_5^\mu + (-4+d)y^\mu \\ &= (d-4)(l_1^\mu + l_2^\mu) + 3p_4^\mu\,. \end{aligned} \tag{3.6.30}$$

Using this, we arrive at

$$\Delta\Omega_1^{\rm NP} = \left(-p_4 \cdot \sum W_1\right)\Omega_1^{\rm NP} = -(d-4)p_4\cdot(l_1+l_2)\Omega_1^{\rm NP}\,. \tag{3.6.31}$$

Since the transformation changes the Mandelstam variables as in Eq. (3.6.26), we arrive at a differential equation for the Feynman integral,

$$\left(-\frac{s^2}{2}\frac{\partial}{\partial s} - \frac{t(t+2s)}{2}\frac{\partial}{\partial t}\right)\int \Omega_1^{\rm NP} = -(d-4)\int p_4\cdot(l_1+l_2)\,\Omega_1^{\rm NP}\,. \tag{3.6.32}$$

Since $\Omega_1^{\rm NP}$ has mass dimension $2(d-4)$, we trivially obtain another differential equation from the simultaneous scaling of all Mandelstam variables,

$$\frac{s}{2}\left(s\frac{\partial}{\partial s} + t\frac{\partial}{\partial t}\right)\int \Omega_1^{\rm NP} = \frac{s}{2}(d-4)\int \Omega_1^{\rm NP}\,. \tag{3.6.33}$$

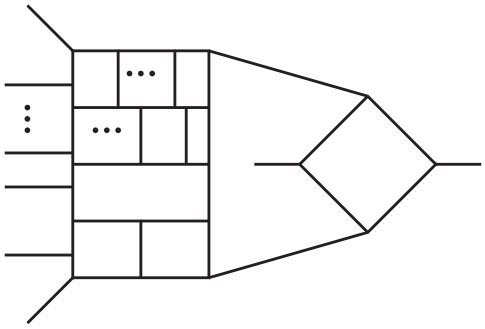

Figure 3.14: An illustrative multi-loop diagram, where an analysis similar to the one for the nonplanar double box in Fig. 3.10 identifies a hidden symmetry.

Adding Eqs. (3.6.32) and (3.6.33), we obtain the derivative of the integral against t only

$$\frac{tu}{2}\frac{\partial}{\partial t}\int \Omega_1^{\rm NP} = \epsilon\left[2\int p_4\cdot(l_1+l_2) - s\right]\Omega_1^{\rm NP}\,. \tag{3.6.34}$$

For the second integrand $\Omega_2^{\rm NP}$ in Eq. (3.6.20), again we read off the weight vector from Fig. 3.13. This leads to results similar to those for $\Omega_1^{\rm NP}$,

$$\Delta\Omega_2^{\rm NP} = \left(-p_4\cdot\sum W_1\right)\Omega_1^{\rm NP} = -(d-4)p_4\cdot(l_1+l_2)\Omega_2^{\rm NP}\,, \tag{3.6.35}$$

and

$$\frac{tu}{2}\frac{\partial}{\partial t}\int \Omega_2^{\rm NP} = \epsilon\left[2\int p_4\cdot(l_1+l_2) - s\right]\Omega_2^{\rm NP}\,. \tag{3.6.36}$$

If there were no infrared singularities, we would be able to set $\epsilon = 0$ and the symmetry would be exact.

It is interesting that a similar analysis extends to any nonplanar diagram with a single crossed box at any loop order, as illustrated in Fig. 3.14. In particular, if we consider this diagram with a numerator obtained from a corresponding planar dual conformal invariant one, except for the single crossed box which is given a similar factor as in the two-loop cases (3.6.19) and (3.6.20), then the resulting nonplanar integral possesses a higher-loop analog of dual conformal symmetry. A way to show the invariance is to remove a three vertex from the crossed box and perform an analysis similar to the one of the previous section for the two-

loop crossed box. In this case, it is convenient to remove a vertex from the crossed double box, instead of the other parts of the diagram. We have checked that the analog of dual conformal symmetry is present for this class of nonplanar integrals, at any loop order. As for the two-loop case, we can use it to generate differential equations to constrain the integrals whose right-hand side is proportional to the dimensional regularization parameter, ϵ.

3.7 Invariance of the nonplanar two-loop four-point $\mathcal{N} = 4$ super-Yang–Mills amplitude

In the previous section we identified a new symmetry of the nonplanar integrands that appear in the two-loop four-point amplitude of $\mathcal{N} = 4$ super-Yang–Mills theory. In this section we comment on symmetries of the full amplitude.

From Eq. (3.15) of Ref. [87] we have the full two-loop four-point amplitude of $\mathcal{N} = 4$ super-Yang-Mills theory as

$$\mathcal{A}_4^{\text{2-loop}} = -\frac{g^6}{4(2\pi)^{2D}} \sum_{\mathcal{S}_4} \Big[c_{1234}^{\text{P}} A^{\text{tree}}(1,2,3,4) \int \Omega^{\text{P}} - c_{1234}^{\text{NP}} \Big(A^{\text{tree}}(1,2,4,3) \int \Omega_1^{\text{NP}} + A^{\text{tree}}(1,2,3,4) \int \Omega_2^{\text{NP}} \Big) \Big] , \tag{3.7.1}$$

where c_{1234}^{P} and c_{1234}^{NP} are the planar and nonplanar color factors obtained by dressing the diagrams in Figs. 3.1 and 3.10 with $\tilde{f}^{abc}$ color factors at each diagram vertex. The planar integrands are given in Eq. (3.4.37) while the nonplanar integrands are given in Eqs. (3.6.19) and (3.6.19). The A^{tree}'s are color-ordered tree amplitudes of $\mathcal{N} = 4$ super-Yang–Mills theory, with the indicated ordering of legs. The overall sum is over all 24 permutations of the external legs; the permutations act on the external color, polarization and momentum labels. The form in Eq. (3.7.1) differs from the one originally given in Ref. [48, 49] by terms that vanish via the color Jacobi identity. In the original form, the individual nonplanar integrals do not reflect the analytic properties of the final amplitude, such as having only

logarithmic singularities and no poles at infinity.

In order to understand the transformation properties we divide the amplitude into sectors determined by the tree amplitude prefactors. These tree amplitudes have differing overall weights under the transformations, which are easy to determine using the identities [25],

$$stA^{\rm tree}(1,2,3,4) = suA^{\rm tree}(1,2,4,3) = tuA^{\rm tree}(1,3,2,4)\,. \tag{3.7.2}$$

From here we can see that the tree amplitudes transform with different overall weights under Eq. (3.6.24),

$$\Delta\left(\frac{A^{\rm tree}(1,2,3,4)}{A^{\rm tree}(1,2,4,3)}\right) = \Delta\left(\frac{t}{u}\right) = -\frac{st}{2u}\,, \tag{3.7.3}$$

where we used Eqs. (3.6.26) and (3.6.27).

In Eq. (3.7.1), the coefficient of each tree amplitude factor is invariant under the four-dimensional symmetry. In Refs. [87], the orderings of the tree factors were chosen to adjust the factors of s, t, and u so that the remaining integrals have unit leading singularities. Not surprisingly, these factors are exactly what is needed to make the coefficient of each tree invariant under the four-dimensional symmetry.

As a side note, we can adjust the transformations in each sector so that a uniform transformation is applied to the external momenta in all sectors of the amplitude. In doing so, the transformations on internal momenta necessarily differ in the various sectors, as expected from the fact that there is no uniform sets of momenta or dual variables in the nonplanar sector. This may be accomplished by adjusting Lorentz and scaling transformations. However, since the different sectors transform with a different weight there is no need to do this.

The transformations described in the previous section can be taken as a direct analog of dual conformal symmetry of planar $\mathcal{N} = 4$ super-Yang–Mills theory, but applicable to the nonplanar sector as well. Like dual conformal symmetry in the planar case, the infinitesimal generators of the new symmetries can be identified as polynomial tangent vectors of unitarity cut surfaces.

This opens the possibility of finding numerators of higher-loop integrals with desired properties of having simple analytic properties and associated DEs, not by detailed studies of the singularity structure of the integrands [83, 84, 86, 87, 116], but by demanding that given integrands be invariant under symmetries analogous to dual conformal symmetry. For nonplanar diagrams that can be obtained from a planar one by a single replacement of a box subdiagram by a crossed box, as in Fig. 3.14, the obvious candidate transformations follow those described in the previous section. It would be very interesting to systematically study these cases, as well as ones with multiple twists. We expect such integrals to be direct building blocks for nonplanar $\mathcal{N} = 4$ super-Yang–Mills amplitudes. More generally, it seems likely that a symmetry along the lines described here is responsible for the simple analytic properties [86, 87, 116] of general nonplanar amplitudes at any loop order.

3.8 Conclusions

In this chapter we studied hidden symmetries of $\mathcal{N} = 4$ super-Yang–Mills theory as a means for generating compact integration-by-parts (IBP) relations [30] and differential equations (DEs) [81, 96] for loop integrals encountered in generic theories. For the planar case, the hidden symmetry is the well-studied dual conformal symmetry [64]. By exploiting the connection between dual conformal symmetry and polynomial tangent vectors of unitarity cut surfaces, we were able to find an analogous symmetry for the nonplanar sector of the two-loop four-point amplitude as well. Besides being useful for generating IBP relations and DEs, this points to the exciting possibility that dual conformal symmetry can be generalized to the nonplanar sector of $\mathcal{N} = 4$ super-Yang–Mills theory.

Dual conformal transformations and their nonplanar analogs have the important property that they do not increase propagator powers, resulting in IBP relations and DEs that are naturally compatible with unitarity [31]. Such IBP relations had been previously described using computational algebraic geometry [31, 34, 74]. Our approach, based on exploiting hidden symmetries, provides new analytic insights and on the practical side gives compact

expressions for the IBP-generating vectors and DEs. In describing the symmetries we found it useful to work with both "direct" dual conformal transformations in d dimensions and the embedding formalism [80], which linearizes the transformations by going to $(d+2)$ dimensions.

To illustrate these ideas, we presented a variety of examples at one and two loops. With up to four massless legs and a small number of mass parameters, it is straightforward to find several dual conformal transformations which leave the external momenta invariant, and lead to a sufficient number of IBP relations to solve generic cases. For example, the dual conformal transformations generate a complete set of IBP relations for the planar two-loop double-box integral. We also studied a five-point example, namely the planar penta-box integral. In this case, we need additional IBP-generating vectors from combining separate conformal transformations for the left loop and right loop, generalizing the strategy of Ref. [33]. These additional vectors still have a simple analytic form. For illustration, we also looked at a simpler three-point nonplanar integral, and obtained IBP relations that reduce all integrals to top-level master integral and daughter integrals.

We also described DEs, where the integrals do not have raised propagator powers, for both planar and nonplanar cases that arise when external momenta are allowed to change under the transformation. For one- and two-loop integrals with appropriately chosen numerators that make the transformation weights cancel in four dimensions, the method directly gives a DEs where the right-hand side is proportional to the dimensional regularization parameter ϵ [83, 84]. This holds before IBP reduction to a basis of master integrals, because the equations follow from a symmetry that is exact in four dimensions. For massless kinematics, the method is applicable with up to five external legs. At higher points, when nontrivial conformal cross ratios are present, the method generates a subset of the DEs.

Our results point to promising directions for future studies. In various one- and two-loop examples we showed the utility of dual conformal invariance for generating both IBP relations and DEs, as well as presented a nonplanar symmetry analogous to dual conformal

symmetry. An obvious direction for future studies is to try to generalize this to arbitrary loop orders and for any number of external legs. The unitarity-compatible IBP-generating vectors and DEs constructed via dual conformal symmetry and its generalizations are particularly simple, making it desirable to extend these ideas as widely as possible. The ability to generate relatively simple DEs becomes especially attractive when existing methods suffer from computational bottlenecks that occur in more complicated cases. It is also worth studying whether the compact expressions generated from our symmetry considerations can improve computational efficiency in numerical unitarity approaches at two loops and beyond [68].

On the more formal side, we know that dual conformal symmetry [64] strongly restricts the analytic properties of the planar sector of $\mathcal{N} = 4$ super-Yang–Mills theory. In particular, the integrands have no double poles or poles at infinity [107]. These analytic properties also appear to carry over to the nonplanar sector [86, 87, 116]. Here we took initial steps to identify a symmetry that can explain this. We explicitly constructed a symmetry of the nonplanar two-loop four-point $\mathcal{N} = 4$ amplitude, and used it to construct a differential equation for determining its value. As in the planar case, the symmetry is intimately connected to polynomial tangent vectors of unitarity cut surfaces. As for dual conformal invariance the symmetry is anomalous due to infrared singularities. We noted that for the class of integrals with a single crossed box and the remaining part planar, the symmetry extends straightforwardly to all loop orders with an arbitrary number of external legs. An important next step would be to extend this to more general nonplanar cases.

We look forward to exploring these ideas for simplifying computations of multi-loop integrals needed for scattering cross sections at particle colliders, as well as for understanding hidden symmetries of the nonplanar sector of $\mathcal{N} = 4$ super-Yang–Mills theory. These two issues are intertwined, as we found here.

3.9 Sub-loop IBP-generating vectors for the penta-box

In this appendix, we tabulate the antisymmetric matrices in Eq. (3.4.49) of Subsection 3.4.5, which parametrize conformal transformations that leave a subset of external momenta invariant. The matrices are,

$$\omega_{(1)} = \begin{pmatrix} 0 & s_{34} & s_{51} & s_{34}-s_{51} & s_{23} & s_{23}s_{34} \\ -s_{34} & 0 & 0 & -s_{34} & s_{12}-s_{45} & -s_{34}s_{45} \\ -s_{51} & 0 & 0 & -s_{51} & s_{23}-s_{45} & -s_{45}s_{51} \\ -s_{34}+s_{51} & s_{34} & s_{51} & 0 & s_{12} & s_{12}s_{51} \\ -s_{23} & -s_{12}+s_{45} & -s_{23}+s_{45} & -s_{12} & 0 & -s_{12}s_{23} \\ -s_{23}s_{34} & s_{34}s_{45} & s_{45}s_{51} & -s_{12}s_{51} & s_{12}s_{23} & 0 \end{pmatrix}, \tag{3.9.1}$$

$$\omega_{(2a)} = \begin{pmatrix} 0 & 0 & 0 & 0 & 0 & 0 \\ 0 & 0 & 0 & 0 & -s_{45} & 0 \\ 0 & 0 & 0 & 0 & 0 & 0 \\ 0 & 0 & 0 & 0 & -s_{23} & 0 \\ 0 & s_{45} & 0 & s_{23} & 0 & s_{23}s_{45} \\ 0 & 0 & 0 & 0 & -s_{23}s_{45} & 0 \end{pmatrix}, \tag{3.9.2}$$

$$\omega_{(2b)} = \begin{pmatrix} 0 & -s_{34} & -s_{23}+s_{51} & 0 & 0 & -s_{23}s_{34} \\ s_{34} & 0 & s_{45} & -s_{12}+s_{34} & 0 & s_{34}s_{45} \\ s_{23}-s_{51} & -s_{45} & 0 & -s_{51} & 0 & -s_{45}s_{51} \\ 0 & s_{12}-s_{34} & s_{51} & 0 & 0 & s_{12}s_{51} \\ 0 & 0 & 0 & 0 & 0 & 0 \\ s_{23}s_{34} & -s_{34}s_{45} & s_{45}s_{51} & -s_{12}s_{51} & 0 & 0 \end{pmatrix}, \tag{3.9.3}$$

$$\omega_{(2c)} = \begin{pmatrix} 0 & 0 & 0 & 0 & s_{23} & 0 \\ 0 & 0 & 0 & 0 & -s_{45} & 0 \\ 0 & 0 & 0 & 0 & 0 & 0 \\ 0 & 0 & 0 & 0 & 0 & 0 \\ -s_{23} & s_{45} & 0 & 0 & 0 & 0 \\ 0 & 0 & 0 & 0 & 0 & 0 \end{pmatrix}. \tag{3.9.4}$$

Chapter 4

Dual Conformal Structure Beyond the Planar Limit

The planar scattering amplitudes of $\mathcal{N} = 4$ super-Yang–Mills theory display symmetries and structures which underlie their relatively simple analytic properties such as having only logarithmic singularities and no poles at infinity. Recent work shows in various nontrivial examples that the simple analytic properties of the planar sector survive into the nonplanar sector, but this has yet to be understood from underlying symmetries. Here we explicitly show that for an infinite class of nonplanar integrals that covers all subleading-color contributions to the two-loop four- and five-point amplitudes of $\mathcal{N} = 4$ super-Yang–Mills theory, symmetries analogous to dual conformal invariance exist. A natural conjecture is that this continues to all amplitudes of the theory at any loop order.

4.1 Introduction

Recent years have seen significant advances in constructing scattering amplitudes, especially for planar $\mathcal{N} = 4$ super-Yang–Mills (sYM) theory. A key feature of planar $\mathcal{N} = 4$ sYM theory that makes this progress possible is its remarkable symmetries and structures. These include dual conformal symmetry [60, 64, 99], Yangian symmetry [100], integrability [101], a

dual interpretation of scattering amplitudes in terms of Wilson loops [102], uniform transcendentality [103], structures that aid various bootstraps [104, 105], and even an all-loop resummation of four- and five-point amplitudes [106]. Scattering amplitudes have been reformulated using on-shell diagrams and the positive Grassmannian [107], which culminated in the geometric concept of the amplituhedron [11, 108]. Some of these advances have been helpful in quantum chromodynamics relevant for collider physics, including improved ways for dealing with polylogarithms that arise in multiloop computations [109] and for finding good choices [83, 86, 87, 110] of integral bases that simplify their evaluation. In fact, the integrals we analyze here for the two-loop five-point amplitude [87, 111] are useful choices for the basis of master integrals for 2-to-3 scattering in generic theories [112].

These symmetries and structures impose nontrivial constraints on the analytic properties of planar $\mathcal{N} = 4$ sYM amplitudes. In particular, the loop-level color-ordered amplitudes $\mathcal{M}_{123\ldots n}$ can be written as

$$\mathcal{M}_{123\ldots n} = \mathrm{PT}_{123\ldots n} \int \mathcal{I} \,, \tag{4.1.1}$$

where the integrand $\mathcal{I}$ has only logarithmic singularities, no poles at infinity [107], and unit leading singularities [113] as tied to the amplituhedron [11, 108]. The prefactor $\mathrm{PT}_{123\ldots n}$ is the standard Parke-Taylor factor [114], as defined in e.g. Ref. [87].

It is unclear how to define dual conformal symmetry in the nonplanar sector given the lack of dual variables to define the symmetry. However, as shown in a variety of examples [86, 87, 115], the key analytic properties of the planar sector implied by its symmetries carry over to the nonplanar sector, even if the symmetries are unclear. In each example, the full amplitude can be expressed as [116]

$$\mathcal{M} = \sum_{k,\sigma,j} a_{\sigma,k,j} c_k \mathrm{PT}_\sigma \int \mathcal{I}^j \,, \tag{4.1.2}$$

where the $a_{\sigma,k,j}$ are rational numbers, the c_k are color factors, the PT_σ are the Parke-Taylor factors corresponding to an ordering σ of external particles, and the $\mathcal{I}^j$ are integrands with

only logarithmic singularities, no poles at infinity, and unit leading singularities. Eq. (4.1.2) is a natural extension of Eq. (4.1.1) to the nonplanar sector. It is nontrivial that such a representation exists where each integrand is expressed in terms of local diagrams. Some structures of the nonplanar sector were also explored at the level of on-shell diagrams [78,117].

In the present chapter we address the following question: Can we identify a hidden symmetry associated with the simple analytic properties for the nonplanar sector uncovered in Refs. [86, 87, 115]? Building on the initial studies in Ref. [2], we answer this question affirmatively and demonstrate that the integrands $\mathcal{I}^j$ in (4.1.2) encoding the simple analytic structure of the full two-loop four- and five-point amplitudes all have hidden symmetries related to dual conformal invariance. These are not hidden symmetries of the full amplitude, but of individual components of the amplitudes, analogous to the situation with dual conformal symmetry in the planar case (4.1.1). We also identify an infinite class of nonplanar integrands with the hidden symmetry. In many cases these symmetries rely on nontrivial identities, making it all the more striking that a symmetry actually exists.

4.2 Dual coordinates and conformal symmetry

To set up our discussion of hidden symmetries in the nonplanar sector, we first briefly review dual conformal symmetry in the planar sector [60, 64, 99]. In general, the momenta (corresponding to edges or lines) in *any* planar diagram can be represented as the difference of adjacent dual coordinates (corresponding to regions). For example, the momenta in the planar double-box diagram on the left of Figure 4.1 can be expressed as

$$\begin{aligned} &p_1 = x_2 - x_1\,, \quad p_2 = x_3 - x_2\,, && p_3 = x_4 - x_3\,, \\ &p_4 = x_1 - x_4\,, \quad l_5 = x_5 - x_1\,, && l_6 = x_1 - x_6\,, \end{aligned} \tag{4.2.1}$$

where the p_i are external momenta, l_5 and l_6 are the loop momenta, and x_i are the dual coordinates with all Lorentz indices omitted. We can perform infinitesimal conformal trans-

formations on these dual coordinates,

$$\delta x_i^\mu = \frac{1}{2} x_i^2 b^\mu - (x_i \cdot b) x_i^\mu \,, \tag{4.2.2}$$

where b^μ is an infinitesimal boost vector. The transformation of the square of proper distance is

$$\delta (x_i - x_j)^2 = -b \cdot (x_i + x_j) \, (x_i - x_j)^2 \,. \tag{4.2.3}$$

In general, if a quantity f transforms as $\delta f = w f$ with w a local function, we say f *rescales* under the transformation with weight w. Thus, under dual conformal transformations, $(x_i - x_j)^2$ carries a weight $-b \cdot (x_i + x_j)$. Note that all massless external legs remain on shell after the transformation. All the inverse propagators have the form $(x_i - x_j)^2$. This implies that locality is maintained for planar loop integrals under dual conformal transformations and allows us to construct simple functions that are invariant.

As a simple illustration, consider an integral associated with the planar double box,

$$I = \int d^D x_5 d^D x_6 \frac{s^2 t}{\prod_k \rho_k} \,, \tag{4.2.4}$$

where $s = (x_1 - x_3)^2 = (p_1 + p_2)^2$ and $t = (x_2 - x_4)^2 = (p_2 + p_3)^2$. The inverse Feynman propagators ρ_k in dual coordinates are

$$\begin{aligned}
&\rho_1 = (x_5 - x_1)^2 \,, \quad \rho_2 = (x_5 - x_2)^2 \,, && \rho_3 = (x_5 - x_3)^2 \,, \\
&\rho_4 = (x_5 - x_6)^2 \,, \quad \rho_5 = (x_6 - x_1)^2 \,, && \rho_6 = (x_6 - x_4)^2 \,, \\
&\rho_7 = (x_6 - x_3)^2 \,.
\end{aligned} \tag{4.2.5}$$

In what follows, we will be interested in the integrand $\mathcal{I}$, defined by $I = \int \mathcal{I}$. With this numerator the integrand has a hidden symmetry exposed by using the dual variables [60, 64,

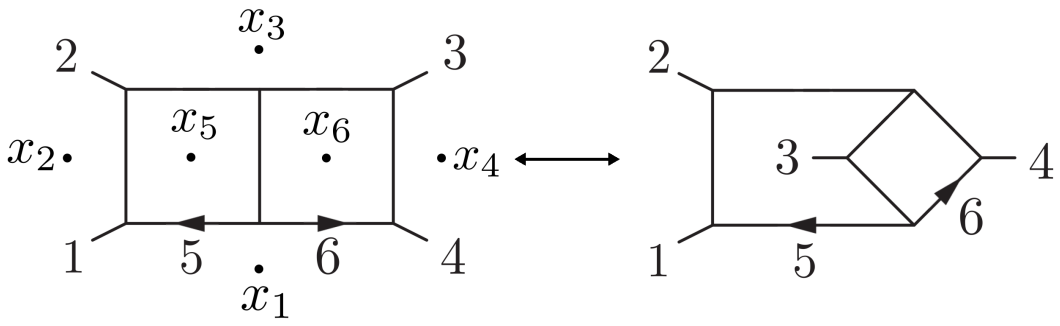

Figure 4.1: Planar double box with dual coordinates and the crossed-box related to it by moving leg 3 to the central rung.

99]. Performing the dual conformal transformation on the integrand (4.2.4) yields

$$\delta\mathcal{I} = -(D-4)\big(b\cdot(x_5+x_6)\big)\mathcal{I}\,, \tag{4.2.6}$$

where we used

$$\delta(d^D x_i) = \Big(\frac{\partial\delta x_i^\mu}{\partial x_i^\mu}\Big) d^D x_i = -D(b\cdot x_i)\, d^D x_i\,. \tag{4.2.7}$$

For $D = 4$ space-time dimensions this integrand is invariant under dual conformal transformations, which is what motivated the choice of numerator s^2t. Outside $D = 4$, this is reminiscent of ϵ-form differential equations [83, 110], but without doubled propagators on the right hand side before reduction to a basis [2, 82, 118].

What is the relevance of this symmetry? It turns out that *all* integrands of planar $\mathcal{N} = 4$ sYM amplitudes possess this property, which then leads to nontrivial constraints on the amplitude after integration. This is the celebrated *dual conformal symmetry* [60, 64, 99] which has spurred many developments. In the following we identify an analogous symmetry in a class of nonplanar diagrams.

4.3 Nonplanar extension

While there are no known global variables for generic nonplanar diagrams, it is natural to require that, as for the planar case, a nonplanar analog of dual conformal transformations also

maintains the local structure for inverse propagators, $\delta\rho_k \propto \rho_k$ [2]. We start by considering a nonplanar diagram that can be made planar by moving the location of one external leg carrying momentum p_k^μ. This is an infinite class of nonplanar integrals, and includes all the nonplanar integrals at two loops with five or fewer external legs. In particular, all of the nonplanar integrals in Figure 4.2 are of this type. For example diagram (a) can be made planar by moving external leg 3. Under this, the momenta of the propagators are modified compared to the planar case at most by adding or subtracting a single external momentum p_k^μ. Thus, the inverse propagators ρ_l therein can be written as either $(x_i - x_j)^2$, or $(x_i - x_j \pm p_k)^2$, when using the dual coordinates of the planar cousin. The key observation here is that if the infinitesimal boost vector b^μ is proportional to a massless external leg p_k^μ, then $(x_i - x_j \pm p_k)^2$ transforms in the same way as $(x_i - x_j)^2$ for any x_i^μ and x_j^μ. Specifically,

$$\frac{\delta(x_i - x_j \pm p_k)^2}{(x_i - x_j \pm p_k)^2} = \frac{\delta(x_i - x_j)^2}{(x_i - x_j)^2} = -b \cdot (x_i + x_j)\,, \tag{4.3.1}$$

implying that all the propagators in this class of nonplanar diagrams satisfy $\delta\rho_k \propto \rho_k$ for this conformal boost.

As a simple first example, consider the crossed double-box diagram on the right of Fig. 4.1, with numerator $N_1 = su(l_5 + p_4)^2$, which is one of the nonplanar pure integrands found in Ref. [115] as a building block of the full amplitude:

$$I^{(\text{np})} = \int \mathcal{I}^{(\text{np})} = \int d^D l_5 d^D l_6 \, \frac{N_1}{\prod_k \rho_k}\,, \tag{4.3.2}$$

where the ρ_k are the inverse propagators. This diagram can be obtained from the planar double box in Fig. 4.1 by moving the external leg 3 to the central rung. Using the dual coordinates of the planar double box, we can write the nonplanar integrand as

$$\mathcal{I}^{(\text{np})} = d^D x_5 d^D x_6 \, \frac{(x_1 - x_3)^2 (x_2 - x_1 + p_3)^2 (x_5 - x_4)^2}{\prod_k \rho_k}\,, \tag{4.3.3}$$

where the propagators are given by

$$\begin{aligned}
&\rho_1 = (x_5 - x_1)^2, \quad \rho_2 = (x_5 - x_2)^2, \quad \rho_3 = (x_5 - x_3)^2, \\
&\rho_4 = (x_5 - x_6)^2, \quad \rho_5 = (x_6 - x_1)^2, \quad \rho_6 = (x_6 - x_4)^2, \\
&\rho_7 = (x_5 - x_6 + p_3)^2,
\end{aligned} \tag{4.3.4}$$

with the x_i defined in Eq. (4.2.1). Applying a dual conformal transformation to the integrand with the boost vector $b^\mu \propto p_3^\mu$ and using equation (4.3.1) we find that

$$\delta \mathcal{I}^{(\text{np})} = -(D-4)(b \cdot (x_5 + x_6))\mathcal{I}^{(\text{np})}\,, \tag{4.3.5}$$

exposing a hidden symmetry in $D = 4$.

A similar analysis holds for the numerator $N_2 = st(l_5 + p_3)^2$, corresponding to the other pure integrand found in Ref. [115]. One can also obtain the crossed box from the planar double box by moving the leg 4 to the central rung (and making a change in the momentum routing of the planar double box), giving a new conformal boost with $b^\mu \propto p_4^\mu$. As can be straightforwardly checked, both numerators N_1 and N_2 give integrands that are invariant in $D = 4$ under this transformation as well.

While we propose these transformations as a natural extension of the planar dual conformal symmetry, it is striking that the numerators N_1 and N_2 are precisely the correct numerators of the building blocks for the two-loop four-point amplitude in $\mathcal{N} = 4$ sYM that unveil their analytic properties [115]. Here we see that we can constrain these numerators from symmetry considerations instead of from imposing desired analytic properties on the integrands. Similar symmetry considerations can be used to match the numerators of a subset of three-loop four-point diagrams in Ref. [86] that can be obtained from planar ones by moving a single external line.

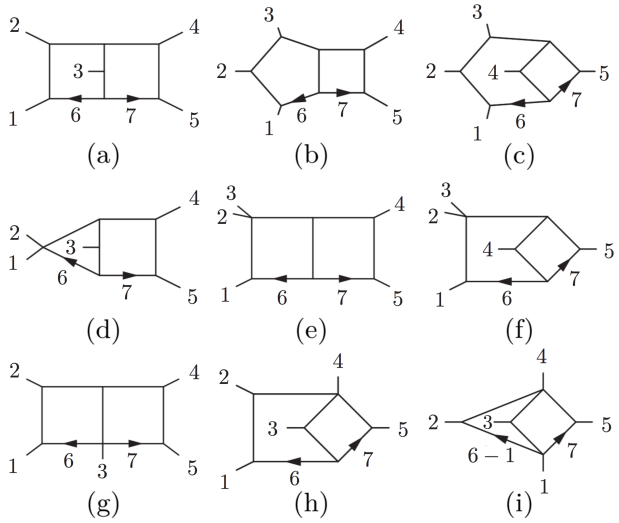

Figure 4.2: Diagrams (a)-(i) from the five-point amplitude in Ref. [87].

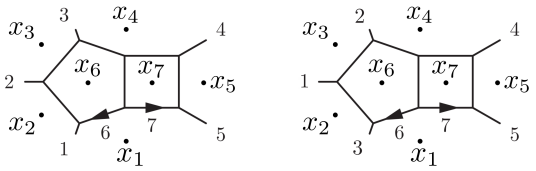

Figure 4.3: Dual variables useful for the two-loop planar pentabox and the nonplanar integrals in Fig. 4.2.

4.4 Two-loop five-point case

As the central nontrivial example consider the two-loop five-point $\mathcal{N} = 4$ sYM amplitude first obtained in Ref. [111]. This amplitude was rewritten in a desired form where each diagram composing the amplitude contains only logarithmic singularities and no pole at infinity [87], as follows from dual conformal symmetry in the planar case. The diagrams composing this amplitude are given in Fig. 4.2. These diagrams are either planar, or in the nonplanar class of diagrams discussed above, so our discussion immediately applies.

Consider diagrams (a), (d), (h), and (i), which can be made planar by moving the external

leg 3, corresponding to choosing $b^\mu \propto p_3^\mu$. Using the dual coordinates

$$\begin{aligned} &p_1 = x_3 - x_2\,, && p_2 = x_4 - x_3\,, && p_3 = x_2 - x_1\,, \\ &p_4 = x_5 - x_4\,, && p_5 = x_1 - x_5\,, && \\ &l_6 = x_6 - x_1\,, && l_7 = x_1 - x_7\,, && \end{aligned} \tag{4.4.1}$$

in the diagram on the right of Figure 4.3, the propagators in the original nonplanar diagrams are a subset of

$$\begin{aligned} &\rho_1 = (x_6 - x_1)^2, && \rho_2 = (x_6 - x_3 + p_3)^2, \\ &\rho_3 = (x_6 - x_4 + p_3)^2, && \rho_4 = (x_7 - x_4)^2, \\ &\rho_5 = (x_7 - x_5)^2, && \rho_6 = (x_7 - x_1)^2, \\ &\rho_7 = (x_6 - x_7)^2, && \rho_8 = (x_6 - x_7 + p_3)^2. \end{aligned} \tag{4.4.2}$$

A crucial difference between integrands at four points and five points is the appearance of spinor helicity variables, which makes the transformation properties less clear. We therefore restrict to $D = 4$ from now on, and the convention for spinors is chosen such that $s_{ij} = (p_i + p_j)^2 = \langle ij\rangle[ji] = \langle i|\, j|i] = (\langle i|_{\dot{a}}\, |j\rangle^{\dot{a}})([i|^a|j]_a) = \langle i|\, p_j|i]$. A complete set of numerators for the diagrams in Figure 4.2 is given in Table 3 of Ref. [87].

To warm up, consider the numerator in diagram (i)

$$N^{(\mathrm{i})} = \langle 2|\, 4|3]\, \langle 3|\, 5|2] - \langle 3|\, 4|2]\, \langle 2|\, 5|3]\,. \tag{4.4.3}$$

This numerator is constructed to follow the S_3 symmetry among legs $2, 3, 5$ of the diagram (up to a sign). By choosing to move leg 3 to make the diagram planar and using the coordinates in Eq. (4.4.1), we recast the numerator as

$$N^{(\mathrm{i})} = \langle 3|\, x_{54}\, x_{43}\, x_{32}|3] + \langle 3|\, x_{23}\, x_{34}\, x_{45}|3]\,, \tag{4.4.4}$$

under momentum conservation and spinor identities. To see that this numerator only rescales with a local weight under the transformation with $b^\mu \propto p_3^\mu$, we need a nontrivial identity

$$\frac{\delta \langle b| x_{i_1 i_2} x_{i_2 i_3} \dots x_{i_{n-1} i_n} |b]}{\langle b| x_{i_1 i_2} x_{i_2 i_3} \dots x_{i_{n-1} i_n} |b]} = -b \cdot (x_{i_1} + \dots + x_{i_n}) \,, \tag{4.4.5}$$

where $x_{ij} \equiv x_i - x_j$ and $\langle b| x_{i_1 i_2} x_{i_2 i_3} \dots x_{i_{n-1} i_n} |b] = (\langle b|_{\dot{a}})(x_{i_1 i_2}^{\dot{a}a})(x_{i_2 i_3, a\dot{b}}) \dots (x_{i_{n-1} i_n}^{\dot{c}d})(|b]_d)$. One can prove this using conformal inversions irrespective of whether the x_{ij}'s are null separated or not. We have directly confirmed Eq. (4.4.5) numerically through $n = 8$. Therefore the numerator in Eq. (4.4.4) is manifestly rescaled under the transformation with weight $-b \cdot (x_2 + x_3 + x_4 + x_5)$. Moreover, accounting for the transformation of the propagators and measure using Eqs. (4.2.7), (4.3.1), and (4.4.2), this is precisely the weight needed to make the integrand invariant.

We can also make diagram (i) planar by moving the leg carrying momentum p_2 or p_5, giving a total of three choices of b^μ for the conformal boosts. We have checked that these three transformations are independent symmetry generators, corresponding to three hidden symmetries of this nonplanar integrand.

A more involved example is diagram (a) in Fig. 4.2. The numerator yielding the desired analytic properties given in Ref. [87] is

$$N_1^{(\mathrm{a})} = \langle 13 \rangle \langle 24 \rangle \Big([24][13](l_7 - l_7^*)^2 (l_6 - l_6^*)^2 - (1 \leftrightarrow 2) \Big) \,, \tag{4.4.6}$$

where $l_7^* = \frac{[54]}{[24]} |5\rangle [2|$ and $l_6^* = p_1 + \frac{[23]}{[13]} |2\rangle [1|$. How this numerator transforms is far from clear in the above form. In fact, the first or second term alone does not rescale with a local weight. However, by using on-shell conditions and Schouten identities it can be rewritten as

$$\begin{aligned} N_1^{(\mathrm{a})} = & - \langle 3| x_{23} x_{34} x_{45} |3] \rho_4 \rho_1 \\ & + \langle 3| x_{23} x_{34} x_{45} x_{57} x_{76} x_{61} x_{14} |3] \,, \end{aligned} \tag{4.4.7}$$

using the dual coordinates in Eq. (4.4.1). With the help of Eq. (4.4.5), each of the two terms in Eq. (4.4.7) above transforms with the weight necessary to make the integrand invariant in $D = 4$. After canceling the propagators, the first term gives rise to the daughter diagram (i) in Fig. 4.2, and the numerator $\langle 3| \, x_{23} x_{34} x_{45} |3]$ also matches to one of the components in Eq. (4.4.4).

Similarly, we can rewrite the original numerators of diagrams (d) and (h) using the dual coordinates in the diagram on the left of Fig. 4.3 as

$$\begin{aligned} N_1^{(\mathrm{d})} &= s_{34}(s_{34} + s_{35}) \Big(l_7 - \frac{\langle 54 \rangle}{\langle 34 \rangle} |3\rangle [5| \Big)^2 \\ &= s_{34}(s_{34} + s_{35}) \rho_6 + \langle 3| \, x_{71} \, x_{15} \, x_{54} |3] \, , \end{aligned} \tag{4.4.8}$$

and

$$\begin{aligned} N_1^{(\mathrm{h})} &= \langle 15 \rangle [35] \langle 23 \rangle [12] \Big(l_6 - \frac{\langle 12 \rangle}{\langle 32 \rangle} |3\rangle [1| \Big)^2 \\ &= (s_{23} s_{35} - \langle 3| \, x_{34} \, x_{45} \, x_{51} |3]) \rho_1 \\ &\qquad - s_{12} \, \langle 3| \, x_{62} \, x_{23} \, \, x_{35} |3] \, , \\ N_3^{(\mathrm{h})} &= -s_{12} \, \langle 3| \, p_1 p_5 l_6 |3] = -s_{12} \, \langle 3| \, x_{35} \, x_{51} \, x_{16} |3] \, . \end{aligned} \tag{4.4.9}$$

In addition there are numerators simply related via diagram symmetries. Using Eqs. (4.2.7), (4.3.1), and (4.4.5), we see that these numerators have weights that make the integrand invariant under the dual conformal boost with $b^\mu \propto p_3^\mu$.

Diagrams (c) and (f) can be made planar by moving the external leg carrying momentum p_4, corresponding to $b^\mu \propto p_4^\mu$. The dual coordinates are defined according to the left of Figure 4.3, analogous to Eq. (4.4.1). The propagators in the original nonplanar diagrams

are a subset of

$$\begin{aligned}
&\rho_1 = (x_6 - x_1)^2, \quad \rho_2 = (x_6 - x_2)^2, && \rho_3 = (x_6 - x_3)^2, \\
&\rho_4 = (x_6 - x_4)^2, \quad \rho_5 = (x_7 - x_5)^2, && \rho_6 = (x_7 - x_1)^2, \\
&\rho_7 = (x_6 - x_7)^2, \quad \rho_8 = (x_6 - x_7 + p_4)^2. && \qquad (4.4.10)
\end{aligned}$$

The numerator of diagram (f) is $N_1^{(\mathrm{f})} = s_{14}s_{45}(l_6 + p_5)^2$ which manifestly rescales with local weight under the transformation. To see the conformal property of diagram (c), we need

$$\begin{aligned}
N_1^{(\mathrm{c})} &= \langle 15\rangle[54]\langle 43\rangle[13]\,(l_6 - l_6^*)^2\,(l_6 + p_4)^2 \qquad (4.4.11)\\
&= (-s_{51}s_{45}\rho_3 + \langle 4|\, x_{46}\, x_{63}\, x_{32}\, x_{21}\, x_{15}|4])\,(l_6 + p_4)^2,
\end{aligned}$$

with the same l_6^* as defined below Eq. (4.4.6). After canceling the propagator, the first term matches $N_2^{(\mathrm{f})}$ of Ref. [87] which is related to $N_1^{(\mathrm{f})}$ under $4 \leftrightarrow 5$.

We have checked all of the two-loop five-point nonplanar integrands from Ref. [87] that manifest the desired analytic properties of the full two-loop five-point amplitude and found that all of them have a hidden symmetry in $D = 4$ closely related to dual conformal symmetry. In cases where more than one conformal boost is available, as for diagrams (c), (f), (h), and (i) in Figure 4.2, we have checked that all such choices of b^μ give symmetries of the integrand. While Eq. (4.3.1) guarantees that all the propagators transform with definite weight, the fact that all the corresponding numerators behave accordingly to make the integrand invariant appears miraculous.

Using Eqs. (4.3.1) and (4.4.5) we can generalize these results to integrals relevant for higher-point amplitudes. As a concrete example, consider diagram (a) in Figure 4.2 but with legs 1,2,4,5 being massive or replaced with arbitrary collections of massless particles, while keeping leg 3 massless. Crucially, the identity in Eq. (4.4.5) holds even for $x_{i,i+1}^2 \neq 0$.

This implies the numerator with the dual variables in Eq. (4.4.1)

$$\langle 3|\, x_{23}\, x_{34}\, x_{45}\, x_{57}\, x_{76}\, x_{61}\, x_{14}|3]\,, \tag{4.4.12}$$

transforms with the proper weight to make the integrand invariant, providing a generalization of the second term in Eq. (4.4.7). Another possible numerator is

$$s_{12}s_{24}\big(\,\langle 3|\, x_{47}\, x_{76}\, x_{61}|3] + \langle 3|\, x_{16}\, x_{67}\, x_{74}|3]\big)\,. \tag{4.4.13}$$

The latter example (4.4.13) is especially interesting since it vanishes in the collinear limit $x_{76}^{\mu} \propto p_3^{\mu}$ and gives an infrared-finite integral, for which the hidden symmetry is *exact* and free of anomalies from divergences. By working in six dimensions, additional finite integrals with the hidden symmetry can be found; such integrals are related to four-dimensional ones via dimension shifting relations [96, 119].

4.5 Conclusions

Following the four-point hints in Ref. [2], here we demonstrated that all sectors of the two-loop five-point $\mathcal{N} = 4$ sYM amplitude, including the nonplanar sector, possess new nontrivial hidden symmetries related to dual conformal symmetry. To show this we demonstrated that each integrand sector identified in Ref. [87] possessing simple analytic properties manifests a hidden symmetry. For some sectors the symmetry is rather unobvious. The construction used for the two-loop five-point amplitude extends to any number of loops and legs, giving an infinite class of integrands with new hidden symmetries. It would be interesting to check if these cases actually appear with nonzero coefficient in $\mathcal{N} = 4$ sYM amplitudes. Even for the cases studied here we can expect a larger set of symmetries than the ones we found; we expect this to be helpful for the important problem of identifying the hidden symmetries of more general cases beyond the ones studied here. It would be interesting to apply the

symmetries to help identify nonplanar integrals of uniform transcendentality, which become nontrivial at high loop orders by directly checking leading singularities [120]. It would also be interesting to understand how the new symmetries described here relate to recent progress in extending integrability to nonplanar theories described in Ref. [121]. Given the useful role hidden symmetries have played in the planar sector of $\mathcal{N} = 4$ sYM theory, we should expect new progress from fully unraveling the corresponding symmetries of the nonplanar sector of the theory.

Chapter 5

Logarithms and Volumes of Polytopes

Describing the geometry of the dual amplituhedron without reference to a particular triangulation is an open problem. In this note we introduce a new way of determining the volume of the tree-level NMHV dual amplituhedron. We show that certain contour integrals of logarithms serve as natural building blocks for computing this volume as well as the volumes of general polytopes in any dimension. These building blocks encode the geometry of the underlying polytopes in a triangulation-independent way, and make identities between different representations of the amplitudes manifest.

5.1 Introduction

Recent years have seen tremendous progress in understanding scattering amplitudes in both gauge and gravity theories. New mathematical structures that are not apparent in textbook formulations of quantum field theory have been uncovered, and many computations have been immensely streamlined in comparison with the standard Feynman diagram approach (see the recent reviews [6,122,123] and references therein). While many of these developments have applications in theories with various amounts of (including no) supersymmetry, the computational simplicity of maximally supersymmetric gauge and gravity theories make them ideal testing grounds for new ideas [124].

One of the major breakthroughs in the study of maximally supersymmetric gauge theories is the discovery of the amplituhedron, an object that encodes all tree-level amplitudes and loop-level integrands in planar $\mathcal{N} = 4$ super-Yang–Mills theory (sYM) [11, 108]. Schematically, and specializing to the case of tree amplitudes, the amplituhedron is a region of a particular positive Grassmannian [11,107,108]. This region encodes the amplitude via a volume form with logarithmic singularities on its boundary, and after stripping off a canonical prefactor from this form what remains (up to some fermionic integrations) is the amplitude. For loop integrands the same is true but with the amplituhedron corresponding to a region of a particular generalization of the positive Grassmannian. In the rest of this note we restrict ourselves to the tree-level case.

For tree-level NMHV amplitudes, the amplitude obtained in this way is naturally interpreted as the volume of a polytope in a $\mathbb{CP}^4$ that is dual to the space in which the amplituhedron lives [11, 108, 125]. N^{k}MHV tree amplitudes with $k \geq 1$ are therefore viewed as a type of "generalized volume" of a dual amplituhedron [125,126]. For $k > 1$ a geometric understanding of the dual amplituhedron is unclear, though there are strong indications that such a picture should exist [126, 127].

In this note we introduce a new way of computing the volume of the tree-level NMHV (or $k = 1$) dual amplituhedron directly in the space in which the polytope lives. The basic objects in this method are contour integrals with simple, closed contours in the complex projective space containing the polytope. In Ref. [125] the authors computed these volumes by integrating a particular volume form over the underlying polytope in the dual space, thus placing the information about the polytope in the contour (which has boundaries). As we will see in section 3, our method differs from that in Ref. [125] by using contours that are closed (i.e., without boundary) and canonically specified by the integrands themselves. This is in contrast to, for example, "dlog" representations of amplitudes, where the contour is not specified by the integrand itself [107]. Additionally, the method we introduce is independent of any particular triangulation of the underlying polytope, and can be used to recover any

such triangulation.

In Ref. [5] we provided a definition of "combinatorial polytopes" which incorporates a general class of polytopes. For these polytopes neither convexity (and therefore positivity) nor even connectivity are necessary. We introduced a set of new objects that we denote by $F_{i_1 \ldots i_n}$ and will now refer to as "vertex objects." The reason for this naming convention is that the subscripts of these vertex objects correspond to the vertices of polytopes in a natural way that we will review shortly. In Ref. [5] we showed that we obtain the volume of a polytope by summing these vertex objects over the vertices of the polytope. This way of expressing the volume of a polytope does not require any triangulation of the polytope to be known, and the volume of the polytope is uniquely expressed in terms of these vertex objects. These observations motivate us to view the vertex objects as basic building blocks for computing volumes of polytopes.

The vertex objects satisfy a simple relation that allows us to easily derive many nontrivial identities between different representations of the tree-level NMHV amplitude, as we will review in the next section. These identities and their more complex analogues for N^{k}MHV amplitudes with $k > 1$ can also be derived using global residue theorems (GRTs) on an auxiliary Grassmannian [128, 129]. In this picture, computing tree amplitudes and loop integrands is equivalent to specifying the correct contour for a particular integrand in the Grassmannian [107], and relations between different representations of the amplitude follow from the GRTs. Introducing this auxiliary space manifests the Yangian symmetry of the amplitudes [130], while the geometry of the underlying space whose volume corresponds to the amplitude gets obscured. By showing that the vertex objects discussed above are naturally given by contour integrals in the dual space directly, we give a formalism that both manifests the relations between different representations of the amplitude while avoiding the introduction of an auxiliary space. This formalism has not been extended to N^{k}MHV amplitudes with $k > 1$, but doing so will likely illuminate the underlying geometry of the dual amplituhedron.

The outline of this note is as follows: In the next section we briefly review some key properties of complex projective space and the standard generalization of volumes of polytopes to projective spaces. We will also briefly describe how NMHV tree amplitudes are expressed as volumes of polytopes and how the vertex objects are defined and used. In section 3 we show how contour integrals of logarithms naturally arise in computing the areas of quadrilaterals and their higher-dimensional analogues. In section 4 we show how the vertex objects correspond to a particular combination of these integrals.

5.2 Polytopes in Projective Space

In this section we review the ideas that will be needed in later sections. After discussing some key facts about (complex) projective spaces, we will review the standard generalization of volumes of polytopes in affine space to that of polytopes in projective space. We then briefly describe the formalism introduced in Ref. [5], where the vertex objects encode the geometry of polytopes as well as give their volumes. Finally, we review how these vertex objects are used to manifest certain properties of the NMHV tree-amplitude. In the remaining sections of this note we show how these vertex objects are given as contour integrals in the space containing the polytope.

5.2.1 Projective Geometry

In this brief review of projective geometry we follow Ref. [131] and the first appendix of Ref. [132], which provide more complete discussions of these ideas.

A point $\mathbb{Z}^\alpha \in \mathbb{CP}^n$ is defined by $n+1$ homogenous coordinates, one for each value of $\alpha = 0, ..., n$. Each such point defines an $(n-1)$-dimensional hyperplane H_Z in the dual $\mathbb{CP}^{n*}$ by placing a single linear constraint on the homogenous coordinates of the dual elements. Namely, we have

$$H_Z \equiv \{A_\alpha \in \mathbb{CP}^{n*} \mid Z \cdot A \equiv Z^\alpha A_\alpha = 0\} \simeq \mathbb{CP}^{n-1} \subset \mathbb{CP}^{n*}. \tag{5.2.1}$$

The subspace H_Z is a linearly embedded $\mathbb{CP}^{n-1}$ in the dual $\mathbb{CP}^{n*}$. We will refer to linearly embedded $\mathbb{CP}^1$'s, $\mathbb{CP}^2$'s, and $\mathbb{CP}^k$'s with $k > 2$ respectively as lines, planes, and hyperplanes, even though the underlying topology of these spaces may be rather different. For example, a $\mathbb{CP}^1$ is a Riemann sphere though we will still refer to it as a line.

Intersections of lines, planes, and hyperplanes always exist in projective geometry. For example, three points Z_1^α, Z_2^α, and Z_3^α in $\mathbb{CP}^2$ give three lines in the dual $\mathbb{CP}^{2*}$ and each pair of lines intersects in a unique point. This is shown in Figure 5.1, where the line dual to Z_i^α is labeled by i, and the intersection of lines i and j is labeled by $\{i, j\}$.

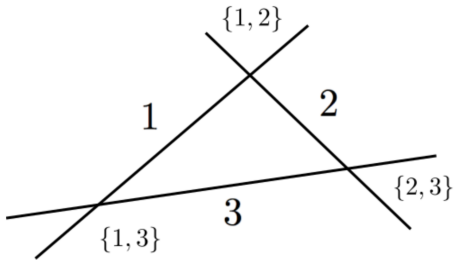

Figure 5.1: Three lines in $\mathbb{CP}^{2*}$ labeled by i corresponding to three points $\{Z_i^\alpha\}_{1 \leq i \leq 3}$ in $\mathbb{CP}^2$. The intersection of lines i and j is denoted by $\{i, j\}$. We note that $\{i, j\} = \{j, i\}$ implicitly.

More generally, any two distinct $(n-1)$-dimensional hyperplanes in $\mathbb{CP}^{n*}$ intersect in a unique $(n-2)$-dimensional hyperplane. Namely, two points Z_1^α and Z_2^α in $\mathbb{CP}^n$ define two $(n-1)$-dimensional hyperplanes H_{Z_1} and H_{Z_2} in $\mathbb{CP}^{n*}$, and we have that

$$H_{Z_1} \cap H_{Z_2} \simeq \mathbb{CP}^{n-2} \subset \mathbb{CP}^{n*}. \tag{5.2.2}$$

We therefore see that n distinct points in $\mathbb{CP}^n$ uniquely define a point in the dual $\mathbb{CP}^{n*}$ via the simultaneous intersection of their n dual hyperplanes.

5.2.2 Volumes of Simplices

There is a natural generalization of the volume of a polytope to projective space. By first understanding this extension for the case of a simplex, the volume of more general polytopes

follows immediately by considering sums of simplices. We will therefore follow Ref. [125] and review how to express the volume of simplices in a projective way.

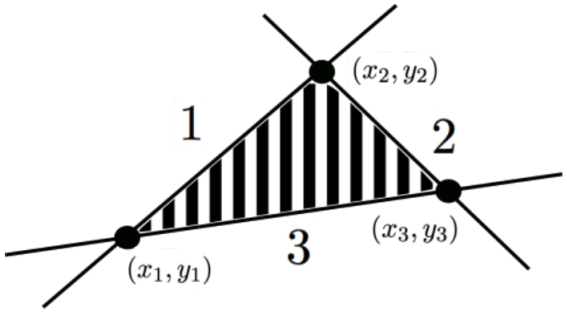

Figure 5.2: A triangle in affine space defined by vertices (x_i, y_i), with faces (edges) labeled by i corresponding to the points $\{Z_i^\alpha\}_{1\leq i\leq 3}$ in the dual space that define them. The Z_i^α's are explicitly defined in terms of the (x_i, y_i) coordinates in the text.

We begin by considering the area of a two-simplex, or a triangle, in real affine space with vertices located at (x_1, y_1), (x_2, y_2), (x_3, y_3), as shown in Figure 5.2. We can write its area A as [125]

$$A = \frac{1}{2}\frac{\langle Z_1 Z_2 Z_3\rangle^2}{\langle Z_1 Z_2 P\rangle\langle Z_2 Z_3 P\rangle\langle Z_3 Z_1 P\rangle} \equiv [123], \tag{5.2.3}$$

where we have introduced the notation $\langle Z_1 ... Z_n\rangle \equiv \varepsilon_{\alpha_1 ... \alpha_n} Z_1^{\alpha_1} ... Z_n^{\alpha_n}$, with the value of n taken from context. We have also defined

$$W_{i\alpha} \equiv \begin{pmatrix} x_i \\ y_i \\ 1 \end{pmatrix}, \qquad P^\alpha = \begin{pmatrix} 0 \\ 0 \\ 1 \end{pmatrix} \tag{5.2.4}$$

as well as

$$Z_1^\alpha \equiv \varepsilon^{\alpha\beta\gamma} W_{1\beta} W_{2\gamma}, \quad Z_2^\alpha \equiv \varepsilon^{\alpha\beta\gamma} W_{2\beta} W_{3\gamma}, \quad Z_3^\alpha \equiv \varepsilon^{\alpha\beta\gamma} W_{3\beta} W_{1\gamma}. \tag{5.2.5}$$

We note that the Z_i^α, $W_{i\alpha}$, and P^α all have three homogenous coordinates, in line with their being elements of $\mathbb{CP}^2$ (or its dual). We have simply "lifted" the affine coordinates into a

particular coordinate patch of projective space by placing a 1 in the third component of the $W_{i\alpha}$'s.

Equation (5.2.3) is projectively well-defined in the Z_i^α's—which, according to the discussion in the previous subsection, determine the faces of the triangle—thus allowing their domain of definition to extend to $\mathbb{CP}^2$. We note that (5.2.3) is not projectively well-defined in P^α since it defines the line at infinity in $\mathbb{CP}^{2*}$ and therefore the scaling of the area—the scaling we choose here corresponds to the choice of placing 1 (as opposed to a different non-zero number) in the third component of the $W_{i\alpha}$'s. Equation (5.2.3) is also completely antisymmetric in the Z_i^α's, corresponding to the two possible orientations of the triangle.

It will be instructive to see explicitly how this works for one-dimensional simplices as well. A one-simplex is simply a line, and the distance L between two points x_1 and x_2 in $\mathbb{R}$ can be written as

$$L = \frac{\langle Z_1 Z_2 \rangle}{\langle Z_1 P \rangle \langle Z_2 P \rangle}. \tag{5.2.6}$$

Here we have defined

$$Z_1^\alpha \equiv \varepsilon^{\alpha\beta} W_{i\beta}, \quad W_{i\alpha} \equiv \begin{pmatrix} x_i \\ 1 \end{pmatrix}, \text{ and } \quad P^\alpha \equiv \begin{pmatrix} 0 \\ 1 \end{pmatrix}. \tag{5.2.7}$$

Equation (5.2.6) indeed reproduces $L = x_1 - x_2$, as expected, and it expresses the length of the line defined by the endpoints $W_{1\alpha}$ and $W_{2\alpha}$ in terms of their duals and the point at infinity defined by P^α. It is projective and antisymmetric in Z_1^α and Z_2^α, corresponding to the two different orientations of the line.

This generalizes to volumes of simplices in any dimension. For any $D{+}1$ points $\{Z_i^\alpha\}_{1 \le i \le D+1}$ in $\mathbb{CP}^D$ there are $D{+}1$ hyperplanes in the dual $\mathbb{CP}^{D*}$, and the volume of the simplex bounded by these hyperplanes is given by [125]

$$V = \frac{1}{D!} \frac{\langle Z_1 ... Z_{D+1} \rangle^D}{\langle Z_1 ... Z_D P \rangle \langle Z_2 ... Z_{D+1} P \rangle ... \langle Z_{D+1} ... Z_{D-1} P \rangle} \equiv [12...(D+1)]. \tag{5.2.8}$$

This expression is projective and totally antisymmetric in the Z_i^α's. The antisymmetry corresponds to the two possible orientations of the simplex.

The dimension most relevant for scattering amplitudes is four, so for completeness we will explicitly write the volume of a four-simplex, bounded by the five faces defined by $Z_1^\alpha, ..., Z_5^\alpha$. Translating the above formula gives

$$V = \frac{1}{4!} \frac{\langle Z_1 Z_2 Z_3 Z_4 Z_5 \rangle^4}{\langle Z_1 Z_2 Z_3 Z_4 P \rangle \langle Z_2 Z_3 Z_4 Z_5 P \rangle \langle Z_3 Z_4 Z_5 Z_1 P \rangle \langle Z_4 Z_5 Z_1 Z_2 P \rangle \langle Z_5 Z_1 Z_2 Z_3 P \rangle} \equiv [12345]. \tag{5.2.9}$$

5.2.3 Volumes of General Polytopes

For a fixed dimension D, we can view any sum of simplices as the volume of a general polytope, expressed through some particular triangulation. For example, four points Z_1^α, Z_2^α, Z_3^α, and Z_4^α in $\mathbb{CP}^2$ define four lines in the dual $\mathbb{CP}^{2*}$. These four lines are depicted in Figure 5.3 and are respectively labeled by 1, 2, 3, and 4.

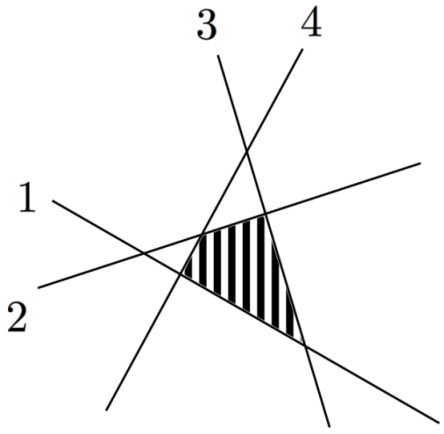

Figure 5.3: A quadrilateral in $\mathbb{CP}^{2*}$ defined by four lines labeled by i according to the points $\{Z_i^\alpha\}_{1 \leq i \leq 4}$ in $\mathbb{CP}^2$ that define them.

The area of the shaded quadrilateral can be written as

$$A = [123] - [124], \tag{5.2.10}$$

which is the area of the triangle bounded by the faces 1, 2, and 3 minus the area of the triangle bounded by the faces 1, 2, and 4. This is depicted in Figure 5.4.

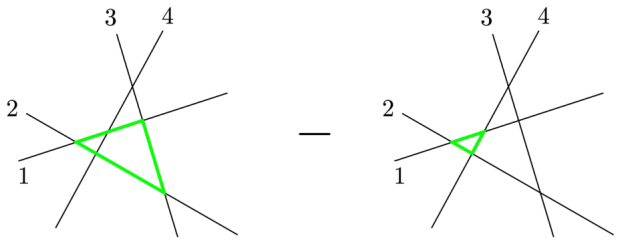

Figure 5.4: The quadrilateral shown in Figure 5.3 viewed as the difference of two triangles.

By inspection of Figure 5.3 we also see that we can write the area of the same region as

$$A = [431] - [432], \tag{5.2.11}$$

by viewing this area as the difference between the area of the triangle bounded by the faces 4, 3, and 1, and the triangle bounded by the faces 4, 3, and 2. We therefore see that we have

$$[123] - [124] = [431] - [432], \tag{5.2.12}$$

which, when one unravels the definition of these 3-brackets, is a nontrivial relation.

Proving this relation through repeated application of Schouten identities on the $\langle ... \rangle$ brackets quickly shows that this geometric proof is more convenient, especially for analogous relations in higher dimensions. However, this geometric proof is not very precise, for a few reasons. For one, we have not been careful to keep track of the orientation of the quadrilateral in our two different triangulations. A second and more serious ambiguity is that our notion of a polytope itself is rather tenuous. Namely, once we extend our underlying space from a real affine space to a complex projective space, any notion of "inside" or "outside" is lost. Moreover, one generally thinks of a D-dimensional polytope in a D-dimensional space as being some full-dimensional region carved out by a finite number of hyperplanes. However, by complexifying our compact space, we end up talking about D-dimensional polytopes

in $\mathbb{CP}^D$, which is a space of $2D$ real dimensions. A third issue with trying to define a polytope as a sum of volumes of simplices is that there are (infinitely) many triangulations that correspond to the same polytope. Some triangulations may make apparent certain geometric qualities of the underlying polytope while masking others.

The amplituhedron makes precise sense of these polytopes as a region in a positive Grassmannian, and for the NMHV case under consideration, this Grassmannian is simply a projective space [11]. In this program one considers convex polytopes, which places positivity constraints on the external kinematics. One then analytically continues to consider general kinematics. In Ref. [5] we instead focused solely on the combinatorial structure of polytopes. We then gave a precise definition of a general type of polytope that is not necessarily convex or even connected. In the next subsection we will briefly review these ideas in two dimensions, as well as introduce the two-dimensional vertex objects $\{F_{ij}\}$. We refer to Ref. [5] for details and the higher-dimensional cases.

5.2.4 The Vertex Formalism

We consider again the quadrilateral in Figure 5.3 and our goal will be to give it a precise definition. While this figure does not correctly depict the topology of the objects involved—as mentioned above, the lines are actually Riemann spheres—it does correctly depict the intersection structure of these objects. We therefore define this polytope by its intersection structure, saying that this is the "quadrilateral" defined by starting at the vertex $\{1,4\}$ and walking along line 4 to arrive at the vertex $\{2,4\}$, then walking along line 2 to arrive at the vertex $\{2,3\}$, then walking along line 3 to arrive at the vertex $\{3,1\}$, and then walking along line 3 to arrive back at the vertex $\{1,4\}$. This is depicted in Figure 5.5.

This set of instructions can be succinctly summarized by the list (1423), which we define to be shorthand for

$$\{1,4\} \to \{4,2\} \to \{2,3\} \to \{3,1\} \to \{1,4\} \tag{5.2.13}$$

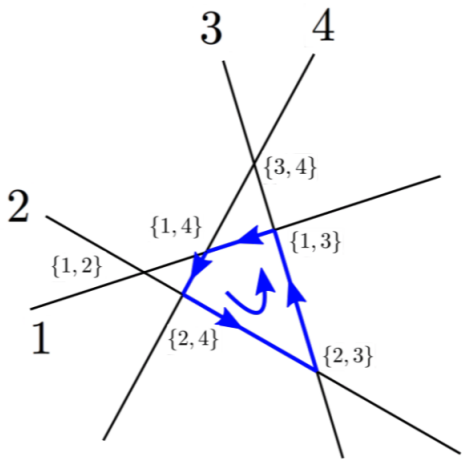

Figure 5.5: The quadrilateral depicted in Figure 5.3 defined solely through the intersection of its faces.

where each "$\rightarrow$" means to travel along the line whose label is common to the vertex on either side of the arrow.

In Ref. [5] we introduced a collection $\{F_{ij}\}$ of vertex objects defined as a particular sum of volumes of simplices. These objects are referred to as vertex objects because a vertex of a two-dimensional polytope is labeled by two lines, as is each F_{ij}. We found that these vertex objects are antisymmetric, so that $F_{ij} = -F_{ji}$, and that they satisfy[1]

$$F_{ij} + F_{jk} + F_{ki} = [ijk] \tag{5.2.14}$$

for any choice of i, j, and k, where we recall that $[ijk]$ is the volume of the two-simplex bounded by the three lines i, j, and k.

We consider the sum $F_{14} + F_{42} + F_{23} + F_{31}$ over the vertices of this quadrilateral. Using

[1]These vertex objects differ from those introduced in Ref. [5] by a factor of 2.

the antisymmetry of each F_{ij} and equation (5.2.14), we find

$$\begin{aligned} F_{14} + F_{42} + F_{23} + F_{31} &= F_{14} + F_{42} + ([231] - F_{12}) \\ &= [123] - (F_{12} + F_{24} + F_{41}) \\ &= [123] - [124], \end{aligned} \tag{5.2.15}$$

which is precisely the volume of the quadrilateral that the list of vertices in (5.2.13) defines. Applying equation (5.2.14) to the left hand side of (5.2.15) in a different order also shows that

$$F_{14} + F_{42} + F_{23} + F_{31} = [431] - [432]. \tag{5.2.16}$$

This gives a quick and rigorous proof of the nontrivial identity (5.2.12). Indeed, all possible triangulations of the quadrilateral can be obtained by applying (5.2.14) to the left hand side of (5.2.15), giving a simple algebraic method for proving many nontrivial identities amongst sums of simplices [5].

This example is a special case of a more general phenomenon—given any set of vertex-connecting instructions defining any polygon, summing the corresponding F_{ij} for each vertex yields the area of that polygon. This process works for general polygons, even disconnected ones. For example, suppose we have six elements $\{Z_i^\alpha\}$, $1 \leq i \leq 6$, defining six lines, as shown on the left hand side of Figure 5.6. We can then define the disconnected polygon shown on the right hand side of this figure by the instructions

$$\{5,1\} \to \{1,6\} \to \{6,2\} \to \{2,4\} \to \{4,5\} \to \{5,6\} \to \{6,3\} \to \{3,5\} \to \{5,1\}. \tag{5.2.17}$$

Analogously to the case of the quadrilateral, this set of instructions corresponds to the list (51624563). It is then the case, rather surprisingly, that the area A of this polygon can be

written simply as

$$A = F_{51} + F_{16} + F_{62} + F_{24} + F_{45} + F_{56} + F_{63} + F_{35}. \tag{5.2.18}$$

This can be checked against any particular triangulation of this polygon. Additionally, any triangulation of this polygon can be obtained from this expression through repeated use of (5.2.14).

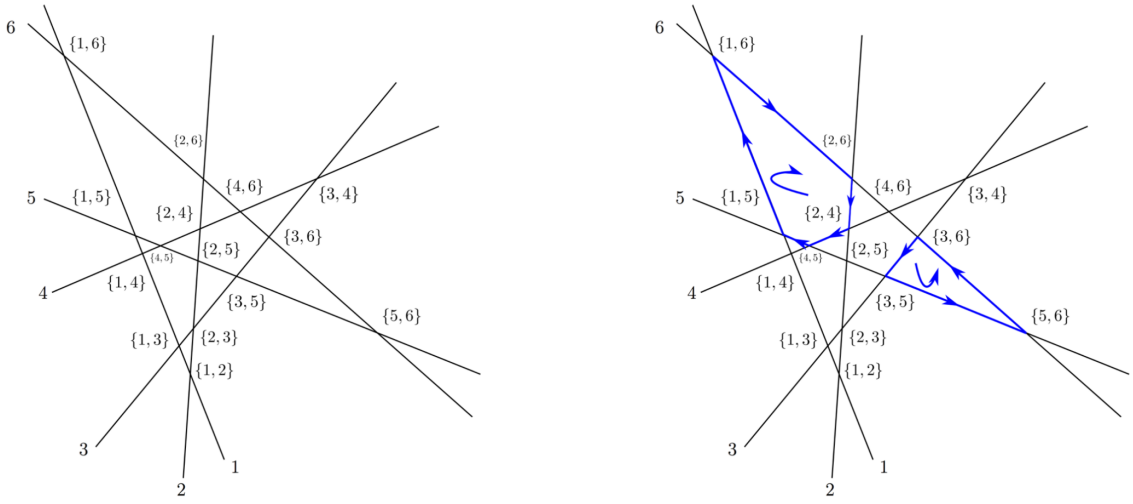

Figure 5.6: A general polygon (right) defined solely through a set of instructions for traversing the intersections of six lines (left). Lines are labeled by i according to the Z_i^α that defines them, and the intersection of two lines i and j is denoted by $\{i, j\}$. It is implied that $\{i, j\} = \{j, i\}$.

The general result can be stated as follows. Let $\{Z_i^\alpha\}$ be a collection of N elements in $\mathbb{CP}^2$ defining N lines in the dual $\mathbb{CP}^{2*}$. The most general polygon in this dual $\mathbb{CP}^{2*}$ is given by a list $(i_1 i_2 ... i_n)$, corresponding to the instructions

$$\{i_1, i_2\} \to \{i_2, i_3\} \to ... \to \{i_{n-1}, i_n\} \to \{i_n, i_1\} \to \{i_1, i_2\}. \tag{5.2.19}$$

The area A of this polygon is then given by the following sum over the vertices:

$$A = \sum_{k=1}^{n} F_{i_k i_{k+1}}, \tag{5.2.20}$$

and from this expression any particular triangulation can be obtained [5]. This form of the area is independent of any particular triangulation and is inherently tied to the data of the polygon itself—its vertices and how we traverse them.

We note that many different lists give rise to the same polygon. For example, any cyclic permutation of a list gives the same polygon. More trivially, the list (1234) is identical to the list (12121234), since the latter corresponds to staying on the vertex $\{1, 2\}$ over and over again before moving on. However, the final result in terms of the vertex objects (up to trivial cancellations) is identical. For example, the sum of these objects corresponding to the list (12121234) is simply

$$F_{12} + F_{21} + F_{12} + F_{21} + F_{12} + F_{23} + F_{34} + F_{41}, \tag{5.2.21}$$

which, after using the antisymmetry of F_{ij} yields the same result as the list (1234). Indeed, the sum in (5.2.20) is dependent only on the equivalence class of lists, where equivalence of lists is defined by their determining the same polygon. In Ref. [5] we show how to extend this definition of polygon to arbitrary higher-dimensional polytopes.

In Ref. [5] we also defined the corresponding vertex objects in higher dimensions. For example, in three dimensions we defined a collection of vertex objects $\{F_{ijk}\}$ completely antisymmetric in their subscripts and satisfying

$$F_{ijk} - F_{jkl} + F_{kli} - F_{lij} = [ijkl] \tag{5.2.22}$$

for any choice of i, j, k, l. We continue to use the term "vertex objects" because for a three-dimensional polytope a vertex is defined by the intersection of three planes, each defined by a Z_i^α, and these planes determine the subscripts of a given F_{ijk}. In four dimensions we defined a collection $\{F_{ijkl}\}$ of vertex objects that are totally antisymmetric in their subscripts and that satisfy

$$F_{ijkl} + F_{jklm} + F_{klmi} + F_{lmij} + F_{mijk} = [ijklm] \tag{5.2.23}$$

for any choice of i, j, k, l, m.

The volume of any polytope is given by the sum over its vertices of these vertex objects. This expression of the volume is unique, and any triangulation of the polytope can be recovered from this expression using (5.2.22), (5.2.23), and their higher-dimensional analogues. Additionally, the expression of the volume of a polytope in terms of the vertex objects also encodes the geometry of all lower-dimensional boundary polytopes and readily gives their volumes as well [5].

We note that equation (5.2.23) is reminiscent of the formula

$$\partial[ijklm] = [ijkl] + [jklm] + [klmi] + [lmij] + [mijk] \tag{5.2.24}$$

given in [125], describing the boundary $\partial[ijklm]$ of the simplex and encoding where the poles of $[ijklm]$ are. Equation (5.2.23) does the same, and is also a genuine equality between the volume of the simplex and objects that correspond to its vertices. Thus the objects on the left of equation (5.2.23) are fundamentally different than those on the right of equation (5.2.24). Similar statements can be made about equations (5.2.14) and (5.2.22) and the lower-dimensional analogues of equation (5.2.24).

5.2.5 Applications to NMHV Amplitudes

Quite surprisingly, the n-point NMHV tree-level superamplitude M^n_{NMHV} in $\mathcal{N} = 4$ planar sYM can be written as the volume of a polytope in $\mathbb{CP}^{4*}$ [125]. Indeed, M^n_{NMHV} can be represented as

$$M^n_{\text{NMHV}} = \sum_{i,j}^{n} [*i(i+1)j(j+1)] \tag{5.2.25}$$

where the $\{Z^\alpha_i\}$ implicitly inside the five-brackets in the sum are n points in $\mathbb{CP}^4$ encoding the external kinematics and Z^α_* is a reference vector in $\mathbb{CP}^4$. The sum on i, j is understood modulo n, and polytopes of this form are known as *cyclic polytopes* [11].

For any given n, M^n_{NMHV} has many different expressions depending on our choice of Z^α_*.

For example, if we choose $Z_*^\alpha = Z_1^\alpha$, then for $n = 6$ we have

$$M^6_{\text{NMHV}} = [12345] + [12356] + [13456], \tag{5.2.26}$$

while if we choose $Z_*^\alpha = Z_2^\alpha$, then we have

$$M^6_{\text{NMHV}} = [23456] + [23461] + [24561]. \tag{5.2.27}$$

Just as the relation (5.2.12) is not obvious at the level of Schouten identities on the $\langle ... \rangle$ brackets, the equivalence of the right hand sides of (5.2.26) and (5.2.27) is nontrivial. These two representations of M^6_{NMHV} were initially found by performing two different BCFW shifts on the amplitude [125, 133, 134]. The geometric interpretation is that they correspond to two different triangulations of the same underlying polytope. As discussed in the introduction, their equality can also be understood by using a global residue theorem in an auxiliary Grassmannian [128, 129]. Part of the utility of the vertex objects is to show that the right hand sides of (5.2.26) and (5.2.27) are equal directly—namely, they are identical when expressed in term of these objects. By using equation (5.2.23) on each simplex in either (5.2.26) or (5.2.27), we find

$$M^6_{\text{NMHV}} = F_{1234} + F_{1245} + F_{1256} + F_{2345} + F_{2356} + F_{2361} + F_{3456} + F_{3461} + F_{4561}. \tag{5.2.28}$$

The amplitude is therefore uniquely expressed in terms of the vertex objects. From this expression and equation (5.2.23), any triangulation of M^6_{NMHV} can be obtained.

For general n, we have

$$\begin{aligned} M^n_{\text{NMHV}} &= \sum_{i,j}^{n} [*i(i+1)j(j+1)] \\ &= \sum_{i,j}^{n} F_{*i(i+1)j} + F_{i(i+1)j(j+1)} + F_{(i+1)j(j+1)*} + F_{j(j+1)*i} + F_{(j+1)*i(i+1)} \\ &= \sum_{i,j}^{n} F_{i(i+1)j(j+1)}, \end{aligned} \tag{5.2.29}$$

where in the second equality we used equation (5.2.23) and in the last equality we used the cyclicity of the sum and antisymmetry of the vertex objects to cancel in pairs any terms with $*$ as a subscript. This shows manifestly that the amplitude is independent of Z^α_* and that the underlying polytope has vertices only where the four hyperplanes defined by Z^α_i, Z^α_{i+1}, Z^α_j, and Z^α_{j+1} intersect.

We refer to Ref. [5] for further discussion of this vertex formalism. In the next two sections we show that these vertex objects are naturally defined as contour integrals of logarithms.

5.3 Volumes and Logarithms

In [5] the vertex objects are defined as a particular sum of simplices. Thus, in some sense, writing the volume of a polytope in terms of these objects may be viewed as simply choosing a particular triangulation. However, we will now show that these objects are naturally defined in terms of contour integrals of logarithms, thus giving them an existence independent of simplices. This further motivates the view that the vertex objects are basic building blocks for computing volumes of polytopes.

As mentioned in the introduction, our integrals differ from those discussed in Ref. [125] in that the latter involve contours with boundaries on the underlying polytope. Evaluating volumes in this way leads to the presence of spurious vertices (which correspond physically to spurious poles) associated to a particular triangulation. For example, the vertex $\{1, 2\}$ is a spurious vertex in the triangulation depicted in Figure 5.4, since it is not present in the

underlying polytope but shows up in individual terms in the triangulation. As we will see, the integrals we use have closed contours, so evaluating them corresponds to a straightforward application of Cauchy's residue theorem. Moreover, they give rise to the vertex objects used in the vertex formalism discussed above, in which only the genuine (i.e., non-spurious) vertices of the polytope play a role.

5.3.1 One Dimension

As a warmup, we begin our discussion in one dimension. Another way of writing the length L of a line from x_1 to x_2 is as

$$L = x_1 - x_2 = \int_{x_1 \leq x \leq x_2} dx = \frac{1}{2\pi i} \int_{x_1 \leq x \leq x_2} 2\pi i \; dx. \tag{5.3.1}$$

By allowing the x variables to be complex, we can define the complex logarithm function $\log\left(\frac{x-x_1}{x-x_2}\right)$ with its branch cut connecting the point x_1 to the point x_2 along the real axis. We can then rewrite $2\pi i$ as $\text{Disc}\big(\log\left(\frac{x-x_1}{x-x_2}\right)\big)$—the discontinuity of the logarithm across its branch cut—giving

$$L = \frac{1}{2\pi i} \int_{x_1 \leq x \leq x_2} \text{Disc}\Big(\log\Big(\frac{x-x_1}{x-x_2}\Big)\Big) \;\; dx. \tag{5.3.2}$$

Unwrapping the contour allows one to drop the "Disc" from the integrand and obtain

$$L = \frac{1}{2\pi i} \oint \log\Big(\frac{x-x_1}{x-x_2}\Big) \;\; dx. \tag{5.3.3}$$

where the contour surrounds the cut. Evaluating this explicitly (for example, by going around the pole at infinity) recovers $L = x_1 - x_2$, as expected.

Making the same definitions as in (5.2.7) we can rewrite (5.3.3) as a contour integral in $\mathbb{CP}^{1*}$ as

$$L = \frac{1}{2\pi i} \oint \log\Big(\frac{Z_1 \cdot X}{Z_2 \cdot X}\Big) \frac{DX}{(P \cdot X)^2}, \tag{5.3.4}$$

where $DX \equiv \varepsilon^{\alpha\beta} X_\alpha dX_\beta$ is the canonical volume form (of weight two) on $\mathbb{CP}^{1*}$ and $X_\alpha \equiv$

$\begin{pmatrix} x \\ 1 \end{pmatrix}$. By explicitly evaluating this integral we find

$$L = \frac{\langle Z_1 Z_2 \rangle}{\langle Z_1 P \rangle \langle Z_2 P \rangle}, \tag{5.3.5}$$

in agreement with equation (5.2.6). In this way, the length of a line is naturally represented as a contour integral of a logarithm.

5.3.2 Two Dimensions

Motivated by the one-dimensional result, we consider the $\mathbb{CP}^{2*}$ integral

$$A = \frac{1}{(2\pi i)^2} \oint \log\Big(\frac{Z_1 \cdot X}{Z_2 \cdot X}\Big) \log\Big(\frac{Z_3 \cdot X}{Z_4 \cdot X}\Big) \frac{DX}{(P \cdot X)^3}, \tag{5.3.6}$$

where $DX \equiv \varepsilon^{\alpha\beta\gamma} X_\alpha dX_\beta dX_\gamma$ is the canonical volume form on $\mathbb{CP}^{2*}$ of weight three. The contour is again defined by the integrand in a canonical way: first go around the branch cut of $\log\big(\frac{Z_3 \cdot X}{Z_4 \cdot X}\big)$ and then go around the branch cut of $\log\big(\frac{Z_1 \cdot X}{Z_2 \cdot X}\big)$. This gives

$$A = [123] - [124], \tag{5.3.7}$$

which is precisely the area of the quadrilateral given in equation (5.2.10). If we swap Z_3^α, and Z_4^α with Z_1^α and Z_2^α in equation (5.3.6) and pick up a minus sign from the change in orientation of the contour, one readily sees that

$$A = -([341] - [342]), \tag{5.3.8}$$

thus proving the identity $[123] - [123] = [431] - [432]$ that we obtained in section 5.2.3. This identity is now made manifest by the integrand of (5.3.6).

We have expressed a two-dimensional area as a closed contour integral whose contour

specification comes naturally with the integrand itself. The objects whose area we compute in this way are quadrilaterals, defined by four lines. Before describing how the vertex objects are obtained from these kinds of integrals, we quickly discuss how we can use these integrals to compute the volume of three- and D-dimensional "quadrilaterals," or hypercubes.

5.3.3 Higher Dimensions

Consider the following contour integral in $\mathbb{CP}^{3*}$:

$$V = \frac{1}{(2\pi i)^3} \oint \log\Big(\frac{Z_1 \cdot X}{Z_2 \cdot X}\Big) \log\Big(\frac{Z_3 \cdot X}{Z_4 \cdot X}\Big) \log\Big(\frac{Z_5 \cdot X}{Z_6 \cdot X}\Big) \frac{DX}{(P \cdot X)^4}, \tag{5.3.9}$$

where $DX \equiv \varepsilon^{\alpha\beta\gamma\delta} X_\alpha dX_\beta dX_\gamma dX_\delta$. The contour is a three-torus $(S^1)^3$ that goes around the branch cut of each logarithm. We find that

$$V = [1235] - [1236] - [1245] + [1246]. \tag{5.3.10}$$

This corresponds to the volume of a three-dimensional "cube," where we simply mean a polytope bounded by 3 pairs of faces. One way to see that equation (5.3.10) is triangulating a "cube" with faces 1 and 2 opposite each other, 3 and 4 opposite each other, and 5 and 6 opposite each other is by examining Figure 5.7, which shows the superposition of the four simplices in (5.3.10) leaving the volume of a "cube."

As in the two-dimensional case, there is more than one expression for the volume of this cube. Namely, just as we could get two different expressions for the area of a quadrilateral by viewing it as the difference between two different pairs of triangles, we can get three expressions for the volume of the cube as a superposition of four simplices. In particular, we also have

$$V = -([3415] - [3416] - [3425] - [3426]) \quad \text{and} \quad V = -([5631] - [5632] - [5641] - [5642]), \tag{5.3.11}$$

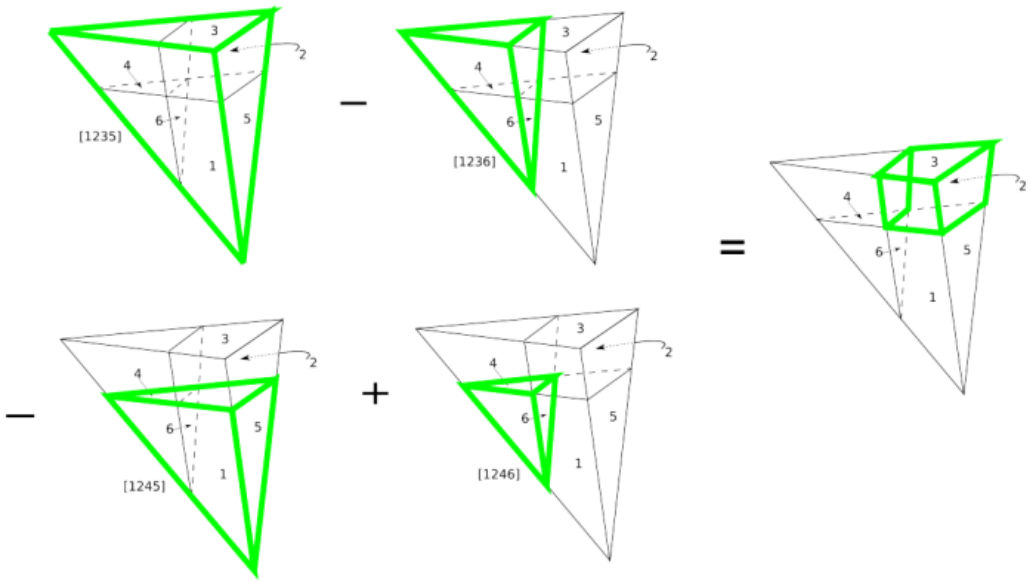

Figure 5.7: A triangulation of the cube using four simplices.

which correspond to the different ways of decomposing the cube analogously to Figure 5.7 corresponding to Figure 5.8. Figure 5.8 is the three-dimensional analog of Figure 5.4. As in the two-dimensional case, these identities are manifest from the integrand in (5.3.9) by swapping, for example, Z_1^α and Z_2^α with Z_3^α and Z_4^α, or with Z_5^α and Z_6^α, and picking up a minus sign from the change in orientation of the contour.

For completeness we write down the contour integral that gives the volume of a D-dimensional "hypercube" bounded by $2D$ faces in "pairs." With $Z_1^\alpha, ..., Z_{2D}^\alpha$ defining the $2D$ faces, we have a generalization of the lower-dimensional cases:

$$V = \frac{1}{(2\pi i)^D} \oint \log\left(\frac{Z_1 \cdot X}{Z_2 \cdot X}\right) ... \log\left(\frac{Z_{2D-1} \cdot X}{Z_{2D} \cdot X}\right) \frac{DX}{(P \cdot X)^{D+1}}, \tag{5.3.12}$$

where DX is the natural generalization of the lower-dimensional volume forms and the contour goes around the branch cut of each logarithm.

We note that these (hyper-)cubes are not directly related to the polytopes that are relevant for scattering amplitudes: equation (5.3.12) applied to $D = 4$ gives the volume of a four-dimensional hypercube, which has 8 codimension-1 faces and 16 vertices, whereas the

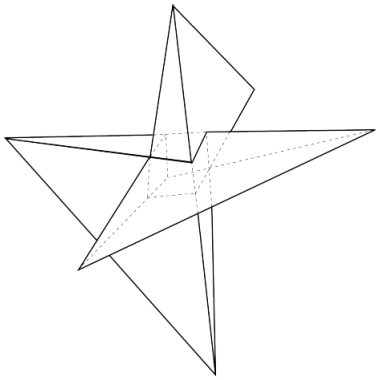

Figure 5.8: The three-dimensional analogue of Figure 5.4, showing the three possible ways of forming a triangulation analogous to that shown in Figure 5.7.

four-dimensional cyclic polytope whose volume is given by equation (5.2.25) corresponding to the scattering of $n = 8$ particles has 8 codimension-1 faces and 20 vertices. However, as we will show in the next section, these volumes of hypercubes can be used to obtain the vertex objects and thus to compute the volumes of general polytopes, including the cyclic polytopes relevant for scattering amplitudes.

5.4 Vertex Objects from Logarithms

5.4.1 Towards The Vertex Objects

We motivate the vertex objects by first seeing how to recover the volume of a simplex from integrals of logarithms. We define

$$T_{12} \equiv \frac{1}{(2\pi i)^2} \oint_{\gamma_{12}} \log\Big(\frac{Z_1 \cdot X}{Z_2 \cdot X}\Big) \log\Big(\frac{Z_3 \cdot X}{Q \cdot X}\Big) \frac{DX}{(P \cdot X)^3} = [123] - [12Q], \tag{5.4.1}$$

where γ_{12} is the same contour that we have described before, only now we are making it explicit. We have also introduced a fixed reference vector Q^α, defining a reference line in

$\mathbb{CP}^{2*}$. Cyclicly permuting 1, 2, and 3, we define

$$T_{23} \equiv \frac{1}{(2\pi i)^2} \oint_{\gamma_{23}} \log\Big(\frac{Z_2 \cdot X}{Z_3 \cdot X}\Big) \log\Big(\frac{Z_1 \cdot X}{Q \cdot X}\Big) \frac{DX}{(P \cdot X)^3} = [231] - [23Q], \tag{5.4.2}$$

as well as

$$T_{31} \equiv \frac{1}{(2\pi i)^2} \oint_{\gamma_{31}} \log\Big(\frac{Z_3 \cdot X}{Z_1 \cdot X}\Big) \log\Big(\frac{Z_2 \cdot X}{Q \cdot X}\Big) \frac{DX}{(P \cdot X)^3} = [312] - [31Q]. \tag{5.4.3}$$

It is important to note that γ_{12}, γ_{23}, and γ_{31} are all different contours, each being the contour defined by the integrand of the corresponding integral—namely, the contour that goes around the branch cut of each logarithm. Performing these integrations and summing them up, we find that

$$T_{12} + T_{23} + T_{31} = 2[123]. \tag{5.4.4}$$

The dependence on Q^α, while present in each T_{ij}, drops out of this sum of integrals and we are left with twice the volume of a single simplex. At the level of the integrated results $T_{ij} = [ijk] - [ijQ]$, the Q^α-independence of this sum results from using the four-term identity in equation (5.2.12), which itself is the result of nontrivial algebra using Schouten identities. At the level of the integrands, however, these cancellations become more manifest, and we will explore them here in some detail.

We begin by rewriting T_{ij}, where $i, j \in \{1, 2, 3\}$ and $k \in \{1, 2, 3\} \setminus \{i, j\}$, as follows:

$$\begin{aligned} T_{ij} &= \frac{1}{(2\pi i)^2} \oint_{\gamma_{ij}} \log\Big(\frac{Z_i \cdot X}{Z_j \cdot X}\Big) \log\Big(\frac{Z_k \cdot X}{Q \cdot X}\Big) \frac{DX}{(P \cdot X)^3}, \\ &= \frac{1}{(2\pi i)^2} \oint_{\gamma_{ij}} \log\Big(\frac{Z_i \cdot X}{Z_j \cdot X}\Big) \log\big(Z_k \cdot X\big) \frac{DX}{(P \cdot X)^3} \\ &\qquad - \frac{1}{(2\pi i)^2} \oint_{\gamma_{ij}} \log\Big(\frac{Z_i \cdot X}{Z_j \cdot X}\Big) \log\big(Q \cdot X\big) \frac{DX}{(P \cdot X)^3}. \end{aligned} \tag{5.4.5}$$

The contour γ_{ij} now goes around the branch cut of $\log(\frac{Z_i \cdot X}{Z_j \cdot X})$ and that of either $\log(Z_k \cdot X)$ or $\log(Q \cdot X)$, depending on which term we are considering. If we now consider only the

Q^α-dependent terms in the sum $T_{12}+T_{23}+T_{31}$, we find

$$\begin{aligned}(T_{12}+T_{23}+T_{31})|_{Q^\alpha-dependent} = -\frac{1}{(2\pi i)^2}\Big(&\oint_{\gamma_{12}} \log\Big(\frac{Z_1\cdot X}{Z_2\cdot X}\Big)\log\big(Q\cdot X\big)\frac{DX}{(P\cdot X)^3} \\ &+\oint_{\gamma_{23}} \log\Big(\frac{Z_2\cdot X}{Z_3\cdot X}\Big)\log\big(Q\cdot X\big)\frac{DX}{(P\cdot X)^3} \\ &+\oint_{\gamma_{31}} \log\Big(\frac{Z_3\cdot X}{Z_1\cdot X}\Big)\log\big(Q\cdot X\big)\frac{DX}{(P\cdot X)^3}\Big).\end{aligned} \tag{5.4.6}$$

By deforming each γ_{ij} to go around the $P\cdot X=0$ pole as opposed to the $\log(\frac{Z_i\cdot X}{Z_j\cdot X})$ branch cut, and thus picking up an overall minus sign, we can bring all of these integrands under the same integral and the integrand vanishes:

$$\begin{aligned}(T_{12}+T_{23}+T_{31})|_{Q^\alpha-dependent} &= \frac{1}{(2\pi i)^2}\Big(\oint_{\gamma}\Big(\log\Big(\frac{Z_1\cdot X}{Z_2\cdot X}\Big)+\log\Big(\frac{Z_2\cdot X}{Z_3\cdot X}\Big)+\log\Big(\frac{Z_3\cdot X}{Z_1\cdot X}\Big)\Big) \\ &\qquad\times\log\big(Q\cdot X\big)\frac{DX}{(P\cdot X)^3}\Big) \\ &= 0,\end{aligned} \tag{5.4.7}$$

where the contour γ goes around the $P\cdot X=0$ pole and the $\log(Q\cdot X)$ branch cut. We can therefore write the sum of T_{ij}'s as

$$\begin{aligned}T_{12}+T_{23}+T_{31} = \frac{1}{(2\pi i)^2}\Big(&\oint_{\gamma_{12}} \log\Big(\frac{Z_1\cdot X}{Z_2\cdot X}\Big)\log\big(Z_3\cdot X\big)\frac{DX}{(P\cdot X)^3} \\ &+\oint_{\gamma_{23}} \log\Big(\frac{Z_2\cdot X}{Z_3\cdot X}\Big)\log\big(Z_1\cdot X\big)\frac{DX}{(P\cdot X)^3} \\ &+\oint_{\gamma_{31}} \log\Big(\frac{Z_3\cdot X}{Z_1\cdot X}\Big)\log\big(Z_2\cdot X\big)\frac{DX}{(P\cdot X)^3}\Big),\end{aligned} \tag{5.4.8}$$

which is manifestly independent of Q^α. However, this representation depends on an implicit choice of line at infinity as this defines the branch of, for example, $\log(Z_3\cdot X)$ that γ_{12} circles. In the following we will therefore keep Q^α and its higher-dimensional analogues in our expressions and note the independence of our expressions on these reference boundaries wherever necessary. We also note that a naive summation of the integrands of the T_{ij}'s would

give a vanishing result, but that performing the integrations along the contours as specified by the branch cuts of their respective integrands gives non-vanishing results.

The Q^α-independence of this sum of integrals can also be directly checked by differentiating with respect to Q^α. In particular, by again using the fact that $\log(\frac{Z_i\cdot X}{Z_j\cdot X})+\log(\frac{Z_j\cdot X}{Z_k\cdot X})+\log(\frac{Z_k\cdot X}{Z_i\cdot X})=0$, it can be easily shown—at the integrand level—that

$$K^\alpha\frac{\partial}{\partial Q^\alpha}(T_{12}+T_{23}+T_{31})=0, \tag{5.4.9}$$

and therefore that this sum is independent of Q^α. In the following we use integrals similar to those defining the T_{ij}'s to define the vertex objects, and we will keep the reference boundaries in these expressions. The sums of these objects that we will be interested in will be independent of these boundaries, and the integrand-level proofs of these statements are similar to those found here.

5.4.2 Two-Dimensional Vertex Objects

Suppose that we have N points $\{Z_i^\alpha\}_{1\leq i\leq N}$ in $\mathbb{CP}^2$, each defining a line in $\mathbb{CP}^{2*}$. We define the following collection of $\binom{N}{2}$ integrals:

$$F_{ij}\equiv\frac{1}{2}\frac{1}{(2\pi i)^2}\oint_{\gamma_{ij}}\log\Big(\frac{Z_i\cdot X}{Z_j\cdot X}\Big)\Big(\sum_{k\neq i,j}\log\Big(\frac{Z_k\cdot X}{Q\cdot X}\Big)\Big)\frac{DX}{(P\cdot X)^3}\equiv\frac{1}{(2\pi i)^2}\oint_{\gamma_{ij}}f_{ij}(X)\frac{DX}{(P\cdot X)^3}, \tag{5.4.10}$$

where the contour γ_{ij} first goes around all of the branch cuts from $Z_k\cdot X=0$ to $Q\cdot X=0$ and then around the branch cut from $Z_i\cdot X=0$ to $Z_j\cdot X=0$. The factor of $\frac{1}{2}$ is conventional. Integrating this gives

$$F_{ij}=\frac{1}{2}\sum_{k\neq i,j}^{N}([ijk]-[ijQ])=\frac{1}{2}\Big(\sum_{k\neq i,j}^{N}[ijk]\Big)-\frac{1}{2}(N-2)[ijQ]. \tag{5.4.11}$$

These are (up to a factor of 2) the vertex objects of Ref. [5] and so in particular we have, for any $i, j, k \in \{1, ..., N\}$, that

$$F_{ij} + F_{jk} + F_{ki} = [ijk]. \tag{5.4.12}$$

Each individual vertex object depends on Q^α as well as all N of the Z_i^α's, but the dependence on Q^α and all other Z_l^α's (i.e., for $l \neq i, j, k$) drops out in the above sum, for reasons identical to those discussed in section 5.4.1.

In equation (5.4.10) we wrote F_{ij} as an integral over a function $f_{ij}(X)$ on the dual space. We readily see that $f_{ij} = -f_{ji}$, and can also show that for any choice of i, j, and k,

$$f_{ij} + f_{jk} + f_{ki} = 0. \tag{5.4.13}$$

The antisymmetry of the f_{ij}'s as well as property (5.4.13) imply that the collection of functions $\{f_{ij}\}$ form a representative of a $\check{C}$ech cohomology class on a subspace of $\mathbb{CP}^{2*}$.

In twistor theory, $\check{C}$ech cohomology is a natural setting in which to discuss the Penrose transform, which takes a cohomology class on (a subspace of) twistor space to a finite-normed on-shell field configuration on space-time [131]. The appearance of $\check{C}$ech cohomology here is of a different nature, and the role it is playing in this discussion is still unclear. For the remainder of this note we will not explore this issue. Instead, we simply note this curious connection to cohomology, as it may be important for generalizing these ideas to the N^{k}MHV amplituhedron with $k > 1$. For now, we simply move on to describing how to construct the higher-dimensional vertex objects in terms of integrals of logarithms.

5.4.3 Higher-Dimensional Vertex Objects

Analogous vertex objects can be defined in any dimension. Namely, in D dimensions there exist objects $F_{i_1 \ldots i_D}$ such that for any choice of $D+1$ hyperplanes defined by $\{Z_{i_k}\}_{1 \leq k \leq D+1}$,

one has the identity

$$F_{i_1 i_2 \ldots i_D} + (-1)^D F_{i_2 i_3 \ldots i_{D+1}} + F_{i_3 i_4 \ldots i_1} + \ldots + (-1)^D F_{i_{D+1} i_1 \ldots i_{D-1}} = [i_1 i_2 \ldots i_{D+1}]. \qquad (5.4.14)$$

Given any polytope in $\mathbb{CP}^D$, one obtains its volume by summing the vertex objects over the vertices of the polytope. In particular, any vertex of the polytope is defined (as reviewed in section 2) by the intersection of D hyperplanes corresponding to $Z_{i_1}, \ldots, Z_{i_D}$, and for this vertex one simply includes an $F_{i_1 \ldots i_D}$. The precise definition of higher-dimensional polytopes in $\mathbb{CP}^D$ is described in Ref. [5], as is the precise way of summing the vertex objects over the vertices. In this subsection, we will see how these higher-dimensional vertex objects arise as contour integrals of logarithms. We will explicitly show this only for dimensions three and four.

Three Dimensions

Let $\{Z_i^\alpha\}_{1 \leq i \leq N}$ be N points in $\mathbb{CP}^3$ defining N planes in the dual $\mathbb{CP}^{3*}$. Motivated by the two-dimensional case, we define

$$F_{ij;k} \equiv \frac{1}{(2\pi i)^3} \oint_{\gamma_{ij;k}} \log\Big(\frac{Z_i \cdot X}{Z_j \cdot X}\Big) \log\Big(\frac{Z_k \cdot X}{Q_2 \cdot X}\Big) \sum_{l \neq i,j,k} \log\Big(\frac{Z_l \cdot X}{Q_1 \cdot X}\Big) \frac{DX}{(P \cdot X)^4}, \qquad (5.4.15)$$

where Q_1^α and Q_2^α are fixed reference points in $\mathbb{CP}^3$ defining fixed reference planes in $\mathbb{CP}^{3*}$. The contour $\gamma_{ij;k}$ is an $(S^1)^3$ contour going around the branch cuts of the logarithms in the natural way. Antisymmetrizing over i, j, and k, and noting that each $F_{ij;k}$ is antisymmetric in its first two indices, we then define

$$F_{ijk} \equiv \frac{1}{2 \cdot 3!} F_{[ij;k]} = \frac{1}{3!}(F_{ij;k} + F_{jk;i} + F_{ki;j}). \qquad (5.4.16)$$

Each F_{ijk} depends on Q_1^α and all N of the Z_i^α's, although it is independent of Q_2^α. To see this Q_2^α-independence, we note that the sum $F_{ij;k} + F_{jk;i} + F_{ki;j}$ gives the exact same cyclic sum

of the $\log(\frac{Z_i\cdot X}{Z_j\cdot X})\log(\frac{Z_k\cdot X}{Q_2\cdot X})$ terms in equation (5.4.15) that appear in the two-dimensional case discussed in section 5.4.1, and thus the arguments used there to prove the Q^α-independence of this sum directly apply.

Having established that each F_{ijk} depends only the reference boundary Q_1^α, it is worth comparing the meaning of this boundary to that of the dummy boundary Z_*^α that appears[2] in the BCFW/CSW triangulation of equation (5.2.25). In the latter, the boundary Z_*^α defines a particular triangulation of the underlying polytope, and the independence of the volume of the polytope on this boundary follows from the general independence of the volume on triangulation. In contrast, Q_1^α determines a boundary that is used to define the branch cuts of the logarithms that appear in the definition of F_{ijk}. The boundary Q_2^α plays a similar role. As discussed in section 5.4.1, a manifestly Q-independent representation of F_{ijk} can be given, at the cost of making an implicit choice of a plane at infinity that determines the branches of the logarithms. Thus, the Q's that make an appearance here can be viewed as generalized "planes at infinity", the intersection of which gives a line at infinity. These boundaries therefore do not play a direct role in defining any triangulation—such a boundary would enter into the subscripts of F_{ijk} itself, as in the middle line of equation (5.2.29). This is in line with the fact that the vertex objects encode triangulation-independent data about the underlying polytope [5]. Moreover, with an explicit choice of endpoints for the branch cuts of the logarithms that define F_{ijk}, these Q^α's can be removed entirely.

It is straightforward to show that the F_{ijk} functions are (up to a factor of $2\times 3!$) the vertex objects defined in Ref. [5]. It then follows that for any choice of $i,j,k,l\in\{1,...,N\}$, one has

$$F_{ijk}-F_{jkl}+F_{kli}-F_{lij}=[ijkl], \tag{5.4.17}$$

where $[ijkl]$ is the volume of the three-simplex bounded by the four faces defined by Z_i^α, Z_j^α, Z_k^α, and Z_l^α. The dependence on Q_1^α and all other Z_m^α's drops out in this sum.

[2]We note that we are currently working in three dimensions, whereas the BCFW/CSW triangulation triangulates a four-dimensional polytope. However, the statements we make here directly carry over to the four dimensional case discussed in the next section.

Four Dimensions

The definition of the four-dimensional vertex objects is similar. Let $\{Z_i^\alpha\}_{1\le i\le N}$ be N points in $\mathbb{CP}^4$ defining N hyperplanes in the dual $\mathbb{CP}^{4*}$. Define

$$F_{ij;k;l} = \frac{1}{(2\pi i)^4}\oint_{\gamma_{ij;k;l}} \log\Big(\frac{Z_i\cdot X}{Z_j\cdot X}\Big)\log\Big(\frac{Z_k\cdot X}{Q_3\cdot X}\Big)\log\Big(\frac{Z_l\cdot X}{Q_2\cdot X}\Big)\sum_{m\neq i,j,k,l}\log\Big(\frac{Z_m\cdot X}{Q_1\cdot X}\Big)\frac{DX}{(P\cdot X)^5}, \tag{5.4.18}$$

where Q_1^α, Q_2^α, and Q_3^α are fixed reference points in $\mathbb{CP}^4$ defining reference hyperplanes in $\mathbb{CP}^{4*}$. The contour $\gamma_{ij;k;l}$ is an $(S^1)^4$ contour going around the branch cuts of the logarithms in the natural way. We define

$$\begin{aligned} F_{ijkl} \equiv \frac{1}{2\cdot 4!}F_{[ij;k;l]} = \frac{1}{4!}(&F_{ij;k;l} - F_{ij;l;k} + F_{ik;l;j} - F_{ik;j;l} + F_{il;j;k} - F_{il;k;j} \\ &+ F_{jk;i;l} - F_{jk;l;i} + F_{jl;k;i} - F_{jl;i;k} + F_{kl;i;j} - F_{kl;j;i}). \end{aligned} \tag{5.4.19}$$

Similarly to the two- and three-dimensional cases, each individual F_{ijkl} is independent of Q_2^α and Q_3^α, though it is dependent on Q_1^α and all N of the Z_i^α's.

Up to a factor of $2\times 4!$, the F_{ijkl} functions are precisely the vertex objects defined in Ref. [5]. It therefore follows that for any choice of i,j,k,l, and m, we have

$$F_{ijkl} + F_{jklm} + F_{klmi} + F_{lmij} + F_{mijk} = [ijklm], \tag{5.4.20}$$

where $[ijklm]$ is the volume of a four-simplex bounded by the five faces defined by Z_i^α, Z_j^α, Z_k^α, Z_l^α, and Z_m^α. Again, the dependence on Q_1^α and all other Z_n^α's drops out in this sum. This completes the proof that the vertex objects of Ref. [5], which can be used as basic building blocks for computing volumes of general polytopes as described in that reference, have a natural definition as simple contour integrals in the same space in which those polytopes live.

5.5 Conclusions

In this chapter we showed that volumes of general polytopes can be computed using contour integrals of logarithms directly in the space in which the polytopes live. The contours of these integrals are canonically specified by the integrands themselves, and the organizing principle for combining these integrals comes directly from the geometry of the polytope—the intersections of its faces—and thus does not rely on any particular triangulation. We also found a surprising connection between the integrands of the two-dimensional vertex objects and Čech cohomology. It would interesting to further explore this connection.

The vertex objects that we have defined are useful for computing NMHV tree-level amplitudes in the planar limit of $\mathcal{N} = 4$ super-Yang–Mills, and we have seen logarithms appear naturally. It would be interesting to see how these ideas might generalize to loop level. Additionally, since our discussion has been limited to tree-level amplitudes, these results readily apply at tree level to Yang–Mills theories with less (and no) supersymmetry. It would therefore be interesting to see if similar ideas can be used for less supersymmetric theories beyond tree level. Taking the planar limit appears to be crucial in this discussion, as momentum (super-)twistors play a fundamental role and these cease to exist in nonplanar theories. Nonetheless, it is worth exploring if and to what extent this discussion can be extended to the nonplanar sector of the theory.

The vertex objects we defined can be used to obtain identities amongst sums of simplices, and these identities can therefore now be viewed as being obtained from contour integrals of logarithms directly in the space containing the polytope. This differs dramatically from the Grassmannian picture discussed in the introduction. Understanding the relation between these two approaches will help extend the method introduced in this note to N^kMHV tree amplitudes for $k > 1$, since the Grassmannian picture is already well-understood for these more complicated cases. Expressing volumes in terms of the vertex objects naturally encodes the geometry of the underlying polytope. If the analogous objects can be found for the $k > 1$

cases, likely by first making a connection to the Grassmannian picture, then this should shed light on the geometry of the dual amplituhedron directly, without a need for any auxiliary spaces.

Chapter 6

Current and Future Work

6.1 A Polytope Picture for N$^{k>1}$MHV Tree Amplitudes

6.1.1 Introduction

A major drawback of the formalism introduced in Chapter 5 is that it only provides a polytope interpretation and computational formalism for tree-level amplitudes in $\mathcal{N} = 4$ sYM in the NMHV sector. The amplitudes in the N$^{k>1}$MHV sectors have elluded any direct interpretation as polytopes, though there are strong hints suggesting that such an interpretation should exist [126].

One such motivation comes directly from using BCFW recursion to compute these higher k amplitudes. The recursion expresses the amplitude as a sum of terms, each having a common form. By choosing different legs on which to base the recursion, one obtains different sums of these terms. Since these expressions must all be equal, one might hope that these are different "triangulations" of the same underlying space. Indeed, this is exactly the case for NMHV amplitudes, where the individual terms coming from the recursion are precisely volumes of simplices in an appropriate space. However, at higher k, there is no clear understanding of how these individual terms correspond to volumes of simplices, so a polytope picture is indirect at best.

We have, however, taken small steps towards uncovering a polytope picture for higher k amplitudes. This has largely involved gaining an even deeper understanding of $k = 1$ (i.e., NMHV) amplitudes, and clarifying exactly at which step the problem for higher k arises. The remainder of this section will summarize this progress.

6.1.2 Review of the Grassmannian Formalism

An alternative way of expressing the R-invariants $[ijklm]$ that make up the NMHV amplitudes is as contour integrals in a Grassmannian [128], which we will now review. We parametrize the kinematics of a $k = 1$, n-point amplitude using $Z_i^I = (Z_i^\alpha, \phi_A \eta_i^A)$, for $i = 1, 2, ..., n$. Here, Z_i^α is the bosonic part of the supertwistor, and η_i^A, with $A = 1, ..., 4$, is a Grassmann odd variable parametrizing the on-shell superspace for $\mathcal{N} = 4$ sYM. We introduce ϕ_A, another Grassmann odd variable, to "bosonify" the supertwistor, placing the supertwistor in $\mathbb{CP}^4$ as opposed to $\mathbb{CP}^{3|4}$ due to its having five bosonic homogenous coordinates. To clarify notation, we note that there are three different kinds of twistor that we are dealing with. We have the purely bosonic part, denoted by Z_i^α (for the i^{th} particle), which lives in $\mathbb{CP}^3$. We then have the supertwistor, $\mathcal{Z}_i^I = (Z_i^\alpha, \eta_i^A)$, which lives in $\mathbb{CP}^{3|4}$. Finally, we have the bosonified supertwistor $Z_i^I = (Z_i^\alpha, \phi_A \eta_i^A)$, which is notationally distinguished from the purely bosonic twistor only by its index, with the latter having a lower-case Greek index. Often, context will make clear which twistors are being considered.

A more thorough review of supertwistors is given in Refs. [125,128], and our notation here is slightly different. The superamplitude can be obtained from the "bosonified" superamplitude simply by integrating over ϕ_A, as will become clearer in what follows. Additionally, we will make little distinction (except where necessary) between the superamplitude and its bosonified form, as the former can be directly and easily obtained from the latter.

We now specialize to the 5-point NMHV amplitude, which we know from Chapter 5 is given simply by the R-invariant [12345]. We can rewrite this R-invariant as a contour integral in the Grassmannian $G(1, 5)$ by introducing the homogenous coordinates T_i, $i = 1, ..., 5$ and

computing the integral [128]

$$\oint \frac{DT}{T_1 T_2 T_3 T_4 T_5} \delta^{4|4}(T\mathcal{Z}^I), \tag{6.1.1}$$

where $T\mathcal{Z}^I$ denotes the linear combination $T_1 Z_1^\alpha + ... + T_5 Z_5^\alpha$ for the bosonic twistor coordinates and $T_1\eta_1^A + ... + T_5\eta_5^A$ for the fermionic twistor coordinates.

The nice thing about writing things in this way is that it readily generalizes not only to higher points but also to higher MHV degree. We will first address the former. Consider an n-point NMHV tree amplitude with momentum supertwistors $Z_i^I = (Z_i^\alpha, \eta_i^A)$, for $i = 1, 2, ..., n$. From Chapter 5 we know that this amplitude is given by

$$\sum_{i,j} \; [*i(i+1)j(j+1)] \tag{6.1.2}$$

where substituting in different values of $*$ gives different but equivalent expressions for the amplitude, reflecting different possible triangulations.

We can also rewrite this amplitude as a contour integral in $G(1, n)$, by introducing the n homogenous coordinates $T_1, ..., T_n$ and considering

$$\oint_{\mathcal{C}} \frac{DT}{T_1 ... T_n} \delta^{4|4}(T\mathcal{Z}^I), \tag{6.1.3}$$

where now $\mathcal{C}$ represents a particular contour in $G(1, n)$. Namely, for a given sum of R-invariants $[i_1 i_2 i_3 i_4 i_5]$, one simply chooses the contour that sets all of the $T_j = 0$ for $j \notin \{i_1, i_2, i_3, i_4, i_5\}$, and uses the delta functions to localize the remaining T_j's. The final contour is then the sum of these contours. While this method clearly recovers a particular triangulation of the underlying polytope, it can also be shown that equalities between different triangulations are simple manifestions of the global residue theorem (GRT). Therefore, once one correct contour $\mathcal{C}$ has been found, all others are related to this one by the global residue theorem.

More nontrivially, however, it turns out that these Grassmannian integrals also encode the

amplitudes for the higher MHV sectors [128]. In particular, an n-point N^{k}MHV amplitude can be written as a contour integral in $G(k,n)$. We begin by introducing homogenous coordinates $T_{i,j}$ on this space, with $i = 1, ..., k$ encoding the MHV degree and $j = 1, ..., n$ encoding the number of particles. By denoting $T_{i,1}Z_1^\alpha + ... + T_{i,n}Z_n^\alpha$ for the bosonic twistor coordinates and $T_{i,1}\eta_1^A + ... + T_{i,n}\eta_n^A$ for the on shell superspace fermionic variables collectively as $T_i Z^I$, we have that the tree amplitude $\mathcal{A}_{k,n}$ can be written as

$$\mathcal{A}_{k,n} = \oint_{\mathcal{C}} \frac{DT}{(1)(2)...(n)} \prod_{i=1}^{k} \delta(T_i \mathcal{Z}^I), \tag{6.1.4}$$

where (i) denotes the i^{th} cyclic minor of the matrix $T_{i,j}$ [128]. All that remains is to find a proper contour $\mathcal{C}$ for the amplitude, and all other expressions for the amplitude can be related to this one by a global residue theorem. It is worth pointing out that these global residue theorems encode many nontrivial identities, often involving dozens or even hundreds of terms.

The problem of finding the appropriate contour $\mathcal{C}$ that represents the amplitude is solved by the geometric formulation of the amplituhedron [11], which gives both a procedure for determining these contours as well as a geometrical interpretation of the region of integration. What the amplituhedron does not do, however, is give a direct geometrical interpretation of the amplitude itself, but rather a more indirect geometrical interpretation of it in terms of structures called positive geometries [107]. In particular, the geometric interpretation of the different terms in these contour integrals is obscured for higher k values.

To summarize, we have from Chapter 5 a formalism for computing volumes of polytopes and therefore NMHV tree amplitudes in terms of objects that both uniquely express the amplitude as well as manifest the underlying geometric interpretation. Moreover, this framework computes the terms in the amplitude via contour integrals within the same space in which the relevant polytope lives. This is in contrast to the Grassmannian and amplituhedron picture, which readily generalizes to tree amplitudes of any MHV degree and encodes

the different triangulations via GRTs but obscures the underlying geometry. It would therefore be ideal to find a framework that enjoys all of these features. Namely, it is an open problem to find a framework that simultaneously encodes all the various equivalent expressions for these amplitudes (which the vertex objects of Chapter 5 do manifestly, and which the Grassmannian formalism does via GRTs), manifests the underlying geometric and/or polytope structure, and generalizes to all MHV degree. In the next subsection we discuss some small steps towards this that we have taken.

6.1.3 Equality of Grassmannian Formalism and Vertex Object Formalism

A natural question to ask is why the vertex object formalism is equivalent to the Grassmannian picture in the first place. In particular, restricting to n-point NMHV amplitudes, the Grassmannian picture computes amplitudes via contour integrals in $G(1,n)$ of the form shown in Eq. (6.1.3), whereas the vertex objects are given as contour integrals around branches of logarithms in dual twistor space. In particular, the space in which these contour integrals live in the case of the vertex objects is the same regardless of the number of points n involved, whereas in principle a different Grassmannian is used for each value of n.

To clarify this confusion as well as to make steps towards understanding it, we consider a simpler class of integrals. Instead of considering supertwistors with four bosonic and four fermionic coordinates (i.e., elements of $\mathbb{CP}^{3|4}$, or $\mathbb{CP}^4$ for bosonified supertwistors), let us consider supertwistors with one bosonic and one fermionic coordinate. These are elements of $\mathbb{CP}^{0|1}$ or $\mathbb{CP}^1$ for bosonified supertwistors, since the latter have two homogeneous bosonic coordinates. By introducing two such supertwistors $\mathcal{Z}_1^I = (z_1, \eta_1)$ and $\mathcal{Z}_2^I = (z_2, \eta_2)$, we can consider the "2-point amplitude" $\mathcal{A}_2$ formed by computing the Grassmannian contour integral

$$\mathcal{A}_2 = \oint \frac{DT}{T_1 T_2} \delta^{0|1}(T\mathcal{Z}^I). \tag{6.1.5}$$

Since these kinds of calculations will be useful in what is to follow, we will carry this one out in detail[1]. Expanding out the delta function, using the holomorphic delta function for the bosonic coordinate and the usual fermionic delta function for the Grassmann odd coordinate, we find

$$\begin{aligned}\mathcal{A}_2 &= \oint \frac{DT}{T_1 T_2} \delta^{0|1}(TZ^I) \\ &= \oint \frac{DT}{T_1 T_2} \Big(\frac{T_1\eta_1 + T_2\eta_2}{T_1 z_1 + T_2 z_2} \Big).\end{aligned} \tag{6.1.6}$$

Now we need to fix the $GL(1)$ redundancy in the measure, as the integration variables are only defined up to an overall scaling. One way to do this is to choose $T_2 = 1$, thus giving

$$\mathcal{A}_2 = \oint \frac{dT_1}{T_1} \Big(\frac{T_1\eta_1 + \eta_2}{T_1 z_1 + z_2} \Big) \tag{6.1.7}$$

Finally, going around the $T_1 = -z_2/z_1$ pole (as specified by the delta function) gives

$$\mathcal{A}_2 = \frac{z_1\eta_2 - z_2\eta_1}{z_1 z_2}. \tag{6.1.8}$$

We can arrive at the same result by following the vertex object formalism. Namely, we bosonify the twistors so that $Z_i = (z_i, \phi\eta_i) \in \mathbb{CP}^1$, and we compute

$$\tilde{A}_2 = \oint \frac{DX}{(P\cdot X)^2} \log\Big(\frac{Z_1 \cdot X}{Z_2 \cdot X} \Big) = \frac{\langle 12 \rangle}{\langle 1P \rangle \langle 2P \rangle}, \tag{6.1.9}$$

where we have introduced $P^I = (0, 1)$. It is then clear that

$$\int d\phi \tilde{A}_2 = \mathcal{A}_2, \tag{6.1.10}$$

so that these two contour integrals are indeed computing the same quantities, up to a trivial fermionic integration. A priori it is not obvious why this is so, and our goal for the remainder

[1]We will, however, be completely cavalier about factors of $2\pi i$ arising from contour integration.

of this section will be to find a "master formula" of sorts, which can translate between the Grassmannian and vertex object formalisms.

Our starting point will be the Grassmannian integral 6.1.6. We rewrite it here for convenience, expanding out the delta funcation as before:

$$\mathcal{A}_2 = \oint \frac{DT}{T_1 T_2} \delta^{0|1}(TZ^I) = \oint \frac{DT}{T_1 T_2} \Big(\frac{T_1\eta_1 + T_2\eta_2}{T_1 z_1 + T_2 z_2} \Big). \tag{6.1.11}$$

Recalling that we want to eventually relate this integral to an integral involving bosonified twistors, let us trivially bosonify this expression by replacing each η_i with $\phi\eta_i$ and integrating everything against ϕ. This means we just rewrite things trivially as

$$\mathcal{A}_2 = \oint \frac{DT}{T_1 T_2} \Big(\frac{T_1\eta_1 + T_2\eta_2}{T_1 z_1 + T_2 z_2} \Big) = \int d\phi \oint \frac{DT}{T_1 T_2} \Big(\frac{T_1\phi\eta_1 + T_2\phi\eta_2}{T_1 z_1 + T_2 z_2} \Big). \tag{6.1.12}$$

By recalling that $\phi\eta_i$ is simply the homogenous component Z_i^2 of the bosonofied momentum twistor Z_i^I, and z_i that is similarly Z_i^1, we have

$$\mathcal{A} = \int d\phi \oint \frac{DT}{T_1 T_2} \Big(\frac{T_1 Z_1^2 + T_2 Z_2^2}{T_1 Z_1^1 + T_2 Z_2^1} \Big). \tag{6.1.13}$$

If we introduce the dual twistors $P^I = (0,1)$ and $Q^I = (1,0)$, and recall that we have defined $TZ^I = T_1 Z_1^I + T_2 Z_2^I$, then we can rewrite the above equation as

$$\mathcal{A} = \int d\phi \oint \frac{DT}{T_1 T_2} \frac{\langle TZQ \rangle}{\langle TZP \rangle}. \tag{6.1.14}$$

As it stands, this only holds for the particular Q^I and P^I that we have chosen. However, being motivated by the lack of homogeneity in Q^I and the incorrect scaling of P^I, we can insert a factor of $\langle QP \rangle$ in the denominator of the integrand at no cost, since for these

particular choices of Q^I and P^I we have $\langle QP\rangle = 1$. We can therefore write

$$\mathcal{A} = \int d\phi \oint \frac{DT}{T_1 T_2} \frac{\langle TZQ\rangle}{\langle TZP\rangle\langle QP\rangle}. \tag{6.1.15}$$

It is important to note that expressions like $\langle TZQ\rangle$ are indeed still antisymmetric products of two twistors, and not three. Namely, we have

$$\langle TZQ\rangle = \varepsilon_{IJ} T Z^I Q^J = T_1\langle 1Q\rangle + T_2\langle 2Q\rangle. \tag{6.1.16}$$

This expression for $\mathcal{A}$ is now independent of our choice of Q^I, which can be shown as follows. We differentiate $\mathcal{A}$ with respect to Q^I by applying the differential operator

$$L^I \frac{\partial}{\partial Q^I} \tag{6.1.17}$$

where L_I is an arbitrary twistor. We find

$$\begin{aligned} L^I \frac{\partial}{\partial Q^I}\mathcal{A} &= \int d\phi \oint \frac{DT}{T_1 T_2} L^I \frac{\partial}{\partial Q^I} \frac{\langle TZQ\rangle}{\langle TZP\rangle\langle QP\rangle} \\ &= \int d\phi \oint \frac{DT}{T_1 T_2} \Big(\frac{\langle QP\rangle\langle TZL\rangle - \langle LP\rangle\langle TZQ\rangle}{\langle TZP\rangle\langle QP\rangle^2} \Big) \\ &= \int d\phi \oint \frac{DT}{T_1 T_2} \Big(\frac{\langle TZP\rangle\langle QL\rangle}{\langle TZP\rangle\langle QP\rangle^2} \Big) \\ &= 0, \end{aligned} \tag{6.1.18}$$

where in the third equality we used the Schouten identity and where the final equality holds because the pole that is needed in the Grassmannian (T_i) integral is cancelled.

We therefore have that

$$\mathcal{A} = \int d\phi \oint \frac{DT}{T_1 T_2} \frac{\langle TZQ\rangle}{\langle TZP\rangle\langle QP\rangle}, \tag{6.1.19}$$

and $\mathcal{A}$ is independent of Q^I. We now notice that the integrand

$$\frac{\langle TZQ\rangle}{\langle TZP\rangle\langle QP\rangle} \tag{6.1.20}$$

is precisely the length of the line (as described and computed in Chapter 5) defined by the twistors TZ^I and Q^I, with P^I defining the line at infinity. We therefore know that we can use the vertex object formalism to write this as

$$\frac{\langle TZQ\rangle}{\langle TZP\rangle\langle QP\rangle} = \oint \frac{DX}{(P\cdot X)^2}\log\Big(\frac{TZ\cdot X}{Q\cdot X}\Big). \tag{6.1.21}$$

If we now insert this expression into the integrand above for $\mathcal{A}$, we obtain

$$\mathcal{A} = \int d\phi \oint \frac{DT}{T_1T_2}\oint \frac{DX}{(P\cdot X)^2}\log\Big(\frac{TZ\cdot X}{Q\cdot X}\Big), \tag{6.1.22}$$

This, we claim, is a "master formula" of sorts. In particular, when evaluated one way, it recovers that Grassmannian formalism, and when evaluated another way it recovers the vertex object formalism. To recover the Grassmannian formalism we simply need to undo the steps we took above. Namely, we first evaluate the inner integral (in dual twistor space) to recover Eq. (6.1.19), and then we set $Q_I = (1, 0)$, recall that $P_I = (0, 1)$, and perform the fermionic integration. To recover the vertex object formalism requires a bit more work.

Ideally we would simply swap the order of integrations and perform the Grassmannian integral first, leaving an integral in dual twistor space that recovers the vertex object formalism. Unfortunately, this is not so straightforward. To see why, we consider a simpler example in regular complex analysis. Namely, we have the standard result

$$1 = \frac{1}{2\pi i}\oint_{z=0}\frac{dz}{z}. \tag{6.1.23}$$

We can trivially rewrite this as a double contour integral as

$$1 = \frac{1}{(2\pi i)^2} \oint_{z=0} dz \oint_{w=0} \frac{dw}{w(z-w)}. \tag{6.1.24}$$

Now we cannot naively switch the order of integration here and perform the contour integral around $z = 0$ since the integrand no longer has a pole there. There are, however, a couple of things we can do. One option is to shift the pole location in z to be at $z = w$ as opposed to at $z = 0$, so that we have

$$1 = \frac{1}{(2\pi i)^2} \oint_{w=0} dw \oint_{z=w} \frac{dz}{w(z-w)}, \tag{6.1.25}$$

however for our purposes we will use a different approach. In particular, we first apply the global residue theorem on the z variable. In the original integral there were only two poles, one at $z = 0$ and one at $z = \infty$. We can therefore safely take the z integration around $z = \infty$ by adding a minus sign, and write

$$1 = -\frac{1}{(2\pi i)^2} \oint_{z=\infty} dz \oint_{w=0} \frac{dw}{w(z-w)}. \tag{6.1.26}$$

We then change variables to $z \to 1/z$ to find

$$1 = \frac{1}{(2\pi i)^2} \oint_{z=0} dz \oint_{w=0} \frac{dw}{zw(1-wz)}. \tag{6.1.27}$$

Now the pole that the z contour is circling is exposed and we can safely change the orders of integration. This is the idea we want to apply to our master formula Eq (6.1.22).

We begin by first fixing the $GL(1)$ redundancy by taking $T_2 = 1$, as before. This gives

$$\mathcal{A} = \int d\phi \oint_{\langle TZP\rangle=0} \frac{dT_1}{T_1} \oint \frac{DX}{(P\cdot X)^2} \log\Big(\frac{T_1(Z_1\cdot X)+(Z_2\cdot X)}{Q\cdot X}\Big). \tag{6.1.28}$$

Note that the Grassmannian integral was meant to go around the $\langle TZP\rangle = 0$ pole, which

we have made explicit in this expression. However, this pole is no longer present (naively) in the current rewriting of the integrand[2]. If we look at the original Grassmannian integral, though, then we see that there are three poles in T_1: $\langle TZP\rangle = 0$, $T_1 = 0$, and $T_1 = \infty$. Therefore we can use the global residue theorem to rewrite our master formula as

$$\mathcal{A} = -\int d\phi \oint_{T_1=0,\infty} \frac{dT_1}{T_1} \oint \frac{DX}{(P\cdot X)^2} \log\Big(\frac{T_1(Z_1\cdot X)+(Z_2\cdot X)}{Q\cdot X}\Big). \tag{6.1.29}$$

The contribution from these two poles can now be straightforwardly computed and we find

$$\mathcal{A} = -\int d\phi \oint \frac{DX}{(P\cdot X)^2}\Big[\log\Big(\frac{Z_2\cdot X}{Q\cdot X}\Big) - \log\Big(\frac{Z_1\cdot X}{Q\cdot X}\Big)\Big], \tag{6.1.30}$$

where the first term in the integrand comes from the $T_1 = 0$ pole and the second from the $T_1 = \infty$ pole. Simplifying the integrand gives

$$\mathcal{A} = \int d\phi \oint \frac{DX}{(P\cdot X)^2} \log\Big(\frac{Z_1\cdot X}{Z_2\cdot X}\Big), \tag{6.1.31}$$

which is precisely the expression used in the vertex object formalism. Note also that the Q^I-dependence has dropped out, as expected.

We have therefore introduced a "master formula", Eq. (6.1.22), that simultaneously encodes the Grassmannian as well as the vertex object formalism, at least in this one-dimensional case. In order for this approach to have any hope for extension to higher MHV levels (i.e., $k > 1$), we first need to see how it generalizes to higher dimensions, in which case there is only one additional subtlety that needs to be addressed.

[2]The pole has become a "pinched-contour" pole [79], since when $\langle TZP\rangle = 0$ we have that TZ^I and P^I are colinear and so there is no contour separating the $P\cdot X = 0$ pole from the branch of the logarithm in the integrand.

6.1.4 Higher Dimensions

We consider the Grassmannian integral for an "amplitude" with supertwistors residing in $\mathbb{CP}^{1|2}$, meaning that they have two bosonic and two fermionic coordinates, $\mathcal{Z}_{iI} = (z_i^1, z_i^2, \eta_i^A)$, $A = 1, 2$, and in particular the bosonified supertwistors reside in $\mathbb{CP}^2$ (having three homogenous bosonic coordinates). At n-points we have n such twistors Z_i^I, $i = 1, ..., n$, and for now we restrict to the $n = 3$ case. We will discuss the general n case afterwards. The Grassmannian integral specifying this amplitude is

$$\mathcal{A} = \oint \frac{DT}{T_1 T_2 T_3} \delta^{1|2}(T\mathcal{Z}^I), \tag{6.1.32}$$

which again, using the holomorphic delta function for the bosonic coordinates and the usual delta function for the fermionic coordinates, gives

$$\mathcal{A} = \oint \frac{DT}{T_1 T_2 T_3} \Big(\frac{(T_1\eta_1^1 + T_2\eta_2^1 + T_3\eta_3^1)(T_1\eta_1^2 + T_2\eta_2^2 + T_3\eta_3^2)}{(T_1 Z_{11} + T_2 Z_{21} + T_3 Z_{31})(T_1 Z_{12} + T_2 Z_{22} + T_3 Z_{32})} \Big). \tag{6.1.33}$$

It is now straightforward to obtain a "master formula" in this case as well. Namely, we begin by bosonifying these coordinates and integrating the newly introduced fermionic coordinates back out. It is a straightforward calculation to check that we can write

$$\mathcal{A} = \int d^2\phi \oint \frac{DT}{T_1 T_2 T_3} \Big(\frac{(T_1\phi\cdot\eta_1 + T_2\phi\cdot\eta_2 + T_3\phi\cdot\eta_3)^2}{(T_1 Z_1^1 + T_2 Z_2^1 + T_3 Z_3^1)(T_1 Z_1^2 + T_2 Z_2^2 + T_3 Z_3^2)} \Big). \tag{6.1.34}$$

By introducing the twistors $Q_1^I = (1, 0, 0)$, $Q_2^I = (0, 1, 0)$, and $P^I = (0, 0, 1)$, and realizing that $Z_i^3 = \phi \cdot \eta_i$, it is straightforward to check that this expression is equivalent to

$$\mathcal{A} = \int d^2\phi \oint \frac{DT}{T_1 T_2 T_3} \Big(\frac{\langle TZQ_1Q_2\rangle^2}{\langle TZQ_1P\rangle\langle TZQ_2P\rangle\langle Q_1Q_2P\rangle} \Big), \tag{6.1.35}$$

where we have included $\langle Q_1 Q_2 P\rangle$ in the denominator since for this particular choice of Q_1^I and Q_2^I we have that $\langle Q_1 Q_2 P\rangle = 1$. The benefit of doing this is that the integrand becomes

independent of both Q_1^I and Q_2^I, as can be checked in an analogous manner as in the one-dimensional case in the previous subsection. Our ability to freely choose Q_1^I and Q_2^I will become important for us soon.

The key step towards obtaining a "master formula" in this case is to realize that the integrand in Eq. (6.1.35) is precisely the volume of a simplex bounded by the planes defined by TZ^I, Q_1^I, and Q_2^I. In the vertex object formalism we know how to write this volume as a sum of contour integrals in dual twistor space. Namely,

$$\begin{aligned}\frac{\langle TZQ_1Q_2\rangle^2}{\langle TZQ_1P\rangle\langle TZQ_2P\rangle\langle Q_1Q_2P\rangle} &= \oint_{\gamma_1}\frac{DX}{(P\cdot X)^3}\log\Big(\frac{TZ\cdot X}{Q_1\cdot X}\Big)\log\Big(\frac{Q_2\cdot X}{K\cdot X}\Big)\\ &+\oint_{\gamma_2}\frac{DX}{(P\cdot X)^3}\log\Big(\frac{Q_2\cdot X}{TZ\cdot X}\Big)\log\Big(\frac{Q_1\cdot X}{K\cdot X}\Big)\\ &+\oint_{\gamma_3}\frac{DX}{(P\cdot X)^3}\log\Big(\frac{Q_1\cdot X}{Q_2\cdot X}\Big)\log\Big(\frac{TZ\cdot X}{K\cdot X}\Big),\end{aligned} \tag{6.1.36}$$

where we have introduced K^I as a dummy twistor, and where γ_i is a contour going around the two branch cuts of the logarithms in the the integrand, as discussed in more detail in Chapter 5. We can now substitute this expression into Eq. (6.1.35) to find

$$\begin{aligned}\mathcal{A} = \int d^2\phi\oint\frac{DT}{T_1T_2T_3}\Big[&\oint_{\gamma_1}\frac{DX}{(P\cdot X)^3}\log\Big(\frac{TZ\cdot X}{Q_1\cdot X}\Big)\log\Big(\frac{Q_2\cdot X}{K\cdot X}\Big)\\ &+\oint_{\gamma_2}\frac{DX}{(P\cdot X)^3}\log\Big(\frac{Q_2\cdot X}{TZ\cdot X}\Big)\log\Big(\frac{Q_1\cdot X}{K\cdot X}\Big)\\ &+\oint_{\gamma_3}\frac{DX}{(P\cdot X)^3}\log\Big(\frac{Q_1\cdot X}{Q_2\cdot X}\Big)\log\Big(\frac{TZ\cdot X}{K\cdot X}\Big)\Big].\end{aligned} \tag{6.1.37}$$

Now, we claim that for the 3-point case, this is the master formula that we are looking for. In particular, we can readily recover from it the Grassmannian integral by simply rerunning the above steps in reverse. To recover the vertex object formalism, we again use the global residue theorem, but with one small addition. Namely, the contour in the original Grassmannian integral surrounds the poles $\langle TZQ_1P\rangle = 0$ and $\langle TZQ_2P\rangle = 0$. If we fix the $GL(1)$ redunancy by setting $T_3 = 1$, we can say that T_1 circles the first of these poles and

T_2 the second. However, in the original Grassmannian integrals, both T_1 and T_2 have poles at infinity. In the one-dimensional case the pole at infinity was not a problem, but in higher dimensions it complicates the use of the GRTs. Instead, we can simply get rid of these poles by setting, for example, $Q_1^I = Z_1^I$ and $Q_2^I = Z_2^I$. This is because the numerator factor

$$\langle TZQ_1Q_2\rangle = T_1\langle 1Q_1Q_2\rangle + T_2\langle 2Q_1Q_2\rangle + \langle 3Q_1Q_2\rangle \tag{6.1.38}$$

simply becomes $\langle 123\rangle$, and so there is no T_1 or T_2 dependence in the numerator, thus getting rid of the poles at infinity. Therefore, with this choice of Q_1^I and Q_2^I, the global residue theorem tells us that we can trade the contour around $\langle TZQ_1P\rangle = 0$ and $\langle TZQ_2P\rangle = 0$ for the contours around $T_1 = 0$ and $T_2 = 0$. We can therefore write Eq. (6.1.37) as (using our choice of Q_1^I and Q_2^I)

$$\begin{aligned}\mathcal{A} = \int d^2\phi \oint_{T_1=0,T_2=0} \frac{dT_1 dT_2}{T_1T_2}\Big[\\ \oint_{\gamma_1} \frac{DX}{(P\cdot X)^3}\log\Big(\frac{T_1(Z_1\cdot X)+T_2(Z_2\cdot X)+(Z_3\cdot X)}{Z_1\cdot X}\Big)\log\Big(\frac{Z_2\cdot X}{K\cdot X}\Big) \\ + \oint_{\gamma_2} \frac{DX}{(P\cdot X)^3}\log\Big(\frac{Z_2\cdot X}{T_1(Z_1\cdot X)+T_2(Z_2\cdot X)+(Z_3\cdot X)}\Big)\log\Big(\frac{Z_1\cdot X}{K\cdot X}\Big) \\ + \oint_{\gamma_3} \frac{DX}{(P\cdot X)^3}\log\Big(\frac{Z_1\cdot X}{Z_2\cdot X}\Big)\log\Big(\frac{T_1(Z_1\cdot X)+T_2(Z_2\cdot X)+(Z_3\cdot X)}{K\cdot X}\Big)\Big].\end{aligned} \tag{6.1.39}$$

Evaluating the integrand at $T_1 = 0$ and $T_2 = 0$ then trivially gives

$$\begin{aligned}\mathcal{A} = \int d^2\phi\Big[\oint_{\gamma_1} \frac{DX}{(P\cdot X)^3}\log\Big(\frac{Z_3\cdot X}{Z_1\cdot X}\Big)\log\Big(\frac{Z_2\cdot X}{K\cdot X}\Big) \\ + \oint_{\gamma_2} \frac{DX}{(P\cdot X)^3}\log\Big(\frac{Z_2\cdot X}{Z_3\cdot X}\Big)\log\Big(\frac{Z_1\cdot X}{K\cdot X}\Big) \\ + \oint_{\gamma_3} \frac{DX}{(P\cdot X)^3}\log\Big(\frac{Z_1\cdot X}{Z_2\cdot X}\Big)\log\Big(\frac{Z_3\cdot X}{K\cdot X}\Big)\Big],\end{aligned} \tag{6.1.40}$$

which we recognize as the way the vertex object formalism computes the volume [123], which we know is the correct expression for this amplitude.

We therefore see that Eq. (6.1.37) can reproduce both the Grassmannian and the vertex object formalisms in the 3-point case. In order to do so in the n-point case, one follows a similar procedure and simply needs to choose different Q_1^I and Q_2^I for each simplex in order to easily apply the global residue theorem. Namely, at n-points the Grassmannian integral gives a sum of simplices, each one being characterized by taking $n-3$ of the T_i's around $T_i = 0$. From there, we can gauge fix the $GL(1)$ redundancy by setting one of the remaining T_i's to 1, and we can recover the vertex object formalism by setting Q_{1I} and Q_{2I} to equal the two twistors whose T_i's have not been set to either 0 or 1.

It is therefore the case that a master formula exists in this two-dimensional case at n-points, and we have checked that a similar formula can be found at n-points in any number of dimensions (i.e., for (bosonic) supertwistors living in $\mathbb{CP}^M$ for any M) via a similar process. This therefore represents a step towards finding a formalism that preserves the benefits of both Grassmannian and vertex object formalisms by combining them into one "master formula" for the $k = 1$ case. Unfortunately such a framework for higher k has yet to be found, but in the next subsection we discuss some steps that have been taken and a concrete place at which we are stuck.

6.1.5 Attempt at Higher k

We quickly recall that our main goal is to find a formalism at higher k that perserves whatever geometric content underlies the amplitudes. Since the vertex object formalism does this manifestly for $k = 1$, our goal is to uncover an analogous formalism for higher k. To do so, we will start with the Grassmannian formalism, which is known to produce the correct amplitudes at higher k, at the expense of a direct geometric understanding. If the Grassmannian formalism can be recast into a "master formula" as in the $k = 1$ case in the previous subsection, then by integrating out the Grassmannian variables (via a GRT or any other method), one can hope to land on a vertex object formalism. Unfortunately it is still not known how this can be done, and in this subsection we will summarize how far we have

gotten along these lines.

We first restrict our supertwistors to reside in $\mathbb{CP}^{1|2}$, so that the supertwistors have two bosonic coordinates and two fermionic coordinates. This dimension with $k = 2$ gives the first nontrivial example. In particular, for $k = 2$, we bosonify the supertwistors slightly differently. We introduce two sets of dummy fermionic coordinates, ϕ_1^A and ϕ_2^A, (where $A = 1, 2$). The bosonic supertwistors then have four homogenous coordinates given by $Z_i^I = (z_i^1, z_i^2, \phi_1 \cdot \eta_i, \phi_2 \cdot \eta_i)$. These bosonified supertwistors have four (bosonic) homogeneous coordinates. This allows us to consider integrals over $G(2, 4)$, which is the first nontrivial Grassmannian.

For simplicity we will restrict ourselves to four points so that we have four supertwistors Z_i^I, $i = 1, ..., 4$. The Grassmannian integral we are concerned with is

$$\mathcal{A} = \oint \frac{DT}{(1)(2)(3)(4)} \delta^{1|2}(T_1 Z^I) \delta^{1|2}(T_2 Z^I), \tag{6.1.41}$$

where $T_i Z^I \equiv T_{i1} Z_1^I + T_{i2} Z_2^I + T_{i3} Z_3^I + T_{i4} Z_4^I$, with $i = 1, 2$. In particular, the homogenous coordinates on the $G(2, 4)$ in which this integral is taking place form the matrix

$$\begin{pmatrix} T_{11} & T_{21} & T_{31} & T_{41} \\ T_{12} & T_{22} & T_{32} & T_{42} \end{pmatrix}. \tag{6.1.42}$$

The minors (i) in the denominator of the measure are simply the determinant of the submatrix formed from the i^{th} and $(i+1)^{th}$ columns of this matrix.

It is now a straightforward calculation, analogous to what we did in the $k = 1$ case in the previous subsections, to show that

$$\mathcal{A} = \int d^2\phi_1 d^2\phi_2 \oint \frac{DT}{(1)(2)(3)(4)} \Big(\frac{\langle T_1 Z T_2 Z Q_1 Q_2 \rangle^2}{\langle T_1 Z Q_1 P_1 P_2 \rangle \langle T_1 Z Q_2 P_1 P_2 \rangle \langle T_2 Z Q_1 P_1 P_2 \rangle \langle T_2 Z Q_2 P_1 P_2 \rangle} \Big), \tag{6.1.43}$$

where we have introduced the twistors $Q_1^I = (1, 0, 0, 0)$, $Q_2^I = (0, 1, 0, 0)$, $P_1^I = (0, 0, 1, 0)$,

and $P_2^I = (0, 0, 0, 1)$. Using a similar approach as we did in the $k = 1$ case, we can show that this expression is independent of both Q_1^I and Q_2^I. It turns out that the result of this integral is

$$\mathcal{A} = \frac{\langle 1234\rangle^2}{\langle 12P_1P_2\rangle\langle 23P_1P_2\rangle\langle 34P_1P_2\rangle\langle 41P_1P_2\rangle}. \tag{6.1.44}$$

In order to proceed, it is worthwhile to note the similarity of this integral with, say, that in Eq (6.1.35.) In that equation, the result of the integral is

$$[123] = \frac{\langle 123\rangle^2}{\langle 12P\rangle\langle 23P\rangle\langle 31P\rangle}, \tag{6.1.45}$$

which is of the same form as the Grassmannian integrand. Our approach there was to rewrite the integrand as an integral in dual twistor space and then use the global residue theorem to perform the Grassmannian integration in order to recover the vertex object formalism from the master formula. In the current $k = 2$ case we find ourselves in a similar situation. We have rewritten the Grassmannian integral Eq. (6.1.41) in a form where the integrand has the same form as the answer.

Therefore, if we can find an integral representation for expressions like that Eq. (6.1.44) in dual twistor space, then inserting this representation into the integrand of Eq. (6.1.43) would give a "master formula" for the first nontrivial $k = 2$ example. This master formula would allow one to recover the Grassmannian representation by simply carrying out the inner integral, and the vertex object formulation (or more precisely whatever the vertex object formalism would be in the $k = 2$ case, as it is still unknown) by using the global residue theorem to perform the Grassmannian integration. Unfortunately such an integral representation in dual twistor space for Eq. (6.1.44) is not currently known[3]. It is our hope and our goal that such a representation can be found, in which case it is almost certain that new geometric insights into these amplitudes and the entire amplituhedron construction will

[3]There is a representation given in Ref. [125], but it is not very conducive to generalization to even higher k and we believe that a better (albeit related) representation should exist. Further investigation is still needed.

follow shortly thereafter.

6.2 Numerically Solving The Scattering Equations

In this section we make a departure away from the amplituhedron construction and instead focus on the scattering equations and a method for computing their numerical solutions quickly. The scattering equations play an interesting and important role in computing scattering amplitudes with only massless particles [135–137]. In particular, one can use the solutions to the scattering equations to compute tree amplitudes in various scalar, gauge, and gravity theories, so long as these theories consist of only massless particles. We begin by giving a very brief introduction to how this is done.

We assume we are scattering n massless particles, each with momentum vector k_i^μ, $i = 1, ..., n$ with $k_i^2 = 0$ and $s_{ij} \equiv 2k_i \cdot k_j$,. The scattering equations are defined to be the following n equations, one for each $i = 1, ..., n$,

$$\sum_j \frac{s_{ij}}{\sigma_i - \sigma_j} = 0. \tag{6.2.1}$$

Here, the kinematic variables s_{ij} are given and fixed, and the σ_i are complex coordinates on the Riemann sphere for which we are solving.

For n external particles, there are n equations in total, but due to the $SL(2, \mathbb{R})$ invariance of these equations there are only $n - 3$ independent equations. It is well known that there are $(n - 3)!$ independent solutions to these equations [135–137].

If one is able to find a full set of solutions $S_i = \{\sigma_{i1}, ..., \sigma_{in}\}$ for $i = 1, ..., (n - 3)!$, to the scattering equations, then one can compute tree amplitudes in various theories by simply computing the sum

$$\mathcal{A}_{\text{tree}} = \sum_{i=1}^{(n-3)!} J^{-1}(\{\sigma_i\}) f(\{\sigma_i\}), \tag{6.2.2}$$

where $J(\{\sigma\})$ is a universal Jacobian factor and f is a function of the σ's which carries all of

the theory-dependence of the amplitudes. Namely, the scattering equations themselves are theory-independent, and recovering scalar, gauge, and/or gravity theory amplitudes from Eq. (6.2.2) is simply a matter of choosing different functions f.

The details of how this is done will not be a concern for us here. We will instead focus on the solutions to the scattering equations themselves. By convention, we choose $\sigma_{n-2}, \sigma_{n-1}$, and σ_n to be fixed at 0, 1, and ∞, respectively, which we can do thanks to the $SL(2,\mathbb{R})$ symmetry of the scattering equations. The scattering equations can then be thought of as finding the $(n-3)!$ extrema of the potential [138]

$$V(\{\sigma_i\}_{1\leq i\leq n-3}) = -\sum_{1\leq i<j\leq n-3} s_{ij}\log(|\sigma_i-\sigma_j|) - \sum_{i=1}^{n-3} s_{i(n-2)}\log|\sigma_i| - \sum_{i=1}^{n-3} s_{i(n-1)}\log|1-\sigma_i|. \tag{6.2.3}$$

For given, numerical kinematics s_{ij}, this is a problem that Mathematica can handle up to 8 or 9 points in a reasonable amount of time on a laptop, and there have been recent developments that use a statistical approach for speeding up this computation [140]. In particular, Ref. [140] has obtained significant speed-up when specializing to four dimensions, where complete sets of solutions up to 12 points in certain MHV sectors have been found. In this section we will introduce a method that finds all $(n-3)!$ numerical solutions in general dimensions, with a speed-up that can compute all solutions at 12 points in a half hour on a single laptop, with little optimization, and in a highly parallelizable way.

In order to do this, we must first restrict ourselves to a subregion of kinematic space. In particular, Cachazo, Mizera, and Zhang showed that if we restrict the variables s_{ij} for $1 \leq i,j \leq n-3$ as well as $s_{i(n-2)}$ and $s_{i(n-1)}$ for $1 \leq i \leq n-3$ to be positive, then the solutions $\{\sigma_i\}$ all lie on the real line [138]. Moreover, when we choose $\sigma_{n-2}=0$, $\sigma_{n-1}=1$, and $\sigma_n=\infty$, then the solutions all lie on the unit interval, i.e., $\{\sigma_i\} \in [0,1]$ for $1 \leq i \leq n-3$.

The authors of Ref. [138] mention that they are able to use this restriction to find individual solutions to the scattering equations for up to 60 points. For the remainder of this section we will discuss how this restriction of the kinematics can be used to solve the

scattering equations in full. In other words, we will describe an algorithm for computing all $(n-3)!$ solutions (as opposed to individual solutions) to the scattering equations with the kinematics restricted to this positive subregion[4].

6.2.1 Convexity of the Potential and Gradient Descent

The key realiziation in regards to solving these equations quickly and in full is the following. By restricting the kinematic variables to this positive region and gauge-fixing the $SL(2,\mathbb{R})$ symmetry as discussed above, we are ensuring that all $n-3$ of the remaining σ's lie on the unit interval, meaning that every solution is associated with an ordering of the remaining, unfixed σ's. There are $n-3$ unfixed σ's, and therefore $(n-3)!$ orderings of these variables. Perhaps unsurprisingly, it turns out that the orderings are in one-to-one correspondence with the solutions [138].

This is a useful realization when it comes to solving these equations numerically. To see why, it is worthwhile to review a standard numerical optimization technique known as gradient descent. This involves taking a function $f(x_1,...,x_m)$ of some number of variables x_i, and trying to find a minimum of it by repeatedly taking steps in the direction of the negative gradient. Namely, we choose some (arbitrary) starting point $x_1^*,...,x_m^*$, compute the gradient of f at this point, and then update this starting point via the equation

$$x_{i,\text{new}} = x_{i,\text{old}} - \alpha \frac{\partial f}{\partial x_i}|_{x_{i,\text{old}}}, \tag{6.2.4}$$

where α is an arbitrary small number known as the learning rate, which determines the size of the step taken in the negative gradient direction. By iterating this process several times, one arrives at a set of x_i that minimize f. However, this will only find local minima—namely the minimum which can be obtained from the arbitrary starting point by simply "flowing" downhill. One approach to solving the scattering equations, then, is to keep picking new

[4]We note that this positive region of kinematic space is not the same as, but is related to, that discussed in, for example, Ref. [139].

starting points until $(n-3)!$ distinct solutions have been found. This is slowed down greatly, however, by the fact that it becomes more and more likely to flow to previously-found solutions as the number of previously-found solutions increases.

All of this can be overcome if the function f enjoys a property known as convexity. Convexity is defined, in essence, to mean that for any line segment in the domain of the function, the average of the function at the two endpoints of the line segment is greater than or equal to the value of the function at the midpoint of the line segment. In practice, what this means is that a local minimum of a convex function will be a global minimum, which in turn means that gradient descent can only flow to one unique minimum.

The main insight here is then the following. It turns out that for a fixed ordering of the remaining $n-3$ σ's, the potential in Eq. (6.2.3) is convex [138]. For example, at 5 points, where we have two remaining variables σ_1 and σ_2, the potential is convex on the region where $\sigma_1 < \sigma_2$ as well as on the region $\sigma_2 < \sigma_1$. This means that if we take our starting values of σ_1 and σ_2 in gradient descent to obey a particular ordering, then that ordering will be preserved at each step and gradient descent will flow to the solution corresponding to that ordering.

Indeed, we have implemented a simple Mathematica program that chooses the starting position for the σ's at evenly spaced intervals on the unit interval, one for each ordering of the σ's. We then let Mathematica find the local minimum for each ordering, and verify afterwards that we have found $(n-3)!$ distinct solutions to the scattering equations. With this approach, we have been able to find full solutions to the scattering equations up to 12 points in a half an hour on a single laptop.

Future work in this regard would involve optimization, possibly writing the code ourselves in a compiled language like c++. We also note that even the Mathematica approach is highly parallelizable, with each separate ordering being completely independent of the others, so that one can easily obtain many factors of speed up from simple multi-threading.

This approach, combined with recent developments in regards to using homotopy theory

to "flow" to an arbitrary solution given any other solution [141], appears to be a way forward for computing full solutions to the scattering equations at very high numbers of external points. This data would be valuable for numerical checks and tests of other procedures for computing amplitudes, and may give insight into the analytic structure of these solutions, of which little is currently known.

Bibliography

[1] Z. Bern, M. Enciso, J. Parra-Martinez, M. Zeng, JHEP **1705**, 137 (2017) [arXiv:1703.08927 [hep-th]].

[2] Z. Bern, M. Enciso, H. Ita and M. Zeng, Phys. Rev. D **96**, no. 9, 096017 (2017) [arXiv:1709.06055 [hep-th]].

[3] Z. Bern, M. Enciso, C. H. Shen, M. Zeng Phys. Rev. Lett. **121**, 121603 (2018) [arXiv:1806.06509 [hep-th]];

[4] M. Enciso, JHEP **1804**, 016 (2018) [arXiv:1612.07370 [hep-th]].

[5] M. Enciso, JHEP **1710**, 071 (2017) [arXiv:1408.0932 [hep-th]].

[6] H. Elvang, Y.-t. Huang, *Scattering Amplitudes in Gauge Theory and Gravity*, Cambridge University Press, (2015), [arXiv:1308.1697 [hep-th]].

[7] E. Witten, Commun. Math. Phys. 252 (2004) 189-258 [arxiv:0312171 [hep-th]]

[8] Z. Bern, S. Davies, T. Dennen and Y.-t. Huang, Phys. Rev. Lett. **108**, 201301 (2012) [arXiv:1202.3423 [hep-th]].

[9] Z. Bern, S. Davies and T. Dennen, Phys. Rev. D **90**, 105011 (2014) [arXiv:1409.3089 [hep-th]].

[10] Z. Bern, S. Davies, T. Dennen and Y. t. Huang, Phys. Rev. D **86**, 105014 (2012) [arXiv:1209.2472 [hep-th]].

[11] N. Arkani-Hamed and J. Trnka, JHEP **1410**, 030 (2014) [arXiv:1312.2007 [hep-th]];

[12] G. 't Hooft and M. J. G. Veltman, Ann. Inst. H. Poincare Phys. Theor. A **20**, 69 (1974).

[13] Z. Bern, C. Cheung, H. H. Chi, S. Davies, L. Dixon and J. Nohle, Phys. Rev. Lett. **115**, 211301 (2015) doi:10.1103/PhysRevLett.115.211301 [arXiv:1507.06118 [hep-th]];
Z. Bern, H. H. Chi, L. Dixon and A. Edison, arXiv:1701.02422 [hep-th].

[14] J. J. M. Carrasco, R. Kallosh, R. Roiban and A. A. Tseytlin, JHEP **1307**, 029 (2013) doi:10.1007/JHEP07(2013)029 [arXiv:1303.6219 [hep-th]];
R. Kallosh, Phys. Rev. D **95**, no. 4, 041701 (2017) doi:10.1103/PhysRevD.95.041701 [arXiv:1612.08978 [hep-th]];
D. Z. Freedman, R. Kallosh, D. Murli, A. Van Proeyen and Y. Yamada, arXiv:1703.03879 [hep-th].

[15] Z. Bern, S. Davies, T. Dennen, A. V. Smirnov and V. A. Smirnov, Phys. Rev. Lett. **111**, no. 23, 231302 (2013) doi:10.1103/PhysRevLett.111.231302 [arXiv:1309.2498 [hep-th]].

[16] E. D'Hoker and D. H. Phong, Nucl. Phys. B **715**, 3 (2005) doi:10.1016/j.nuclphysb.2005.02.043 [hep-th/0501197].

[17] G. Bossard, P. S. Howe, K. S. Stelle and P. Vanhove, Class. Quant. Grav. **28**, 215005 (2011) doi:10.1088/0264-9381/28/21/215005 [arXiv:1105.6087 [hep-th]].

[18] G. Bossard, P. S. Howe and K. S. Stelle, Phys. Lett. B **719**, 424 (2013) doi:10.1016/j.physletb.2013.01.021 [arXiv:1212.0841 [hep-th]];
G. Bossard, P. S. Howe and K. S. Stelle, JHEP **1307**, 117 (2013)

doi:10.1007/JHEP07(2013)117 [arXiv:1304.7753 [hep-th]];

[19] Z. Bern, S. Davies and T. Dennen, Phys. Rev. D **88**, 065007 (2013), doi:10.1103/PhysRevD.88.065007 [arXiv:1305.4876 [hep-th]].

[20] P. Tourkine and P. Vanhove, Class. Quant. Grav. **29**, 115006 (2012) doi:10.1088/0264-9381/29/11/115006 [arXiv:1202.3692 [hep-th]].

[21] S. Mandelstam, J. Phys. Colloq. **43**, no. C3, 331 (1982);
doi:10.1051/jphyscol:1982367 S. Mandelstam, Nucl. Phys. B **213**, 149 (1983);
doi:10.1016/0550-3213(83)90179-7 L. Brink, O. Lindgren and B. E. W. Nilsson, Phys. Lett. **123B**, 323 (1983). doi:10.1016/0370-2693(83)91210-8

[22] P. S. Howe, K. S. Stelle and P. K. Townsend, Nucl. Phys. B **236**, 125 (1984). doi:10.1016/0550-3213(84)90528-5.

[23] Z. Bern, J. J. Carrasco, D. Forde, H. Ita and H. Johansson, Phys. Rev. D **77**, 025010 (2008) doi:10.1103/PhysRevD.77.025010 [arXiv:0707.1035 [hep-th]].

[24] Z. Bern, L. J. Dixon, D. C. Dunbar and D. A. Kosower, Nucl. Phys. B **425**, 217 (1994) doi:10.1016/0550-3213(94)90179-1 [hep-ph/9403226];
Z. Bern, L. J. Dixon, D. C. Dunbar and D. A. Kosower, Nucl. Phys. B **435**, 59 (1995) doi:10.1016/0550-3213(94)00488-Z [hep-ph/9409265].

[25] Z. Bern, J. J. M. Carrasco and H. Johansson, Phys. Rev. D **78**, 085011 (2008) doi:10.1103/PhysRevD.78.085011 [arXiv:0805.3993 [hep-ph]].

[26] Z. Bern, J. J. M. Carrasco and H. Johansson, Phys. Rev. Lett. **105**, 061602 (2010) doi:10.1103/PhysRevLett.105.061602 [arXiv:1004.0476 [hep-th]].

[27] D. C. Dunbar and P. S. Norridge, Nucl. Phys. B **433**, 181 (1995) doi:10.1016/0550-3213(94)00385-R [hep-th/9408014];

D. C. Dunbar, J. H. Ettle and W. B. Perkins, Phys. Rev. D **83**, 065015 (2011) doi:10.1103/PhysRevD.83.065015 [arXiv:1011.5378 [hep-th]].

[28] Z. Bern, C. Boucher-Veronneau and H. Johansson, Phys. Rev. D **84**, 105035 (2011) doi:10.1103/PhysRevD.84.105035 [arXiv:1107.1935 [hep-th]].

[29] C. Boucher-Veronneau and L. J. Dixon, JHEP **1112**, 046 (2011) doi:10.1007/JHEP12(2011)046 [arXiv:1110.1132 [hep-th]].

[30] F.V. Tkachov, Phys. Lett. B **100**, 65 (1981);
K.G. Chetyrkin and F.V. Tkachov, Nucl. Phys. B **192**, 159 (1981);
S. Laporta, Int. J. Mod. Phys. A **15**, 5087 (2000) doi:10.1016/S0217-751X(00)00215-7, 10.1142/S0217751X00002157 [hep-ph/0102033];
S. Laporta and E. Remiddi, Phys. Lett. B **379**, 283 (1996) doi:10.1016/0370-2693(96)00439-X [hep-ph/9602417];
A. V. Smirnov, Comput. Phys. Commun. **189**, 182 (2015) doi:10.1016/j.cpc.2014.11.024 [arXiv:1408.2372 [hep-ph]];
A. von Manteuffel and C. Studerus, arXiv:1201.4330 [hep-ph].

[31] J. Gluza, K. Kajda and D. A. Kosower, Phys. Rev. D **83**, 045012 (2011) doi:10.1103/PhysRevD.83.045012 [arXiv:1009.0472 [hep-th]];

[32] G. Chen, J. Liu, R. Xie, H. Zhang and Y. Zhou, JHEP **1609**, 075 (2016) doi:10.1007/JHEP09(2016)075 [arXiv:1511.01058 [hep-th]];
A. Georgoudis, K. J. Larsen and Y. Zhang, arXiv:1612.04252 [hep-th];

[33] H. Ita, Phys. Rev. D **94**, no. 11, 116015 (2016), doi:10.1103/PhysRevD.94.116015 [arXiv:1510.05626 [hep-th]].

[34] K. J. Larsen and Y. Zhang, Phys. Rev. D **93**, no. 4, 041701 (2016), doi:10.1103/PhysRevD.93.041701 [arXiv:1511.01071 [hep-th]].

[35] Z. Bern, J. J. M. Carrasco, L. J. Dixon, H. Johansson and R. Roiban, Phys. Rev. D **85**, 105014 (2012) doi:10.1103/PhysRevD.85.105014 [arXiv:1201.5366 [hep-th]].

[36] E. Cremmer, J. Scherk and S. Ferrara, Phys. Lett. B **74**, 61 (1978).

[37] M. T. Grisaru, P. van Nieuwenhuizen and J. A. M. Vermaseren, Phys. Rev. Lett. **37**, 1662 (1976) doi:10.1103/PhysRevLett.37.1662

[38] S. Deser, J. H. Kay and K. S. Stelle, Phys. Rev. Lett. **38**, 527 (1977) doi:10.1103/PhysRevLett.38.527 [arXiv:1506.03757 [hep-th]].

[39] Z. Bern, T. Dennen, Y. t. Huang and M. Kiermaier, Phys. Rev. D **82**, 065003 (2010) doi:10.1103/PhysRevD.82.065003 [arXiv:1004.0693 [hep-th]].

[40] H. Johansson and A. Ochirov, JHEP **1511**, 046 (2015) doi:10.1007/JHEP11(2015)046 [arXiv:1407.4772 [hep-th]];
H. Johansson and A. Ochirov, JHEP **1601**, 170 (2016) doi:10.1007/JHEP01(2016)170 [arXiv:1507.00332 [hep-ph]].

[41] M. B. Green, J. H. Schwarz and L. Brink, Nucl. Phys. B **198**, 474 (1982). doi:10.1016/0550-3213(82)90336-4

[42] Z. Bern, S. Davies, T. Dennen, Y. t. Huang and J. Nohle, Phys. Rev. D **92**, no. 4, 045041 (2015) doi:10.1103/PhysRevD.92.045041 [arXiv:1303.6605 [hep-th]].

[43] J. C. Collins, *Renormalization: An Introduction to Renormalization, the Renormalization Group, and the Operator Product Expansion,* Cambridge University Press, Cambridge (1985).

[44] Z. Bern and D. A. Kosower, Nucl. Phys. B **379**, 451 (1992), doi:10.1016/0550-3213(92)90134-W.

[45] M. T. Grisaru, Phys. Lett. **66B**, 75 (1977), doi:10.1016/0370-2693(77)90617-7;
E. T. Tomboulis, Phys. Lett. **67B**, 417 (1977), doi:10.1016/0370-2693(77)90434-8

[46] Z. Bern, L. J. Dixon and D. A. Kosower, JHEP **0001**, 027 (2000), doi:10.1088/1126-6708/2000/01/027 [hep-ph/0001001].

[47] M. L. Mangano and S. J. Parke, Phys. Rept. **200**, 301 (1991), doi:10.1016/0370-1573(91)90091-Y [hep-th/0509223].

[48] Z. Bern, J. S. Rozowsky and B. Yan, Phys. Lett. B **401**, 273 (1997), doi:10.1016/S0370-2693(97)00413-9 [hep-ph/9702424].

[49] Z. Bern, L. J. Dixon, D. C. Dunbar, M. Perelstein and J. S. Rozowsky, Nucl. Phys. B **530**, 401 (1998), doi:10.1016/S0550-3213(98)00420-9 [hep-th/9802162].

[50] E. Herrmann and J. Trnka, JHEP **1611**, 136 (2016) doi:10.1007/JHEP11(2016)136 [arXiv:1604.03479 [hep-th]].

[51] G. Ossola, C. G. Papadopoulos and R. Pittau, Nucl. Phys. B **763**, 147 (2007), doi:10.1016/j.nuclphysb.2006.11.012 [hep-ph/0609007].

[52] G. Passarino and M. J. G. Veltman, Nucl. Phys. B **160**, 151 (1979), doi:10.1016/0550-3213(79)90234-7

[53] A. A. Vladimirov, Theor. Math. Phys. **43**, 417 (1980) [Teor. Mat. Fiz. **43**, 210 (1980)];
N. Marcus and A. Sagnotti, Nuovo Cim. A **87**, 1 (1985);

[54] Z. Bern, S. Davies and J. Nohle, Phys. Rev. D **93**, no. 10, 105015 (2016) doi:10.1103/PhysRevD.93.105015 [arXiv:1510.03448 [hep-th]].

[55] Z. Bern, A. Edison, D. Kosower, J. Parra-Martinez, Phys. Rev. D **96**, no. 6, 066004 (2017) doi:10.1103/PhysRevD.96.066004 [arXiv:1706.01486 [hep-th]].

[56] P. Mastrolia, T. Peraro and A. Primo, JHEP **1608**, 164 (2016) doi:10.1007/JHEP08(2016)164 [arXiv:1605.03157 [hep-ph]].

[57] Z. Bern, J. J. Carrasco, W. M. Chen, H. Johansson and R. Roiban, Phys. Rev. Lett. **118**, no. 18, 181602 (2017) [arXiv:1701.02519 [hep-th]].

[58] T. P. Cheng and L. F. Li, Oxford, UK: Clarendon (1984) 536 P. (Oxford Science Publications)

[59] S. Caron-Huot and J. M. Henn, JHEP **1406**, 114 (2014) doi:10.1007/JHEP06(2014)114 [arXiv:1404.2922 [hep-th]].

[60] J. M. Drummond, J. Henn, V. A. Smirnov and E. Sokatchev, JHEP **0701**, 064 (2007) [hep-th/0607160];

[61] J. M. Henn, J. Phys. A **44**, 454011 (2011) [arXiv:1103.1016 [hep-th]];

[62] V. Del Duca, L. J. Dixon, J. M. Drummond, C. Duhr, J. M. Henn and V. A. Smirnov, Phys. Rev. D **84**, 045017 (2011) [arXiv:1105.2011 [hep-th]];

[63] B. Basso and L. J. Dixon, Phys. Rev. Lett. **119**, no. 7, 071601 (2017) [arXiv:1705.03545 [hep-th]].

[64] J. M. Drummond, G. P. Korchemsky and E. Sokatchev, Nucl. Phys. B **795**, 385 (2008) [arXiv:0707.0243 [hep-th]].

[65] D. Forde, Phys. Rev. D **75**, 125019 (2007) [arXiv:0704.1835 [hep-ph]].

[66] C. F. Berger, Z. Bern, L. J. Dixon, F. Febres Cordero, D. Forde, H. Ita, D. A. Kosower and D. Maitre, "An Automated Implementation of On-Shell Methods for One-Loop Amplitudes," Phys. Rev. D **78** (2008) 036003 [arXiv:0803.4180 [hep-ph]].

[67] C. F. Berger *et al.*, Phys. Rev. Lett. **102**, 222001 (2009) [arXiv:0902.2760 [hep-ph]];
R. K. Ellis, K. Melnikov and G. Zanderighi, Phys. Rev. D **80**, 094002 (2009) [arXiv:0906.1445 [hep-ph]];
F. Cascioli, P. Maierhofer and S. Pozzorini, Phys. Rev. Lett. **108**, 111601 (2012) [arXiv:1111.5206 [hep-ph]];
G. Bevilacqua, M. Czakon, M. V. Garzelli, A. van Hameren, A. Kardos, C. G. Papadopoulos, R. Pittau and M. Worek, Comput. Phys. Commun. **184**, 986 (2013) [arXiv:1110.1499 [hep-ph]];
G. Cullen, N. Greiner, G. Heinrich, G. Luisoni, P. Mastrolia, G. Ossola, T. Reiter and F. Tramontano, Eur. Phys. J. C **72**, 1889 (2012) [arXiv:1111.2034 [hep-ph]];
S. Badger, B. Biedermann, P. Uwer and V. Yundin, Comput. Phys. Commun. **184**, 1981 (2013) [arXiv:1209.0100 [hep-ph]];;
Z. Bern, L. J. Dixon, F. Febres Cordero, S. Höche, H. Ita, D. A. Kosower, D. Maître and K. J. Ozeren, Phys. Rev. D **88**, no. 1, 014025 (2013) [arXiv:1304.1253 [hep-ph]];
J. Alwall *et al.*, JHEP **1407**, 079 (2014) [arXiv:1405.0301 [hep-ph]];
S. Actis, A. Denner, L. Hofer, J. N. Lang, A. Scharf and S. Uccirati, Comput. Phys. Commun. **214**, 140 (2017) [arXiv:1605.01090 [hep-ph]].

[68] S. Abreu, F. Febres Cordero, H. Ita, M. Jaquier, B. Page and M. Zeng, arXiv:1703.05273 [hep-ph];
S. Abreu, F. Febres Cordero, H. Ita, M. Jaquier and B. Page, Phys. Rev. D **95**, no. 9, 096011 (2017) [arXiv:1703.05255 [hep-ph]].

[69] S. Badger, H. Frellesvig and Y. Zhang, JHEP **1204** (2012) 055 [arXiv:1202.2019 [hep-ph]];
Y. Zhang, JHEP **1209** (2012) 042 [arXiv:1205.5707 [hep-ph]].

[70] P. Mastrolia and G. Ossola, "On the Integrand-Reduction Method for Two-Loop Scattering Amplitudes," JHEP **1111** (2011) 014 [arXiv:1107.6041 [hep-ph]];

P. Mastrolia, E. Mirabella, G. Ossola and T. Peraro, Phys. Lett. B **718** (2012) 173 [arXiv:1205.7087 [hep-ph]];

[71] R. K. Ellis, W. T. Giele and Z. Kunszt, JHEP **0803**, 003 (2008) [arXiv:0708.2398 [hep-ph]];
W. T. Giele, Z. Kunszt and K. Melnikov, JHEP **0804** (2008) 049 [arXiv:0801.2237 [hep-ph]].

[72] H. Hauser and G. Müller, Manuscripta Mathematica, 80(1):309–337, 1993.

[73] Y. Zhang, arXiv:1612.02249 [hep-th].

[74] R. M. Schabinger, JHEP **1201**, 077 (2012) [arXiv:1111.4220 [hep-ph]].

[75] S. J. Parke and T. R. Taylor, Phys. Lett. **157B**, 81 (1985) Erratum: [Phys. Lett. B **174**, 465 (1986)].

[76] Z. Bern, L. J. Dixon and D. A. Kosower, Phys. Rev. Lett. **70**, 2677 (1993) [hep-ph/9302280].

[77] J. M. Drummond, J. Henn, G. P. Korchemsky and E. Sokatchev, Nucl. Phys. B **795**, 52 (2008) [arXiv:0709.2368 [hep-th]].

[78] R. Frassek and D. Meidinger, JHEP **1605**, 110 (2016) [arXiv:1603.00088 [hep-th]].

[79] R. J. Eden, P. V. Landshoff, D. I. Olive and J. C. Polkinghorne, "The Analytic S-Matrix," Cambridge University Press, 1966;
G. F. Sterman, "An Introduction to quantum field theory," Cambridge University Press, 1993.

[80] D. Simmons-Duffin, JHEP **1404**, 146 (2014) [arXiv:1204.3894 [hep-th]].

[81] A. V. Kotikov, Phys. Lett. B **259**, 314 (1991);
E. Remiddi, Nuovo Cim. A **110**, 1435 (1997) [hep-th/9711188].

[82] M. Zeng, JHEP **1706**, 121 (2017) [arXiv:1702.02355 [hep-th]].

[83] J. M. Henn, Phys. Rev. Lett. **110**, 251601 (2013) [arXiv:1304.1806 [hep-th]];

[84] J. M. Henn, J. Phys. A **48**, 153001 (2015) [arXiv:1412.2296 [hep-ph]].

[85] J. M. Henn, A. V. Smirnov and V. A. Smirnov, JHEP **1403**, 088 (2014) [arXiv:1312.2588 [hep-th]].

[86] Z. Bern, E. Herrmann, S. Litsey, J. Stankowicz and J. Trnka, JHEP **1506**, 202 (2015) [arXiv:1412.8584 [hep-th]].

[87] Z. Bern, E. Herrmann, S. Litsey, J. Stankowicz and J. Trnka, JHEP **1606**, 098 (2016) [arXiv:1512.08591 [hep-th]].

[88] D. R. Grayson and M. E. Stillman, "Macaulay2, a software system for research in algebraic geometry", available at http://www.math.uiuc.edu/Macaulay2/;
W. Decker, G.-M. Greuel, G. Pfister, and H. Schönemann, Singular4-0-2 — A computer algebra system for polynomial computations http://www.singular.uni-kl.de, 2015.

[89] S. Laporta and E. Remiddi, Nucl. Phys. B **704**, 349 (2005) [hep-ph/0406160].

[90] S. Müller-Stach, S. Weinzierl and R. Zayadeh, Commun. Num. Theor. Phys. **6**, 203 (2012) [arXiv:1112.4360 [hep-ph]].

[91] R. N. Lee, JHEP **0807**, 031 (2008) [arXiv:0804.3008 [hep-ph]].

[92] D. A. Kosower and K. J. Larsen, Phys. Rev. D **85**, 045017 (2012) [arXiv:1108.1180 [hep-th]];
S. Caron-Huot and K. J. Larsen, JHEP **1210**, 026 (2012) [arXiv:1205.0801 [hep-ph]];

M. Søgaard, JHEP **1309**, 116 (2013) [arXiv:1306.1496 [hep-th]];
H. Johansson, D. A. Kosower and K. J. Larsen, Phys. Rev. D **89**, no. 12, 125010 (2014) [arXiv:1308.4632 [hep-th]];
M. Søgaard and Y. Zhang, JHEP **1312**, 008 (2013) [arXiv:1310.6006 [hep-th]];
M. Søgaard and Y. Zhang, JHEP **1407**, 112 (2014) [arXiv:1403.2463 [hep-th]];
M. Harley, F. Moriello and R. M. Schabinger, JHEP **1706**, 049 (2017) [arXiv:1705.03478 [hep-ph]];
J. Bosma, M. Søgaard and Y. Zhang, arXiv:1704.04255 [hep-th].

[93] S. Abreu, R. Britto, C. Duhr and E. Gardi, JHEP **1706**, 114 (2017) [arXiv:1702.03163 [hep-th]].

[94] L. F. Alday, J. M. Henn, J. Plefka and T. Schuster, JHEP **1001**, 077 (2010) [arXiv:0908.0684 [hep-th]].

[95] Z. Bern and G. Chalmers, Nucl. Phys. B **447**, 465 (1995) [hep-ph/9503236].

[96] Z. Bern, L. J. Dixon and D. A. Kosower, Nucl. Phys. B **412**, 751 (1994) [hep-ph/9306240].

[97] R. J. Gonsalves, Phys. Rev. D **28**, 1542 (1983);
G. Kramer and B. Lampe, J. Math. Phys. **28**, 945 (1987).

[98] H. Ita, PoS LL **2016**, 080 (2016) [arXiv:1607.00705 [hep-ph]].

[99] Z. Bern, M. Czakon, L. J. Dixon, D. A. Kosower and V. A. Smirnov, Phys. Rev. D **75**, 085010 (2007) [hep-th/0610248];
J. M. Drummond, J. Henn, G. P. Korchemsky and E. Sokatchev, Nucl. Phys. B **828**, 317 (2010) [arXiv:0807.1095 [hep-th]].

[100] I. Bena, J. Polchinski and R. Roiban, Phys. Rev. D **69**, 046002 (2004) [hep-th/0305116];
J. M. Drummond, J. M. Henn and J. Plefka, JHEP **0905**, 046 (2009) [arXiv:0902.2987

[hep-th]];

N. Beisert, J. Broedel and M. Rosso, J. Phys. A **47**, 365402 (2014) [arXiv:1401.7274 [hep-th]].

[101] N. Beisert and M. Staudacher, Nucl. Phys. B **670**, 439 (2003) [hep-th/0307042].

[102] J. M. Drummond, J. Henn, G. P. Korchemsky and E. Sokatchev, Nucl. Phys. B **815**, 142 (2009) [arXiv:0803.1466 [hep-th]];

A. V. Belitsky, G. P. Korchemsky and E. Sokatchev, Nucl. Phys. B **855**, 333 (2012) [arXiv:1103.3008 [hep-th]];

L. J. Mason and D. Skinner, JHEP **1012**, 018 (2010) [arXiv:1009.2225 [hep-th]].

[103] A. V. Kotikov, L. N. Lipatov, A. I. Onishchenko and V. N. Velizhanin, Phys. Lett. B **595**, 521 (2004) Erratum: [Phys. Lett. B **632**, 754 (2006)] [hep-th/0404092];

A. V. Kotikov and L. N. Lipatov, Nucl. Phys. B **769**, 217 (2007) [hep-th/0611204].

[104] B. Basso, A. Sever and P. Vieira, Phys. Rev. Lett. **111**, no. 9, 091602 (2013) [arXiv:1303.1396 [hep-th]];

B. Basso, A. Sever and P. Vieira, JHEP **1401**, 008 (2014) [arXiv:1306.2058 [hep-th]].

[105] L. J. Dixon, J. M. Drummond, C. Duhr and J. Pennington, JHEP **1406**, 116 (2014) [arXiv:1402.3300 [hep-th]];

L. J. Dixon and M. von Hippel, JHEP **1410**, 065 (2014) [arXiv:1408.1505 [hep-th]];

L. J. Dixon, J. Drummond, T. Harrington, A. J. McLeod, G. Papathanasiou and M. Spradlin, JHEP **1702**, 137 (2017) [arXiv:1612.08976 [hep-th]];

S. Caron-Huot, L. J. Dixon, A. McLeod and M. von Hippel, Phys. Rev. Lett. **117**, no. 24, 241601 (2016) [arXiv:1609.00669 [hep-th]].

[106] Z. Bern, L. J. Dixon and V. A. Smirnov, Phys. Rev. D **72**, 085001 (2005) [hep-th/0505205];

L. F. Alday and J. M. Maldacena, JHEP **0706**, 064 (2007) [arXiv:0705.0303 [hep-th]].

[107] N. Arkani-Hamed, J. L. Bourjaily, F. Cachazo, A. B. Goncharov, A. Postnikov and J. Trnka, arXiv:1212.5605 [hep-th].

[108] N. Arkani-Hamed and J. Trnka, JHEP **1412**, 182 (2014) [arXiv:1312.7878 [hep-th]].

[109] A. B. Goncharov, M. Spradlin, C. Vergu and A. Volovich, Phys. Rev. Lett. **105**, 151605 (2010) [arXiv:1006.5703 [hep-th]].

[110] D. Chicherin, J. M. Henn and E. Sokatchev, arXiv:1804.03571 [hep-th].

[111] J. J. Carrasco and H. Johansson, Phys. Rev. D **85**, 025006 (2012) [arXiv:1106.4711 [hep-th]].

[112] T. Gehrmann, J. M. Henn and N. A. Lo Presti, Phys. Rev. Lett. **116**, no. 6, 062001 (2016) Erratum: [Phys. Rev. Lett. **116**, no. 18, 189903 (2016)] [arXiv:1511.05409 [hep-ph]];
D. Chicherin, J. Henn and V. Mitev, JHEP **1805**, 164 (2018) [arXiv:1712.09610 [hep-th]].

[113] N. Arkani-Hamed, J. L. Bourjaily, F. Cachazo, S. Caron-Huot and J. Trnka, JHEP **1101**, 041 (2011) [arXiv:1008.2958 [hep-th]].

[114] S. J. Parke and T. R. Taylor, Phys. Rev. Lett. **56**, 2459 (1986);
M. L. Mangano, S. J. Parke and Z. Xu, Nucl. Phys. B **298**, 653 (1988).

[115] N. Arkani-Hamed, J. L. Bourjaily, F. Cachazo and J. Trnka, Phys. Rev. Lett. **113**, no. 26, 261603 (2014) [arXiv:1410.0354 [hep-th]].

[116] N. Arkani-Hamed, J. L. Bourjaily, F. Cachazo, A. Postnikov and J. Trnka, JHEP **1506**, 179 (2015) [arXiv:1412.8475 [hep-th]].

[117] S. Franco, D. Galloni, B. Penante and C. Wen, JHEP **1506**, 199 (2015) [arXiv:1502.02034 [hep-th]];

J. L. Bourjaily, S. Franco, D. Galloni and C. Wen, JHEP **1610**, 003 (2016) [arXiv:1607.01781 [hep-th]].

[118] J. Bosma, K. J. Larsen and Y. Zhang, Phys. Rev. D **97**, no. 10, 105014 (2018) [arXiv:1712.03760 [hep-th]].

[119] Z. Bern, L. J. Dixon and D. A. Kosower, Phys. Lett. B **302**, 299 (1993) Erratum: [Phys. Lett. B **318**, 649 (1993)] [hep-ph/9212308]; O. V. Tarasov, Phys. Rev. D **54**, 6479 (1996) [hep-th/9606018].

[120] R. H. Boels, T. Huber and G. Yang, JHEP **1801**, 153 (2018) [arXiv:1711.08449 [hep-th]].

[121] B. Eden, Y. Jiang, D. le Plat and A. Sfondrini, JHEP **1802**, 170 (2018) [arXiv:1710.10212 [hep-th]];
T. Bargheer, J. Caetano, T. Fleury, S. Komatsu and P. Vieira, arXiv:1711.05326 [hep-th];
R. Ben-Israel, A. G. Tumanov and A. Sever, arXiv:1802.09395 [hep-th].

[122] L.J. Dixon, *Calculating Scattering Amplitudes Efficiently*, arXiv:9601359 [hep-ph]

[123] J. M. Henn, J. C. Plefka, *Scattering Amplitudes in Gauge Theories*, Lecture Notes in Physics 883, Heidelbera: Springer (2014).

[124] N. Arkani-Hamed, F. Cachazo, J. Kaplan, JHEP **1009**, 016 (2010) [arXiv:0808.1446 [hep-th]].

[125] N. Arkani-Hamed, J. Bourjaily, F. Cachazo, A. Hodges, J. Trnka, JHEP **1204**, 081 (2012) [arXiv:1012.6030 [hep-th]].

[126] N. Arkani-Hamed, A. Hodges, J. Trnka, JHEP **1508**, 030 (2015) [arXiv:1412.8478 [hep-th]].

[127] F. Livia, T. Lukowski, A. Orta, M. Parisi, JHEP **1603**, 014 (2016) [arXiv:1512.04954 [hep-th]].

[128] L. Mason, D. Skinner, JHEP **0911**, 045 (2009) [arXiv:0909.0250 [hep-th]].

[129] N. Arkani-Hamed, F. Cachazo, C. Cheung, J. Kaplan, JHEP **1003**, 020 (2010) [arXiv:0907.5418 [hep-th]].

[130] J. M. Drummond, J. M. Henn and J. Plefka, JHEP **0905**, 046 (2009) [arXiv:0902.2987 [hep-th]].

[131] S. Huggett and K. Tod, *An Introduction to Twistor Theory*. Cambridge University Press, 1994.

[132] L. Hughston and T. Hurd, Phys. Rept. **100** (1983) pg. 275-326.

[133] A. Hodges, JHEP **1305**, 135 (2013) [arXiv:0905.1473 [hep-th]].

[134] R. Britto, F. Cachazo, F. Feng, E. Witten, Phys.Rev.Lett. 94 (2005) 181602 [arXiv:0501052 [hep-th]]

[135] F. Cachazo, S. He, E. Y. Yuan, Phys.Rev.Lett. 113 (2014) 171601 [arXiv:1307.2199 [hep-th]]

[136] F. Cachazo, S. He, E. Y. Yuan, JHEP **1407**, 033 (2014) [arXiv:1309.0885 [hep-th]]

[137] F. Cachazo, S. He, E. Y. Yuan, JHEP **1507**, 149 (2015) [arXiv:1412.3479 [hep-th]]

[138] F. Cachazo, S. Mizera, G. Zhang, JHEP **1703**, 151 (2017) [arXiv:1609.00008 [hep-th]]

[139] N. Arkani-Hamed, Y. Bai, S. He, G. Yan, JHEP **1805**, 096 (2018) [arXiv:1711.09102 [hep-th]]

[140] J. Farrow JHEP **1808**, 085 (2018) [arXiv:1806.02732 [hep-th]]

[141] Z. Liu, X. Zhao [arXiv:1810.00384 [hep-th]]